The Pennsylvania State University
The Graduate School
College of Engineering

COMPUTATIONALLY EFFICIENT ONLINE MODEL-BASED CONTROL AND ESTIMATION FOR LITHIUM-ION BATTERIES

A Dissertation in
Mechanical Engineering
by
Ji Liu

Submitted in Partial Fulfillment
of the Requirements
for the Degree of

Doctor of Philosophy

May 2017

The dissertation of Ji Liu was reviewed and approved* by the following:

Hosam K. Fathy
Associate Professor of Mechanical Engineering
Dissertation Advisor, Chair of Committee

Christopher D. Rahn
Professor of Mechanical Engineering

Chao-Yang Wang
Professor of Mechanical Engineering

Constantino Lagoa
Professor of Electrical Engineering

Karen A. Thole
Professor of Mechanical Engineering
Department Head of Mechanical and Nuclear Engineering

*Signatures are on file in the Graduate School.

Abstract

This dissertation presents a framework for computationally-efficient, health-conscious online state estimation and control in lithium-ion batteries. The framework builds on three main tools, namely, (i) battery model reformulation and (ii) pseudo-spectral optimization for (iii) differential flatness. All of these tools already exist in the literature. However, their application to electrochemical battery estimation and control, both separately and in an integrated manner, represents a significant addition to the literature. The dissertation shows that these tools, together, provide significant improvements in computational efficiency for both online moving horizon battery state estimation and online health-conscious model predictive battery control. These benefits are demonstrated both in simulation and using an experimental case study.

Two key facts motivate this dissertation. First, lithium-ion batteries are widely used for different applications due to their low self-discharge rates, lack of memory effects, and high power/energy densities compared to traditional lead-acid and nickel-metal hydride batteries. Second, lithium-ion batteries are also vulnerable to aging and degradation mechanisms, such as lithium plating, some of which can lead to safety issues. Conventional battery management systems (BMS) typically use model-free control strategies and therefore do not explicitly optimize the performance, life span, and cost of lithium-ion battery packs. They typically avoid internal damage by constraining externally-measured variables, such as battery voltage, current, and temperature. When pushed to charge a battery quickly without inducing excessive damage, these systems often follow simple and potentially sub-optimal charge/discharge trajectories, e.g., the constant-current/constant-voltage (CCCV) charging strategy. While the CCCV charging strategy is simple to implement, it suffers from its poor ability to explicitly control the internal variables causing battery aging, such as side reaction overpotentials. Another disadvantage is the inability of this strategy to adapt to changes in battery dynamics caused by aging.

Model-based control has the potential to alleviate many of the above limitations of classical battery management systems. A model-based control system can

estimate the internal state of a lithium-ion battery and use the estimated state to adjust battery charging/discharging in a manner that avoids damaging side reactions. By doing so, model-based control can (i) prolong battery life, (ii) improve battery safety, (iii) increase battery energy storage capacity, (iv) decrease internal damage/degradation, and (v) adapt to changes in battery dynamics resulting from aging. These potential benefits are well-documented in the literature. However, one major challenge remains, namely, the computational complexity associated with online model-based battery state estimation and control. The goal of this dissertation is to address this challenge by making five contributions to the literature. Specifically:

- Chapter 2 exploits the differential flatness of solid-phase lithium-ion battery diffusion dynamics, together with pseudo-spectral optimization and diffusion model reformulation, to decrease the computational load associated with health-conscious battery trajectory optimization significantly. This contribution forms a foundation for much of the subsequent work in this dissertation, but is limited to isothernal single-particle battery models with significant time scale separation between anode- and cathode-side solid-phase diffusion dynamics.

- Chapter 3 extends the results of Chapter 2 in two ways. First , it exploits the law of conservation of charge to enable flatness-based, health-conscious battery trajectory optimization for single particle battery models even in the absence of time scale separation between the negative and positive electrodes. Second, it performs this optimization for a combined thermo-electrochemical battery model, thereby relaxing the above assumption of isothermal battery behavior and highlighting the benefits of flatness-based optimization for a nonlinear battery model.

- Chapter 4 presents a framework for flatness-based pseudo-spectral combined state and parameter estimation in lumped-parameter nonlinear systems. This framework enables computationally-efficient total least squares (TLS) estimation for lumped-parameter nonlinear systems. This is quite relevant to practical lithium-ion battery systems, where both battery input and output measurements can be quite noisy.

- Chapter 5 utilizes the above flatness-based TLS estimation algorithm for moving horizon state estimation using a coupled thermo-electrochemical equivalent circuit model of lithium-ion battery dynamics.

- Chapter 6 extends the battery estimation framework from Chapter 5 to enable moving horizon, flatness-based TLS state estimation in thermo-electrochemical

single-particle lithium-ion battery models, and demonstrates this framework using laboratory experiments.

The overall outcome of this dissertation is an integrated set of tools, all of them exploiting model reformulation, differential flatness, and pseudo-spectral methods, for computationally efficient online state estimation and health-conscious control in lithium-ion batteries.

Table of Contents

List of Figures

List of Tables

Acknowledgments

Looking back on the experience as a Ph.D. candidate, only now do I realize that getting a Ph.D. degree is more about a journey than a degree. I would like to sincerely thank my advisor Dr. Hosam K. Fathy for all the guidance and support you have given me through my Ph.D. study. I would like to thank you for trusting me and giving me the prestigious opportunity to join our great, friendly, diverse, and fun lab. I would like to thank you for giving me continuous technical support whenever I need and being very patient and tolerant. I would like to thank you for your encouragement which makes me believe my research could have some positive impact to our community. I would like to thank you for guiding me to be a better student, scholar, and collaborator. Without your wisdom, knowledge, guidance, and support, I would not even be able to enter my favorite area, dynamics control and optimization and I would not have the opportunity to enjoy my research. Additionally, I would like to thank my committee members, Dr. Chris Rahn, Dr. Chao-Yang Wang, and Dr. Constantino Lagoa. With your valuable input, ideas, and suggestion, this dissertation has become much better.

Second, I would like to thank my families for your endless love, understanding, support, and encouragement. Without the love, encouragement, and understanding from my parents, Jiangwei Liu and Xiujuan Ji, I would not be able to be so decided to pursue the Ph.D. degree at early stage during my undergrad life and I would not ever be able to finish the Ph.D. study. Without the love and understanding from my wife, Lejiao Wang, I would not live such a happy, although challenging, life during my Ph.D. study. My families are the ones of only a few people who know me very well, who understand why I continue being energetic and conscientious, and more importantly, who believe that I can reach my dreams and realize my social values in the future.

Third, I need to say a big thank you to the COOL Lab members and without you guys, my Ph.D. life would definitely crash. Abdullah, the king, thank you for being patient and tolerant on me. I wish I could be even as 50% calm as you are. Donald, you are so nice to me and you are always patient to listen to what

I said and provide any help I need. Sergio, you do not know how much I learned from you, not only from your research but also from how you communicate and negotiate with people. Mohammed, or Cup (thank for coming up with this name, Sergio!), you are so nice and smart and I do not doubt you will change the world. Partha, thank you for your support and wisdom on the hardware tests and I am looking forward to seeing your company for self-balancing setup with photovoltaic cells, batteries, and everything. Michelle, you do not know how much I learned from your presentation and writing skills. Oh my God, Wahaba, (I treat you as a pseudo-member of our lab), as a singular point in the office, thank you for your stories and introducing me to college football.

Finally, I would like to thank the financial support from the AMPED program in Advanced Research Projects Agency - Energy (ARPA-E) in U.S. Department of Energy.

Chapter 1
Introduction

1.1 Motivation

This dissertation examines the fundamental challenge of online health-conscious model-based control and estimation for lithium-ion batteries. Lithium-ion batteries are widely used for different applications, such as electronic devices, electric vehicles, and the smart grid [5]. The popularity of lithium-ion batteries is due to their low self-discharge rates, lack of memory effects, and high power/energy densities compared to traditional lead-acid and nickel-metal hydride batteries [6,7]. However, the improper use of lithium-ion batteries can result in reduced life, reduced capacity/power, and even catastrophic thermal runaway [8]. Examples highlighting the lithium-ion battery safety challenge include the thermal runaway accidents of the Boeing 787 Dreamliner fleet [8].

The vulnerability of lithium-ion batteries to abuse and extreme conditions makes it necessary to design some onboard mechanisms, i.e., battery management systems (BMS), that can manage lithium-ion batteries properly. Two key roles of a BMS are (i) to control the usage of battery cells and (ii) estimate their internal states. The control function in a BMS is needed for protecting the cells from excessive degradation and guaranteeing their safety while satisfying user demand. The estimation function is needed for predicting how much charge is left in a cell and also for estimating the internal states that are not measurable directly through sensors.

Conventional BMS can limit battery performance, jeopardize safety, and increase cost unnecessarily. This is because they mostly use model-free control strategies

that fail in constraining the internal variables responsible for aging (e.g., side reaction overpotentials). These algorithms also suffer from poor adaptation to battery aging. More specifically, traditional BMSs typically avoid internal damage by constraining externally-measured variables such as battery voltage, current, and temperature. When pushed to charge a battery as fast as possible without inducing excessive damage, these systems often follow simple charge/discharge strategies such as the constant-current/constant-voltage (CCCV) strategy [9]. The advantage of traditional control strategies is their simplicity: they do not need a battery model, and any constraints they use for ensuring safety are imposed on directly-measured signals. However, the literature shows that these traditional control strategies can be conservative for new batteries and aggressive (hence damaging) for old batteries [10]. For instance, with constant cell voltage bounds, a fresh battery can reach the voltage limit while there is still space for safe operation. However, when the battery ages, it can be dangerous to use the same voltage bounds, since the aged electrodes can experience dangerous side reactions while within those bounds. From the estimation perspective, conventional BMS systems estimate available charge by integrating input current: a method known as Coulomb counting. While simple and model-free, Coulomb counting suffers from significant estimation error due to (i) incorrect initial state of charge (SOC) estimates, (ii) current sensor bias, and (iii) incorrect cell capacity estimates. To alleviate the above estimation/control challenges, battery packs are typically oversized [5]. This typically improves battery safety and longevity, at the expense of increased cost.

The literature shows that model-based control is superior to the traditional model-free approach with regard to battery performance, lifespan, and cost. The use of battery models makes it possible to predict battery dynamics and internal variables that are related to battery aging phenomena, such as solid-electrolyte interface (SEI) layer growth and lithium plating [10]. Physics-based battery models are also able to predict degradation in terms of parameters and variables that have physical significance. The literature shows that model-based battery control can prolong effective battery life by about 20-40% [11], improve battery safety [9, 12], increase battery energy-storing capacity [13], and decrease damage and degradation [12]. Moreover, model-based control has the ability to *adapt* to variations in battery health with time by charging new batteries more aggressively and old batteries more safely [9]. To develop and implement a model-based controller in BMS in real time,

one needs (i) a parameterized battery model that can capture battery dynamics; (ii) an estimation algorithm to estimate state variables; (iii) a model-based control algorithm for online battery control.

1.2 Key Challenges in Model-Based Battery Estimation and Control

Model-based battery state estimation and control may, as explained above, have many potential benefits, but it also comes a price. Two potential challenges that motivate this dissertation are: (i) the computational cost associated with model-based battery control; and (ii) the estimation accuracy required for such control. Theses challenges are discussed below.

1.2.1 Challenge 1: The Computational Cost of Model-Based Battery Control

Model predictive control (MPC) is one particularly attractive approach for online battery management. It has the advantages of being well-suited for enforcing health-related battery control constraints. It also has the attractive feature of re-optimizing the battery charge/discharge trajectory at every sampling instant, thereby potentially achieving some degree of robustness to battery modeling uncertainties. The tools used in this dissertation are useful for many battery control design methods, including both MPC and other design approaches (e.g., offline trajectory optimization, model-reference adaptive control, etc.). However, MPC is particularly useful for illustrating the fundamental need for computational efficiency in model-based battery control. An MPC controller must be capable of using a battery model for trajectory optimization at every time step of controller operation. Moreover, this optimization must be completed in less than one time step. This is quite problematic for the following reasons:

Challenge 1.1: Physics-based battery models are computationally complex. It is necessary for model-based control purposes to adopt battery models that can represent the underlying dynamics governing battery performance and aging as accurately as possible. There is a broad spectrum of lithium-ion battery models in the literature, with many different levels of fidelity and complexity.

At one end of this spectrum are lumped-parameter equivalent-circuit models (ECM), which represent battery dynamics using simple circuit elements such as resistors and capacitors. These models are limited in their ability to provide direct physical insights into internal battery phenomena, such as solid- and solution-phase diffusion dynamics. This motivates the literature's exploration of higher-fidelity, physics-based models such as single-particle models (SPMs), extended single particle models (ESPMs), and porous pseudo-two dimensional (P2D) models such as the well-known Doyle-Fuller-Newman (DFN) model [7, 14]. The distinctions between these models can be explained, quite simply, as follows: a single-particle model represents each battery electrode's solid-phase diffusion dynamics by modeling the behavior of just one representative solid particle per electrode, neglecting the dynamics of the battery's electrolyte. An enhanced single-particle model also represents each electrode's solid-phase dynamics by a single particle, but adds electrolytic diffusion effects between the representative particles in the negative and positive electrodes. Finally, a porous pseudo-2D model allows solid-phase diffusion dynamics to be different at different points along the thickness of the battery, and also accounts for solution-phase diffusion dynamics. This leads to a "pseudo"-2D model because there are now two dimensions in which diffusion can occur: the thickness of the electrode, and the radius of each solid-phase particle. These solid- and solution-phase diffusion processes are governed by one-dimensional partial differential equations (PDEs), with coupling at the boundaries between these PDEs [15]. All of these models can be enhanced to capture not just electrochemical battery behavior, but also the coupling between thermal and electrochemical behaviors, leading to models such as the temperature-enhanced single-particle battery model (SPM-T) [16].

An important question in model-based lithium-ion battery control is: *which of the above models should one use for control*? All of the above models certainly have value for optimization and control studies. However, one can argue that only the physics-based, rather than equivalent-circuit, models are suitable for predicting internal battery variables associated with aging and degradation phenomena, e.g., the side reaction overpotentials responsible for lithium plating and solid electrolyte interphase (SEI) layer growth. One can also observe that physics-based lithium-ion battery models, such as the SPM, ESPM, SPM-T, and DFN models, typically utilize partial differential equations (PDEs) to describe internal battery diffusion dynamics. This makes the models infinite-dimensional, thereby making model-based control

potentially computationally challenging.

There is a rich existing literature on discretizing, or "reformulating", PDE-based lithium-ion battery models to reduce them into lumped-parameter models with finite numbers of state variables. The spatial dimension can be discretized using finite difference or finite element methods, which often furnish high-order lumped-parameter models [17]. Subramanian *et al.* approximate the solid phase concentration profile using parabolic and quadratic polynomials, respectively [18]. Long *et al.* reduce battery models using the orthogonal collocation on finite elements, which is shown to be better than the finite volume approach with equal discretization points [19]. Smith *et al.* approximate the diffusion dynamics using the residue grouping method, which has good spatial resolution even with a low order model [17]. Forman *et. al.* apply the Padé approximation tool to the spherical diffusion centered at low frequency, thereby obtaining analytic reduced-order transfer function representation of solid-phase diffusion dynamics [20]. Both the residue grouping and the Padé approximation are important in the sense that the residue grouping method is more robust to a wide frequency window and the Padé approximation is more accurate at a target frequency [21]. Finally, Kehs *et al.* and Mayhew *et al.* adopt projection-based model reduction techniques for solid-phase diffusion dynamics [22, 23].

The above use of model reformulation is quite valuable for extracting accurate finite-dimensional representations of lithium-ion battery dynamics from the underlying infinite-dimensional diffusion PDEs. This reduces the computational cost of model-based lithium-ion battery control significantly, and model reformulation is in fact an important foundation for the work in this dissertation. However, even with model reformulation, accurately capturing the dynamics of lithium-ion battery behavior - particularly at high charge/discharge rates - often requires reformulated models with a significant number of state variables. This can be quite challenging for optimization and control applications.

Challenge 1.2: Battery trajectory optimization problems are computationally difficult to solve. Battery dynamics are typically nonlinear [24]. For the single-particle model with temperature dynamics (SPM-T), for instance, the nonlinearity is introduced by at least five factors. First, the Butler-Volmer equation which relates the intercalation rates in the positive and negative battery electrodes to the corresponding overpotentials is nonlinear. Second, heat generation

in a lithium-ion battery is also nonlinear in terms of the battery's internal states and inputs. This is true for both reversible heating, which is a function of input current squared, and irreversible heating, which is a bilinear function of input current and temperature. Third, the Arrhenius equation, which expresses the dependency of battery model parameters on temperature, is also nonlinear. Fourth, the relationship between solid-phase ion concentrations and electrode reference potentials in both the positive and negative electrodes is also nonlinear for most battery chemistries, especially over a broad range of states of charge. Finally, lithium-ion battery electrode entropy coefficients, which govern reversible internal heat generation during charge/discharge, also typically vary in a nonlinear manner with state of charge. The nonlinearity of battery dynamics, and non-convexity of the resulting model-based optimal battery control problems, can make model-based optimal battery control computationally very challenging even for low-order battery models.

The literature presents at least five different families of algorithms for model-based battery charge/discharge trajectory optimization, grounded in: (i) dynamic programming [25], (ii) genetic algorithm [26, 27], (iii) reference governor methods [5, 12], (iv) direct transcription [28, 29], and (v) pseudospectral optimization [30, 31]. All of these algorithms are valuable, in the sense that they contribute to a growing literature showing the potential benefits of model-based battery control. However, in light of the above discussion on nonlinearity/non-convexity, it is natural to ask whether these approaches are well-suited for online model-based optimal battery control. Dynamic programming and evolutionary optimization algorithms are both appealing for non-convex optimization problems, but their computational cost is prohibitive for most online control applications. This raises the question of whether other trajectory optimization methods from the literature, such as pseudo-spectral methods, can be used for solving model-based optimal battery control problems in a manner that is computationally tractable and does, indeed, improve battery performance and longevity compared to classical BMS controllers. A key goal of this dissertation is to explore the degree to which pseudo-spectral optimization, in particular, can be combined with battery model reformulation and differential flatness to enable computationally tractable, nonlinear health-conscious battery control. In pursuing this goal, the dissertation does not attempt to provide mathematical guarantees of global control optimality or proximity to

global optimality. However, it does explore the degree to which one can use the above tools for computationally tractable, health-conscious online battery control.

1.2.2 Challenge 2: Battery State of Charge Estimation Accuracy

To fully achieve the benefits of model-based battery control, one must be able to estimate the state variables of underlying battery models accurately. Inaccurate estimation of internal battery state variables can lead to accidental cell damage and reduced battery life. The state variables are used to describe the internal dynamics of charge diffusion and accumulation in a lithium-ion battery. For instance, one particularly important state variable in any battery model is the battery's state of charge (SOC), defined as the amount of charge stored in the battery divided by its nominal charge capacity. Because there is no sensor that can "measure" SOC directly, one has to estimate it.

There is a significant existing literature that examines both battery SOC estimation and the factors affecting SOC estimation accuracy. Examples of these factors include sensor noise, mismatch between the order of a battery model and the order a battery's true dynamics, and inaccuracy in battery parameter estimation [32–34]. One can classify existing SOC estimation algorithms into open-loop and closed-loop algorithms [35]. Open-loop SOC estimation, also known as Coulomb counting, is vulnerable to at least three major sources of estimation error, namely: (i) incorrect initialization of the SOC estimate, (ii) current sensor bias, and (iii) incorrect estimation of cell charge capacity. Closed-loop estimation algorithms are typically less sensitive to these three sources of error. Some of the methods used for closed-loop battery SOC estimation in the literature include Luenberger filtering [36, 37], backstepping [38], recursive least squares estimation [39], Kalman filtering [40–46], and optimization-based estimation [47, 48].

The SOC estimation literature is quite rich and mature, in the sense that it offers many different algorithms for SOC estimation and also different perspectives on the accuracy of these algorithms. However, one critical challenge remains relatively unexplored in this literature. To estimate a battery's SOC, one typically measures physical quantities such as battery input current, terminal voltage, and temperature (ambient, surface, and/or internal). All of these measurements can be

quite noisy in practical battery applications: a fact that motivates the use of total least squares (TLS) for the online estimation of battery state variables (including SOC). A key goal of this dissertation is to perform nonlinear TLS battery state estimation online, in a computationally efficient manner, using a moving-horizon approach. A closely-related goal is to validate the resulting estimation algorithm experimentally. The use of nonlinear total least squares for moving-horizon online battery state estimation, in a computationally efficient manner, using a physics-based combined thermo-electrochemical battery model, is in and of itself a novel addition to the literature. There is some existing work in the literature, for example, on moving-horizon battery SOC estimation using simple equivalent-circuit models, rather than physics-based ones [49–51]. The work in this dissertation expands significantly beyond this existing work, and also validates the resulting estimation algorithm experimentally.

1.3 Contributions

The overarching goal of this dissertation is to address the above challenges and furnish a computationally tractable framework for online health-conscious model-based battery control and state estimation estimation. In pursuing this goal, the dissertation builds on three key tools from the literature.

First, the dissertation exploits the differential flatness of lithium-ion battery dynamics, including the flatness of Fick's second law of diffusion, to optimize the trajectory of a small number of flat output variables that capture all of the underlying battery dynamics. The concept of the differential flatness originated in a seminal work by Fliess *et al.* [52]. A dynamic system is differentially flat if there exists a flat output such that the system's states and the inputs can be directly expressed in terms of the flat output and a finite number of its derivatives. The concept of flatness can be considered an extension of the classical notion of controllability from linear system theory to nonlinear systems [52] and has been used in optimization, trajectory planning, and control design [53–56]. Fick's second law of diffusion is a special case of the generalized heat diffusion equation presented in [57], and is therefore differentially flat [1, 58, 59]. One major benefit of adopting differential flatness in optimization is that only the flat output trajectory needs to be optimized and all the states and inputs can be expressed as functions of

the flat output and a finite number of its derivatives. As a result, the number of continuous-time optimization variables is reduced significantly: a fact that boosts computational efficiency significantly, especially for nonlinear battery dynamics, e.g., electrochemical-thermal battery models.

Second, the dissertation employs an efficient model order reduction technique (namely, Legendre polynomial-based orthogonal projection) to represent the dynamics of each battery electrode using a small number of state equations. For orthogonal projection-based model order reduction, lithium-ion concentration is expressed as a sum of Legendre spatial basis functions following [22]. Since the only unknown variables are the coefficients associated with Legendre polynomials, the dissertation reformulates the dynamics using 3 state variables in an efficient and accurate way. The specific choice of spatial basis functions for model reformulation does not limit the work presented in this dissertation: other choices (e.g., Chebyshev polynomials) can be used with equal ease [60]. For Padé approximation, the PDEs governing spherical diffusion are Laplace transformed and approximated using a rational polynomial transfer function centered at a low frequency.

Third, the dissertation optimizes the above flat output trajectory using pseudospectral methods because such methods: (i) have high convergence rates, are computationally very efficient, and (ii) can solve nonlinear and nonconvex optimization problems [61,62]. Originally developed for the numerical solution of differential equations, pseudospectral methods have been recently adopted as efficient tools for solving optimal control problems [63,64]. These methods transform a continuous optimization problem into a nonlinear programming (NLP) problem which can be solved using well-developed NLP algorithms [61,63].

The above three tools, together, constitute a framework that makes it possible, in this dissertation, to solve two interconnected optimization problems, namely: (i) optimal battery state estimation and (ii) health-conscious optimal battery control. The dissertation solves both of these problems using an online, moving-horizon approach. For the health-conscious model-based battery control problem, the work in this dissertation furnishes a nonlinear model-predictive control (NMPC) algorithm.The fact that NMPC involves re-optimizing the battery control trajectory every time step can be quite attractive in the presence of modeling uncertainties [65, 66]. For battery SOC estimation, the work in this dissertation furnishes a moving-horizon estimation (MHE) technique with a total least squares (TLS) estimation

objective. One particularly appealing feature of MHE is its ability to explicitly incorporate constraints on state estimates [67].

All of the above tools build on established concepts from the control literature, such as differential flatness, pseudo-spectral optimization, and model reformulation. This dissertation applies these tools in a unified framework for more efficient and better battery model-based control and estimation. Specifically, the dissertation makes 5 contributions to the literature:

1. Chapter 2 exploits the differential flatness of solid-phase lithium-ion battery diffusion dynamics, together with pseudo-spectral optimization and diffusion model reformulation, to decrease the computational load associated with health-conscious battery trajectory optimization significantly. This contribution forms a foundation for much of the subsequent work in this dissertation, but is limited to isothermal single-particle battery models with significant time scale separation between anode- and cathode-side solid-phase diffusion dynamics.

2. Chapter 3 extends the results of Chapter 2 in two ways. First , it exploits the law of conservation of charge to enable flatness-based, health-conscious battery trajectory optimization for single particle battery models even in the absence of time scale separation between the negative and positive electrodes. Second, it performs this optimization for a combined thermo-electrochemical battery model, thereby relaxing the above assumption of isothermal battery behavior and highlighting the benefits of flatness-based optimization for a nonlinear battery model.

3. Chapter 4 presents a framework for flatness-based pseudo-spectral combined state and parameter estimation in lumped-parameter nonlinear systems. This framework enables computationally-efficient total least squares (TLS) estimation for lumped-parameter nonlinear systems. This is quite relevant to practical lithium-ion battery systems, where both battery input and output measurements can be quite noisy.

4. Chapter 5 utilizes the above flatness-based TLS estimation algorithm for moving horizon state estimation using a coupled thermo-electrochemical equivalent circuit model of lithium-ion battery dynamics.

5. Chapter 6 extends the battery estimation framework from Chapter 5 to enable moving horizon, flatness-based TLS state estimation in thermo-electrochemical single-particle lithium-ion battery models, and demonstrates this framework using laboratory experiments.

The remainder of this dissertation highlights these above contributions in battery model-based control and estimation and Chapter 7 concludes the dissertation with a brief summary of the completed work.

Chapter 2
Flatness-Based Optimization of Lithium-Ion Battery Charging

2.1 Introduction

This chapter examines the problem of optimizing the charge trajectory of a lithium-ion battery cell to meet a desired target state of charge (SOC) while avoiding damaging side reactions such as lithium plating. The degradation side reaction emphasized in this chapter is lithium plating. Unlike the CCCV strategy with fixed voltage constraint, this chapter places physics-based constraints on the overpotential governing the lithium plating side reaction. This leads to optimized input protocols that can increase battery life and safety by protecting the battery from lithium plating. [1]

Traditional battery management systems typically avoid internal damage by constraining externally-measured variables such as battery voltage and current. When pushed to charge a battery as fast as possible without inducing excessive damage, these systems often follow the simple and well-known constant-current/constant-voltage (CCCV) charging strategy [9]. This is an excessively conservative approach. In fact, the literature shows that compared to this traditional approach, model-based control can prolong effective battery life by about 20-40% [11], improve battery safety [9, 68], increase battery energy-storing capacity [13], and decrease damage/degradation [69]. Moreover, model-based control has the ability to *adapt* to

[1] The work presented in this chapter is based on a peer-reviewed journal publication by the dissertation's author. The publication has already appeared in the ASME Journal of Dynamic Systems, Measurement and Control [58].

variations in battery health with time by charging new batteries more aggressively and old batteries more safely [9].

The above advantages of model-based battery management come at a price. Physics-based battery trajectory optimization problems can be computationally expensive for at least two reasons:

- First, battery trajectory optimization problems are typically nonlinear and nonconvex. In this chapter, for instance, the Butler-Volmer equation relating the rates of intercalation reactions to the overpotentials driving these reactions is nonconvex. Additional nonlinearity and nonconvexity are introduced by the relationship between solid-phase concentrations and reference potential in the positive electrode. Moreover, the side reaction overpotential governing lithium plating is a nonconvex function with respect to the solid-phase concentrations.

- Second, the dynamics of lithium-ion batteries are governed by coupled partial differential equations describing effects such as diffusion, migration, and intercalation. When these dynamic systems are discretized in space, the resulting models can be high-order, which furnishes optimization problems with large numbers of variables.

The literature presents at least four different families of algorithms for battery model-based charge/discharge trajectory optimization, grounded in (i) dynamic programming [25], (ii) genetic algorithms [26, 27], (iii) direct transcription [28, 29], and (iv) pseudospectral optimization [30]. All of these algorithms are valuable, in the sense that they contribute to a growing literature showing the potential benefits of model-based battery control. However, these algorithms also have limitations. The tools of dynamic programming and genetic algorithms are computationally expensive: a fact that limits their suitability to extensive optimization and control studies. Additionally, while pseudospectral methods are known for their computational advantages [61, 63], the use of pseudospectral methods and other direct transcription methods in the literature fails to exploit the additional computational benefits attainable because of the differential flatness of battery diffusion dynamics.

This chapter addresses these computational limitations and proposes a tractable framework for battery charge/discharge trajectory optimization by combining four key tools. First, the chapter exploits time scale separation to obtain a singularly perturbed single particle model (SPM) that neglects the electrode with

faster diffusion dynamics. Specifically, this model represents the faster electrode's dynamics using an integrator while retaining the dynamics of the slower electrode. This reduces the number of state variables required for the trajectory optimization by half.

Second, the chapter employs efficient orthogonal projection techniques to represent the dynamics of the slow battery electrode using only 3 state equations. The lithium ion concentration is expressed as a sum of Legendre spatial basis functions following [22]. Since the only unknown variables are the coefficients (which are functions of time) associated with the Legendre polynomials, the chapter reformulates the dynamics using 3 state variables in an efficient and accurate way. The specific choice of spatial basis functions for model reformulation does not limit the work presented in this chapter: other choices (e.g., Chebyshev polynomials) can also be used [60].

Third, the chapter exploits the differential flatness property of Fick's second law of diffusion to optimize a single scalar trajectory of a flat output variable that captures all of the battery's dynamics. The concept of differential flatness is introduced by Fliess *et al.* [52]. A dynamic system is differentially flat if there exists a flat output such that the states and the inputs can be directly expressed in terms of the flat output and a finite number of its derivatives. Fick's second law of diffusion is a special case of the generalized heat diffusion equation presented in [57], and is known to be differentially flat. One major benefit of adopting differential flatness in optimization is that only the flat output trajectory needs to be optimized and all the states and inputs can be expressed as functions of the flat output and a finite number of its derivatives. As a result, the number of continuous-time optimization variables is reduced to one: a fact that boosts computational efficiency significantly.

Finally, the chapter optimizes the above flat output trajectory using pseudospectral methods because such methods: (i) have high convergence rates and are computationally efficient, (ii) can solve nonlinear and nonconvex optimization problems [61, 62]. Originally developed for the numerical solutions of differential equations, pseudospectral methods have been recently adopted as efficient tools for solving optimal control problems [63, 64]. When solving battery trajectory optimization problems using traditional discretization methods, one can easily end up with hundreds or thousands of optimization variables. Pseudospectral methods,

in contrast, discretize problems using a set of unevenly distributed collocation points and are known to be very efficient [70]. These methods transform a continuous optimization problem into a nonlinear programming (NLP) problem which can be solved using well-developed NLP algorithms [61, 63].

All of the above tools build on established concepts from the control literature, but this chapter combines them into a single, unified framework for computationally efficient battery charge/discharge trajectory optimization. The end product is a toolset that makes it possible to solve nonconvex battery charge/discharge trajectory optimization in a manner that accounts for physics-based side reaction constraints and is 5 times more computationally efficient than pseudospectral optimization alone. In addition to this important computational benefit, this chapter exploits differential flatness for electrochemical battery trajectory optimization. Further work building on this chapter extends this research to online battery model predictive control, and is discussed in subsequent chapters [1].

The remainder of the chapter is structured as follows. Section 2.2 presents the assumptions and governing equations for the SPM. Section 2.3 formulates the optimization problem with a physics-based side reaction constraint. Section 2.4 briefly introduces differentially flat systems and demonstrates that battery diffusion dynamics are differentially flat. Section 2.5 briefly describes the Gauss pseudospectral method and the flatness-based Gauss pseudospectral method. In Section 2.6, the results and discussion are presented and compared to the standard charging strategy. We also demonstrate the efficiency of the proposed framework. Finally, the chapter is concluded in Section 2.7.

2.2 Single Particle Model

It is necessary for model-based control to adopt battery models which can represent the dynamics of lithium-ion batteries with enough accuracy and computational efficiency. The dynamics of a lithium-ion battery can be described by several models with different assumptions and fidelities. Commonly used models include equivalent circuit models (ECM), the SPM model, extended SPM model, and the Doyle-Fuller-Newman (DFN) model [1,14–16]. This chapter utilizes the SPM model to achieve different levels of tradeoff between accuracy and computational efficiency.

In this section, the assumptions and governing equations of the SPM model

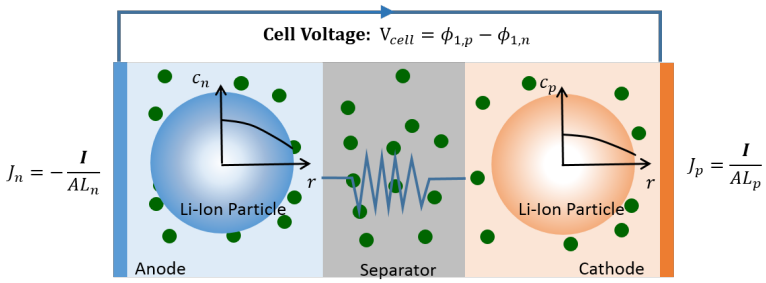

Figure 2.1: Single particle model (SPM)

are briefly described. Then model order reduction techniques are introduced to transform the partial differential equations into ordinary differential equations. Model parameters are obtained from [3] for a commercial A123 $LiFePO_4$ (LFP) 26650 2.3Ah cell and the reference potential curve for each electrode is obtained from [2].

The SPM assumes that [6, 71]:

1. Electrolytic diffusion is sufficiently fast, and the electrolyte is sufficiently concentrated, such that electrolyte concentration c_e can be treated as constant throughout the spatial and temporal domains;

2. Ohmic effects in both the solid and electrolyte phases can be represented by a single lumped resistance;

3. The spatial distribution of charge across the thickness of each electrode is almost uniform, such that representing each electrode by an “averaged" single particle is justified.

2.2.1 Governing Equations

The governing equations for the SPM are presented as follows. Solid phase diffusion dynamics are central to a SPM, and are represented by Fick’s second law of diffusion. The governing differential equation is

$$\frac{\partial c_{s,j}(r,t)}{\partial t} = \frac{D_{s,j}}{r^2}\frac{\partial}{\partial r}\left(r^2\frac{\partial c_{s,j}(r,t)}{\partial r}\right) \tag{2.1}$$

where $c_{s,j}$ is the lithium-ion concentration in the solid particles, $D_{s,j}(T)$ is the solid phase diffusion coefficient, r is the radial coordinate, $j = p$ corresponds to the

positive electrode, and $j = n$ corresponds to the negative electrode.

The boundary conditions at the particle center ($r = 0$) and particle surface ($r = R_j$) are

$$\left.\frac{\partial c_j(r,t)}{\partial r}\right|_{r=0} = 0 \tag{2.2}$$

$$\left.\frac{\partial c_j(r,t)}{\partial r}\right|_{r=R_j} = -\frac{J_j(t)}{FD_{s,j}a_j} \tag{2.3}$$

where F is Faraday's number and a_j is the specific interfacial area defined as

$$a_j = \frac{3\varepsilon_j}{R_j} \tag{2.4}$$

The term R_j is the particle radius and ε_j is active material volume fraction.

The molar flux of lithium ions J_i is defined as

$$\begin{aligned} J_n(t) &= -\frac{I(t)}{S_n L_n} \text{ for negative electrode} \\ J_p(t) &= \frac{I(t)}{S_p L_p} \text{ for positive electrode} \end{aligned} \tag{2.5}$$

where I is the input current, defined as positive for charging, S_j is the sheet area of electrode j, and L_n and L_p are the thickness of the negative and positive electrode, respectively.

The bulk state of charge (SOC) is defined as

$$SOC_j(t) = \frac{c_{s,j,avg}(t)}{c_{s,j,max}} \tag{2.6}$$

where $c_{s,j,avg}(t)$ is the average lithium-ion concentration of the electrode, i.e.,

$$c_{s,j,avg}(t) = \int_0^{R_j} c_{s,j} dr \tag{2.7}$$

and $c_{s,j,max}$ is the maximum concentration of lithium-ions of electrode.

The surface SOC is defined as

$$SOC_j^{surf}(t) = \frac{c_{s,j}^{surf}(t)}{c_{s,j,max}} \tag{2.8}$$

where $c_{s,j}^{surf}(t) = c_{s,j}(R_j, t)$ is the surface lithium-ion concentration of electrode.

Battery SOC, SOC_{cell}, is related to the electrode bulk SOC, SOC_j, using the stoichiometry relationship shown below:

$$SOC_{cell} = \frac{SOC_n(t) - \theta_{n,0}}{\theta_{n,100} - \theta_{n,0}} \tag{2.9}$$

$$SOC_{cell} = \frac{\theta_{p,100} - SOC_p(t)}{\theta_{p,100} - \theta_{p,0}} \tag{2.10}$$

where the stoichiometry values $\theta_{n,0}$, y_0, $\theta_{n,0}$, and $\theta_{p,100}$ are defined as follow

$$\theta_{n,0} = \frac{c_{s,n,avg,0\%}(t)}{c_{s,n,max}}, \quad \theta_{n,100} = \frac{c_{s,n,avg,100\%}(t)}{c_{s,n,max}} \tag{2.11}$$

$$\theta_{p,0} = \frac{c_{s,p,avg,0\%}(t)}{c_{s,p,max}}, \quad \theta_{p,100} = \frac{c_{s,p,avg,100\%}(t)}{c_{s,p,max}} \tag{2.12}$$

where $c_{s,j,avg,0\%}(t)$ is the minimum concentration of electrode j and $c_{s,j,avg,100\%}(t)$ is the maximum concentration of electrode j. For instance, when the battery is empty, the negative electrode concentration is $c_{s,n,avg,0\%}$ and positive electrode concentration is $c_{s,p,avg,100\%}$. The stoichiometry value is the ratio of bulk concentration in each electrode to the max concentration.

The Butler-Volmer equation describes the relationship between the molar flux of lithium ions and the potential difference between the solid and solution phases at the reaction boundary and can be expressed as

$$J_j(t) = i_{0,j}(t) \left[\exp\left(\frac{\alpha_a F}{RT} \eta_j(t) \right) - \exp\left(-\frac{\alpha_c F}{RT} \eta_j(t) \right) \right] \tag{2.13}$$

where α_a is the negative electrode transfer coefficient, α_c is the positive electrode transfer coefficient, R is the ideal gas constant, T is the cell temperature, and η is the overpotential. The exchange current density i_0 is defined as

$$i_{0,j}(t) = a_j k_j (c_{s,j,\max} - c_{s,j}^{surf})^{\alpha_a} (c_{s,j}^{surf}(t))^{\alpha_c} c_e^{\alpha_a} \tag{2.14}$$

where k_j is the reaction rate constant and c_e is the lithium-ion concentration in solution.

The overpotential η_j is defined as the difference between the solid and solution

potential minus the open-circuit potential (OCP) of electrode

$$\eta_j(t) = \phi_{1,j}(t) - \phi_{2,j}(t) - U_j(SOC_j^{surf}(t)) \tag{2.15}$$

where $\phi_{1,j}$ is the solid phase potential, and $\phi_{2,j}$ is the solution phase potential. The term U_j is the OCP as a function of surface SOC.

The potential drop in the solution phase between two electrodes is

$$\phi_{2,p}(t) - \phi_{2,n}(t) = I(t)R_{cell} \tag{2.16}$$

where $R_{cell}(T)$ is a lumped parameter.

The cell voltage is defined as the potential difference between positive and negative electrode

$$V_{cell}(t) = \phi_{1,p}(t) - \phi_{1,n}(t) \tag{2.17}$$

This chapter adopts a physics-based side reaction constraint from [9] for health-conscious optimal charging. This side reaction represents lithium plating and can be expressed as

$$\begin{aligned} \eta_{sr}(t) &= \phi_{1,n}(t) - \phi_{2,n}(t) - U_{sr}(SOC_n^{surf}(t)) \geq 0 \\ &= \eta_n(t) + U_n(SOC_n^{surf}(t)) - U_{sr}(SOC_n^{surf}(t)) \geq 0 \end{aligned} \tag{2.18}$$

where η_{sr} is the side reaction overpotential and U_{sr} denotes the equilibrium potential of the side reaction and is zero due to the deposit of metallic lithium for lithium-ion batteries [9, 10].

2.2.2 Model Order Reduction

For efficient optimization we first employ time-scale separation for the SPM. For the model parameters used in this study, the dynamics of the positive electrode are much (about 100 times) faster than the negative electrode, as seen by comparing the eigenvalues of the dynamics of the two electrodes. This makes it possible to retain the electrode with slower dynamics while modeling the electrode with faster diffusion dynamics as a pure integrator. To achieve this, we consider the differential equation (2.1) and its boundary conditions (2.2)-(2.3) only for the negative electrode. The lithium-ion concentration of the positive electrode is

recovered using the law of conservation of lithium-ions. The concentration of lithium ions in the positive electrode is, therefore, described only by the bulk SOC. The fact that bulk SOC is computed for both electrodes means that the pure integration dynamics associated with bulk SOC occur twice in a SPM. Elimination of this redundancy in state variables furnishes a minimal realization of battery dynamics where only the dynamics of the slower electrode are modeled, and bulk SOC for the faster electrode is an algebraic function of the slower electrode's bulk SOC. This reduces the total number of state variables by half.

Fick's law of diffusion (2.1) is a partial differential equation, and needs to be discretized into a set of ordinary differential equations before a SPM can be used for control studies. This discretization process is often referred to as "model reformulation" in the electrochemistry literature [60]. We achieve this reformulation by projecting Fick's law onto Legendre spatial basis functions using a Galerkin method, as presented in [22]. The reformulated SPM represents diffusion dynamics using only 3 state variables. The above process is briefly shown below and more details on how to implement Legendre polynomials and orthogonal projection can be found in [22].

The lithium-ion concentration in the negative electrode $c_n(r,t)$ can be approximated by a linear combination of Legendre polynomials, which separates the temporal and spatial dynamics as

$$c_n(r,t) \approx \sum_{i=0}^{N_L} P_i(r)\beta_{i,j}(t) \tag{2.19}$$

where $P_i(r)$ with even subscripts $i = 0, 2 \ldots, N_L$ are Legendre polynomials, and $\beta_{i,j}$ is the unknown coefficient for the negative electrode n. Because of the boundary condition (2.2), we can only adopt the symmetric Legendre polynomials, i.e., $i = 0, 2 \ldots, N_L$.

The Legendre polynomials are then normalized such that

$$\int_0^{R_n} P_i(r)P_k(r)dr = \begin{cases} 0 & \text{if } i \neq k \\ 1 & \text{if } i = k \end{cases} \tag{2.20}$$

where R_n is the radius of the particles in the negative electrode.

Substituting Eq. (2.19) into Eq. (2.1) gives

$$\sum_{i=0}^{N_L} P_i(r)\dot{\beta}_{i,j}(t) = D_{s,n}\left[\frac{2}{r}\sum_{i=0}^{N_L}\frac{dP_i(r)}{dr}\beta_{i,j}(t) + \sum_{i=0}^{N_L}\frac{d^2P_i(r)}{dr^2}\beta_{i,j}(t)\right] \tag{2.21}$$

where $\dot{\beta}_{i,j}(t)$ is the derivative with respect to time. Then we use the orthogonal projection techniques by pre-multiplying both sides of (2.21) by $\left[P_0, P_2, \ldots, P_{N_L}\right]^T$ and then integrating both sides in space from 0 to R_n. This furnishes the dynamics of the coefficients $\left[\beta_{0,j}, \beta_{2,j}, \ldots, \beta_{N_L,j}\right]^T$.

In this chapter, we employ 4 symmetric Legendre polynomials, as suggested in [72], to represent the negative concentration, i.e., $N_L = 6$. In [72], the Legendre-based projection method is used to discretize the PDE diffusion dynamics. It shows that in the radial dimension one can approximate diffusion dynamics relatively accurately with only 4 polynomials. There is little improvement in accuracy with more polynomials than 4. Therefore, in this chapter, four polynomials are chosen.

The diffusion dynamics Eq. (2.1) can then be expressed as the following

$$\begin{bmatrix}\dot{\beta}_{0,n}\\ \dot{\beta}_{2,n}\\ \dot{\beta}_{4,n}\\ \dot{\beta}_{6,n}\end{bmatrix} = \frac{D_{s,n}}{R_n^2}\begin{bmatrix}0, & 9\sqrt{5}, & 20, & 29.4\sqrt{13}\\ 0, & 0, & 35\sqrt{5}, & 16.8\sqrt{65}\\ 0, & 0, & 0, & 46.2\sqrt{13}\\ 0, & 0, & 0, & 0\end{bmatrix}\begin{bmatrix}\beta_{0,n}\\ \beta_{2,n}\\ \beta_{4,n}\\ \beta_{6,n}\end{bmatrix} \tag{2.22}$$

Similarly, the boundary condition in Eq. (2.3) can be expressed as

$$\frac{3}{R_n}\sqrt{\frac{5}{2R_n}}\beta_{2,n} + \frac{10}{R_n}\sqrt{\frac{9}{2R_n}}\beta_{4,n} + \frac{21}{R_n}\sqrt{\frac{13}{2R_n}}\beta_{6,n} = -\frac{J_n(t)}{D_{s,n}a_n} \tag{2.23}$$

From Eq.(2.22), it can be seen that the term β_6 does not have dynamics and can be expressed as a function of $\beta_{0,n}, \beta_{2,n}, \beta_{4,n}$ using the Eq. (2.23). Since current I is chosen to be the input of the battery in this chapter, one needs to substitute Eq. (2.5) into Eq. (2.23). Then based on (2.22) and (2.23), we can derive the state space model describing the dynamics of the negative electrode as

$$\dot{x}_n = A_n x_n + B_n u \tag{2.24}$$

where the state vector is defined as $x_n = [\beta_{0,n}, \beta_{2,n}, \beta_{4,n}]^T$, and the input u is the

current I. Different outputs can be computed algebraically from these state and input variables, including the expansion coefficient $\beta_{6,n}$ and the electrode surface concentration $c_n(R,t)$. Computing the surface concentration is important because the main and side reaction reference potentials are defined with respect to it.

Note that the diffusion model (2.24) only represents the negative electrode (the one with slower dynamics). The SPM using time-scale separation relates the positive electrode (representee using an integrator) to the negative electrode via the fact that the current going through both electrodes is the same. Specifically, we assert that because of conservation of charge, there is an affine relationship between the bulk ion concentrations in the negative and positive electrodes. This furnishes a dynamic model for the whole battery.

2.3 Problem Formulation

While the chapter proposes an efficient framework for general battery trajectory optimization, the optimal charging problem is used to for demonstration purposes. To charge a battery in a health-conscious manner, the optimization problem is constrained by a side reaction constraint governing the rate of degradation via

lithium-ion plating

$$
\begin{aligned}
&\min_{u(t)} \; J = \int_{t_0}^{t_f} \left(SOC_{cell}(t) - SOC_{ref}\right)^2 dt \\
&\quad \text{s.t:} \\
&\qquad \dot{x}_n(t) = A_n x_n(t) + B_n u(t) \\
&\qquad SOC_{cell} = \frac{SOC_n(t) - \theta_{n,0}}{\theta_{n,100} - \theta_{n,0}} \\
&\qquad SOC_n(t) = \frac{c_{s,n,avg}(t)}{c_{s,n,max}} \\
&\qquad SOC_n^{surf}(t) = \frac{c_{s,n}^{surf}(t)}{c_{s,n,max}} \\
&\qquad c_{s,n,avg}(t) = \int_0^{R_n} c_{s,n} dr \\
&\qquad c_n(r,t) \approx \sum_{i=0}^{M} \beta_{n,i}(t) P_i(r) \\
&\qquad J_n(t) = i_{0,n}(t) \left[\exp\left(\frac{\alpha_a F}{RT}\eta_n(t)\right) - \exp\left(-\frac{\alpha_c F}{RT}\eta_n(t)\right)\right] \\
&\qquad \eta_{sr}(t) = \eta_n + U_n(SOC_n^{surf}(t)) \geq 0 \\
&\qquad 0 \leq I(t) \leq I_{\max} \\
&\qquad SOC_{cell}(t_0) = SOC_{ini}
\end{aligned}
\tag{2.25}
$$

where η_{sr} is side reaction overpotential, $I_{\max}$ is the maximum allowed current, SOC_{ref} is the reference SOC level, and SOC_{ini} is the known initial SOC.

The goal of this problem is to charge the cell to a desired SOC, SOC_{ref}, while avoiding internal charge concentrations and overpotentials conducive to damaging side reactions such as lithium plating. While there is no explicit constraint on SOC, the fact that lithium plating is more likely to occur at higher SOCs [73] means that the above formulation provides implicit protection against overcharging. We adopt the physics-based constraint Eq. (2.18) governing the reaction rate of lithium plating which is essentially is a function of the state variables. This side reaction constraint is very valuable compared to the standard CCCV charging strategy which uses only voltage and current limits. Chaturvedi *et al.* show that with this side reaction constraint, one can charge cells in a more robust manner in the sense that one can charge new cells more aggressively and aged cells more

safely compared to the CCCV strategy [10].

It is challenging to solve problem (2.25) efficiently for at least two reasons. First, the underlying dynamic model can make the optimization problem (2.25) computationally expensive. Electrochemistry-based battery models need to be discretized or reformulated for control purposes. Traditional discretization methods, such as the finite difference method, furnish very large state-space representations of battery dynamics to achieve reasonable levels of accuracy. The model reformulation approach used here is more computationally efficient. However, even after employing model reformulation techniques from Section 2.2 there are still 3 state variables. This can lead to hundreds of optimization variables using traditional nonlinear optimization techniques (e.g., input parameterization method), since these methods need to discretize each optimization variable in the time domain, which will produce high-dimensional optimization problems. Second, problem (2.25) is nonconvex due to its nonconvex constraint set. The side reaction overpotential η_{sr} is a nonconvex function with respect to the negative SOC. This makes the problem difficult to solve.

To address these challenges, this chapter adopts 2 more tools besides time-scale separation and orthogonal projection-based model reformulation. First, we further reformulate the SPM from the previous section by exploiting the differential flatness property, thereby expressing all of the battery's dynamics in terms of a single scalar trajectory of the flat output. Second, we use the Gauss pseudospectral method (GPM) to optimize the trajectory of the flat output. The resulting nonlinear programming problem remains nonconvex. We address this challenge numerically using a multi-start NLP algorithm, but other approaches are possible, including evolutionary optimization techniques.

2.4 Differentially Flat Systems

We begin this section by providing an "intuitive" discussion of differential flatness, then proceed to a formal mathematical definition of the differential flatness.

2.4.1 Introduction to Differential Flatness

To understand the concept of differential flatness, consider Fick's law of diffusion over a spherical medium. If charge concentration as a function of time, t, and radius, r, is $c_j(t, r)$, and if the diffusion medium has a constant diffusivity, then Fick's law translates to the PDE shown in Eq. (2.1). The PDE, in and of itself, is not necessarily differentially flat. Differential flatness relates to both the governing differential equations for a given dynamic system and the boundary conditions acting on this system. In applying Fick's law of diffusion to a spherical medium, one must set the spatial gradient of concentration at the center of the given sphere to zero to satisfy Eq. (2.2). This ensures that no diffusion takes place into or out of the zero-volume center point of the sphere. Moreover, the concentration gradient at the sphere's surface is related to an input forcing term (i.e., an intercalation rate) through a Neumann boundary condition.

Given Fick's law of diffusion and its boundary conditions, suppose that the concentration of charge at the center of the sphere , $c_j(0, t)$, is known completely as a function of time. In other words, the function, $c_j(0, t)$ together with all of its time derivatives is known. What additional information can be derived from this knowledge? For example, can charge concentration at some infinitesimal radius δ_r, be computed from the above information?

To answer this question, one can express the concentration at δ_r using the Taylor series expansion at the center $r = 0$

$$c_j(\delta_r, t) = c_j(0, t) + \frac{\partial c_j(0, t)}{\partial r}\delta_r + \frac{1}{2}\frac{\partial^2 c_j(0, t)}{\partial r^2}\delta_r^2 + H.O.T \tag{2.26}$$

where the term $H.O.T$ stands for higher-order terms which can be neglected for a sufficiently small δ_r. Moreover, the first-order term in the above expansion is zero by virtue of the center point boundary condition on concentration gradient in Eq. (2.2). Thus,

$$c_j(\delta_r, t) \approx c_j(0, t) + \frac{1}{2}\frac{\partial^2 c_j(0, t)}{\partial r^2}\delta_r^2 \tag{2.27}$$

where the approximation becomes more and more accurate as $\delta_r \to 0$. Additionally, applying Fick's law of diffusion in Eq. (2.1) to the center concentration gives

$$\frac{\partial c_j(0, t)}{\partial t} = D_{s,j}\frac{\partial^2 c_j(0, t)}{\partial r^2} \tag{2.28}$$

Substituting Eq. (2.28) into Eq. (2.27) gives

$$c_j(t, \delta_r) \approx c_j(t, 0) + \frac{1}{2D_{s,j}} \frac{\partial c_j(0, t)}{\partial t} \delta_r^2 \tag{2.29}$$

Equation (2.29) is interesting, because it shows that knowledge of charge concentration at the center of the spherical diffusion medium as a function of time is enough for predicting charge concentration in the "neighborhood" of that center point as a function of time. In fact, further mathematical analysis (omitted here for brevity) shows that *knowledge of the charge concentration at the center of the spherical diffusion medium as a function of time is sufficient for predicting charge concentration everywhere in the diffusion medium as a function of time.* Moreover, this knowledge is also sufficient for predicting the boundary input to the diffusion process and thus the input current using Eq. (2.3) and Eq. (2.5).

The above mathematical property is called *differential flatness*, and is central to this chapter. Differential flatness is a attractive mathematical property because it makes it possible to optimize the entire time history of all solid-phase concentrations in the SPM by optimizing only the center point concentration as a function of time. This is true for diffusion processes governed by both linear and nonlinear versions of Fick's law of diffusion. In fact, the literature shows that Fick's law, as a special case of the heat equation, is differentially flat even in the nonlinear case where the diffusion coefficient, $D_{s,j}$, is concentration-dependent [58].

2.4.2 Definition: Differentially Flat Systems

Mathematically, a system is *differentially flat* if there exists a fictitious variable, the *flat output* z, such that

1. the state x and input u can be expressed in terms of the trajectory of the flat output z and a finite number of its derivatives

$$x = f_x(z, \dot{z}, \ldots, z^{(\alpha)}) \tag{2.30a}$$

$$u = f_u(z, \dot{z}, \ldots, z^{(\beta)}) \tag{2.30b}$$

2. the flat output z can be expressed in terms of state x, input u, and a finite

number of the input's derivatives

$$z = f_z(x, u, \dot{u}, \cdots, u^{(\gamma)}) \tag{2.31}$$

where α, β, γ are integers which vary for different systems and $z^{(r)}$ is the r^{th} derivative with respect to time [52, 74]. The dimension of the flat output vector z is the same as the number of the inputs to the system [52].

2.4.3 Application to Batteries

Lithium-ion battery diffusion dynamics can be shown to be differentially flat by comparing battery dynamics with the flat linear diffusion equation representing heat dynamics shown in [57]. Laroche *et al.* proved the following one-dimension linear diffusion equation is differentially flat [57]

$$\frac{\partial \theta(x,t)}{\partial t} = f_1(x)\frac{\partial^2 \theta(x,t)}{\partial x^2} + g_1(x)\frac{\partial \theta(x,t)}{\partial x} + h_1(x)\theta(x,t) \tag{2.32}$$

where $x \in [0, 1]$, $f_1(\theta) > 0$, g_1 and h_1 are analytic functions. The boundary conditions are

$$\left.\frac{\partial \theta(x,t)}{x}\right|_{x=0} = 0 \tag{2.33}$$

$$\left.\theta(x,t)\right|_{x=1} = u(t) \tag{2.34}$$

where u is the control input, θ is the temperature along x coordinate and t is the time.

Battery diffusion dynamics are governed by Fick's second law of diffusion (2.1). It can be expressed in a more general form as below

$$\frac{\partial c_{s,j}(r,t)}{\partial t} = f(r)\frac{\partial^2 c_{s,j}(r,t)}{\partial r^2} + g(r)\frac{\partial c_{s,j}(r,t)}{\partial r}, \quad r \in [0, R_j] \tag{2.35}$$

where $c_{s,j}$ is the lithium-ion concentration, r is the radial coordinate, and $f(r) > 0$. The boundary conditions at particle center ($r = 0$) and particle surface ($r = R_j$) are

$$\left.\frac{\partial c_{s,j}(r,t)}{\partial r}\right|_{r=0} = 0$$
$$\left.\frac{\partial c_{s,j}(r,t)}{\partial r}\right|_{r=R_j} = au(t) \tag{2.36}$$

where a is a constant.

Comparing with Eq. (2.32) and its boundary condition Eq. (2.33), it is apparent that Eq. (2.35) is a special case of Eq. (2.32) and therefore the battery diffusion dynamics in each electrode are flat.

Differential flatness can be seen as an extension of the concept of controllability to nonlinear systems. In fact, for linear systems, a system is differentially flat if and only if it is controllable [52]. The diffusion dynamics in each electrode of battery are controllable and hence differentially flat. As a result, only one flat output trajectory (rather than all state and input variables) is required to represent the system dynamics in each electrode. The state and inputs can then be recovered using the flat output trajectory.

The flat output for the single electrode SPM is found by transforming the reformulated diffusion sub-model for each electrode into the controllable canonical form. According to the definition of differential flatness shown in Eq. (2.30) and Eq. (2.31), one needs one flat output $z \in \mathbb{R}^1$ to represent the dynamics of single electrode SPM. Suppose the state vector $x = [\beta_{0,j}, \beta_{2,j}, \beta_{4,j}]^T$ corresponds to diffusion dynamics of slower electrode (i.e., negative electrode in this dissertation). One can transform the original state space representation Eq. (2.24) into the controllable canonical form

$$\dot{\bar{x}}_n(t) = \begin{bmatrix} 0 & 1 & 0 \\ 0 & 0 & 1 \\ -\alpha_{1,n} & -\alpha_{2,n} & -\alpha_{3,n} \end{bmatrix} \bar{x}_n(t) + \begin{bmatrix} 0 \\ 0 \\ 1 \end{bmatrix} u(t) \tag{2.37}$$

where $\alpha_{i,n}$ are the coefficients of characteristic equation of the state matrix A_n in Eq. (2.24) and $\bar{x}_n$ is transformed state vector for the electrode, defined as

$$x_(t) = M_n \bar{x}_n(t) \tag{2.38}$$

The matrix M_n is the similarity transformation matrix required to obtain a con-

trollable canonical state representation [75]. Given this state representation, one can define the following flat output:

$$z(t) = \bar{x}_1(t) \tag{2.39}$$

The remaining state variables can then be expressed using the flat output and a finite number of its derivatives

$$x(t) = f_x(z(t), \dot{z}(t), \ddot{z}(t)) = M \left(\begin{bmatrix} 1 & 0 & 0 \\ 0 & 1 & 0 \\ 0 & 0 & 1 \end{bmatrix} \begin{bmatrix} z(t) \\ \dot{z}(t) \\ \ddot{z}(t) \end{bmatrix} \right) \tag{2.40}$$

where the product in parentheses is the transformed state $\bar{x}_j$. The terms $\dot{z}$, $\ddot{z}$, and $\dddot{z}$ represent the first, second, and third derivatives of the flat output with respect to time. The input can be expressed similarly as well

$$\begin{aligned} u(t) &= f_u(z(t), \dot{z}(t), \ddot{z}(t), \dddot{z}(t)) \\ &= [-\alpha_1, -\alpha_2, -\alpha_3, 1] \begin{bmatrix} z(t) \\ \dot{z}(t) \\ \ddot{z}(t) \\ \dddot{z}(t) \end{bmatrix} \end{aligned} \tag{2.41}$$

The above equations demonstrate how one can use differential flatness property to represent diffusion dynamics of each electrode using one flat output.

2.5 Flatness-Based Pseudospectral Methods

Pseudospectral methods are a class of direct methods which transform the original problem into a nonlinear programming (NLP) problem that can be solved using well-developed NLP algorithms. The Gauss pseudospectral method (GPM) is adopted in this chapter. The collocation points τ_i in the GPM are the Legendre-Gauss (LG) points which are the roots of N^{th} degree Legendre polynomials $P_N(\tau_i)$ and are located in the interior of the range $[-1, 1]$, i.e., $\tau_i \in (-1, 1)$ [61]. The discretization points are collocation points plus the boundaries, i.e., $\tau_0 = -1$ and $\tau_{N+1} = 1$. The

remainder of this section describes how to use the GPM to optimize the flat output trajectory for differentially flat systems.

First, the time $t \in [t_0, t_f]$ needs to be mapped into τ domain to use collocation points

$$t = \frac{(t_f - t_0)\tau + (t_f + t_0)}{2} \tag{2.42}$$

The GPM approximates the trajectories of flat output as a linear combination of $N+1$ Lagrange polynomials at N collocation points and the initial point $\tau_0 = -1$. The flat output z_j (the subscript represents the electrode j) is approximated

$$z_j(\tau) \approx \mathbf{z}_j(\tau) = \sum_{k=0}^{N} L_k(\tau) z_j(\tau_k) \tag{2.43}$$

where $\mathbf{z}_j(\tau)$ is the approximated trajectory of the flat output in the electrode j and $L_k(\tau)$ is the Lagrange polynomial bases. The property of Lagrange polynomials leads to

$$\mathbf{z}_j(\tau_k) = z_j(\tau_k) \tag{2.44}$$

as stated in [1].

One benefit of using pseudospectral methods is that one can express the derivatives of variables analytically by differentiating Eq. (2.43). The first derivative of the flat output evaluated at collocation points gives

$$\mathbf{z}_j^{(l)}(\tau_i) = \sum_{k=0}^{N} L_k^{(l)}(\tau_i) \mathbf{z}_j(\tau_k) \tag{2.45}$$

where the term $L_k^l(\tau_i)$ represents the l-th derivative of Lagrange polynomials evaluated at time τ_i and can be expressed using the differentiation matrix $D_l(i,k) = L_k^{(l)}(\tau_i)$.

Therefore, the l-th derivative of the flat output in Eq. (2.45) can be expressed using a more compact way

$$Z_j^{(l)} = D_l Z_j \tag{2.46}$$

where $Z_j := [\mathbf{z}_j(\tau_0), \mathbf{z}_j(\tau_1), \cdots, \mathbf{z}_j(\tau_N)]^T$ and $Z_j^{(l)}$ is a vector of the l-th derivative of $\mathbf{z}_j(\tau_i)$. Therefore, the following equations holds $\bar{X}_{j,1} = Z_j$, $\bar{X}_{j,2} = D_1 Z_j$, and $\bar{X}_{j,3} = D_2 Z_j$, where $\bar{X}_{j,k} := [\bar{\mathbf{x}}_{j,k}(\tau_1), \bar{\mathbf{x}}_{j,k}(\tau_2), \cdots, \bar{\mathbf{x}}_{j,k}(\tau_N)]^T$, where the $\bar{x}_{j,k}$ is the k^{th} transformed state defined in (3.23).

As a result, the trajectory of the state x_j evaluated at collocation points can be expressed using the flat output trajectory with Eq. (2.40). Equation (2.41) provides the mapping from z_j to u

$$\begin{aligned} U &= [u(\tau_0), u(\tau_1), \cdots, u(\tau_N)]^T \\ &= -\alpha_{j,1} I_N Z_j - \alpha_{j,2} D_1 Z_j - \alpha_{j,2} D_2 Z_j - \alpha_{j,3} D_3 Z_j \end{aligned} \tag{2.47}$$

where I_N is an identity matrix.

Moreover, pseudospectral methods integrate the cost function J using the LG quadrature rule

$$\begin{aligned} J &= \int_{t_0}^{t_f} \left(SOC_n(\tau) - SOC_{ref}\right)^2 d\tau \\ &\approx \frac{t_f - t_0}{2} \sum_{i=1}^{N} w_i \left(SOC_n(\tau_i) - SOC_{ref}\right)^2 \end{aligned} \tag{2.48}$$

The Gauss weights w_i are determined by

$$w_i = \frac{2}{1 - \tau_i^2} \left[\dot{P}_N(\tau_i)\right]^2 \tag{2.49}$$

The term $\dot{P}_N(\tau_i)$ is the first derivative of the N^{th} degree of Legendre polynomials $P_N(\tau_i)$ evaluated at collocation point τ_i.

The resulting optimization problem with the application of differential flatness

is shown as follows

$$
\begin{aligned}
&\min_{Z_n} J = \frac{t_f - t_0}{2} \sum_{i=1}^{N} \omega_i \left(SOC_{cell}(\tau_i) - SOC_{ref} \right)^2 \\
&\quad \text{s.t:} \\
&\qquad x_n = f_x(z(\tau_i), \dot{z}(\tau_i), \ldots, z^{(\alpha)}(\tau_i)) \\
&\qquad u_n = f_{u_n}(z(\tau_i), \dot{z}(\tau_i), \ldots, z^{(\beta)}(\tau_i)) \\
&\qquad z = f_z(x(\tau_i), u(\tau_i), \dot{u}(\tau_i), \cdots, u^{(\gamma)}(\tau_i)) \\
&\qquad SOC_{cell} = \frac{SOC_n(\tau_i) - \theta_{n,0}}{\theta_{n,100} - \theta_{n,0}} \\
&\qquad SOC_n(\tau_i) = \frac{c_{s,n,avg}(\tau_i)}{c_{s,n,max}} \\
&\qquad SOC_n^{surf}(\tau_i) = \frac{c_{s,n}^{surf}(\tau_i)}{c_{s,n,max}} \\
&\qquad c_{s,n,avg}(\tau_i) = \int_0^{R_n} c_{s,n} dr \\
&\qquad c_n(r, \tau_i) \approx \sum_{i=0}^{M} \beta_{n,i}(\tau_i) P_{n,i}(r) \\
&\qquad J_n(\tau_i) = i_{0,n}(\tau_i) \left[\exp\left(\frac{\alpha_a F}{RT} \eta_n(\tau_i) \right) - \exp\left(-\frac{\alpha_c F}{RT} \eta_j n(\tau_i) \right) \right] \\
&\qquad \eta_{sr}(\tau_i) = \eta_n + U_n(SOC_n^{surf}(t)) \geq 0 \\
&\qquad 0 \leq u(\tau_i) \leq u_{\max} \\
&\qquad \eta_{sr}(\tau_i) \geq 0 \\
&\qquad SOC_{cell}(\tau_0) = SOC_{ini} \\
&\qquad \text{where } i = 1, 2, \cdots, N
\end{aligned}
\tag{2.50}
$$

where the optimization variable is $Z_n \in \mathbb{R}^N$.

This problem formulation explicitly optimizes the trajectories of z_n, subject to model dynamics and inequality constraints. The term N is the number of collocation points in the prediction horizon. Additionally, unlike the formulation in problem (2.25), there is no explicit model dynamic constraint Eq. (2.24). This is because model dynamics are automatically satisfied by exploiting the flatness property using Eq. (2.40) and Eq. (2.41). The resulting NLP is then solved with well-developed algorithms.

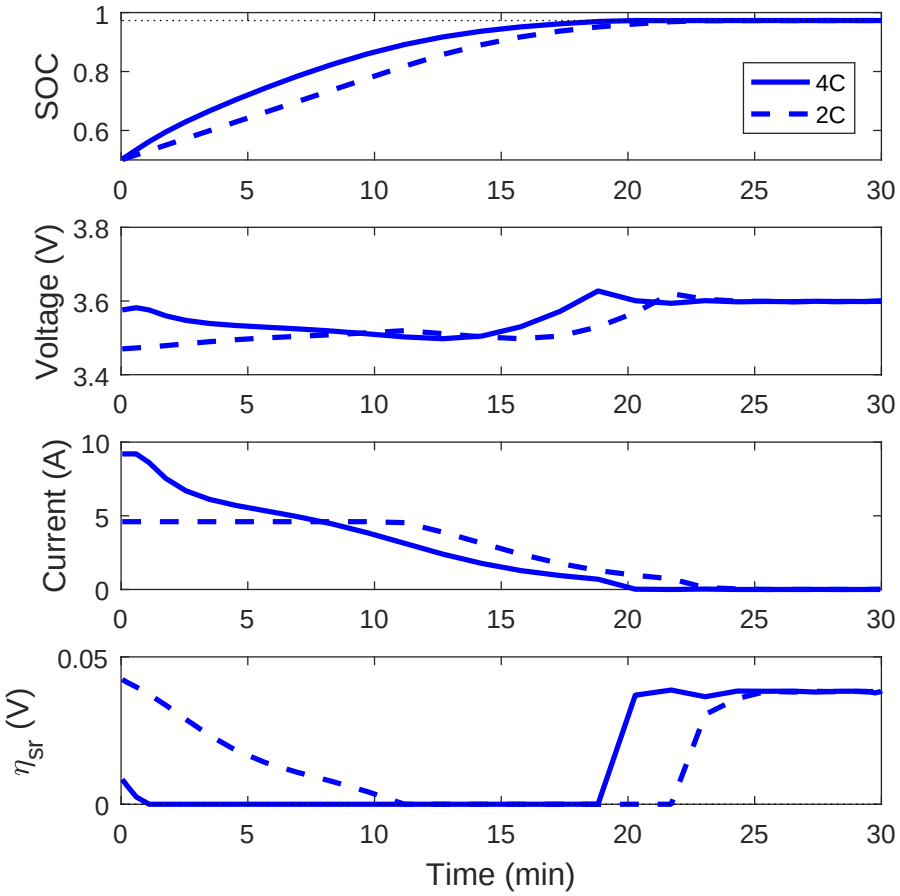

Figure 2.2: Simulation results for problem (2.25) applying the flatness-based GPM with $SOC_{ini} = 0.5$ for two current upper limits: $I_{\max} = 9.2A$ (4C) and $I_{\max} = 4.6A$ (2C)

2.6 Results and Discussion

This section presents simulation results for problem (2.25). To show the advantages of model-based control we formulate and solve a standard charging problem, whose results are compared with the ones of problem (2.25). In addition, we demonstrate the efficiency of the proposed flatness-based GPM by solving problem (2.25) using the GPM alone. All optimization problems are solved using the Fmincon function in Matlab.

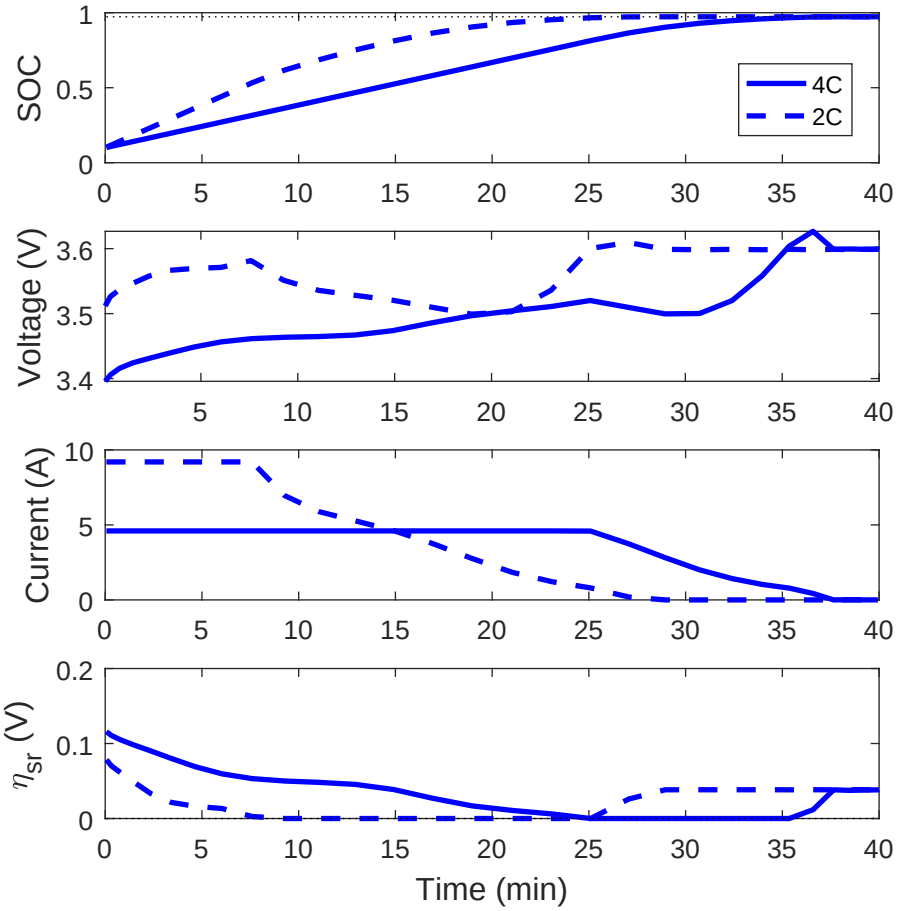

Figure 2.3: Simulation results for problem (2.25) applying the flatness-based GPM with $SOC_{ini} = 0.1$ for two current upper limits: $I_{\max} = 9.2A$ (4C) and $I_{\max} = 4.6A$ (2C)

2.6.1 Optimal Charging Strategy

For the problem (2.25), the reference SOC is set to 0.98 ($SOC_{ref} = 0.96$). The current lower bound is zero and two current upper bounds are used, i.e., $I_{max} = 2C$ and $I_{max} = 4C$. The problem is formulated and solved in MATLAB. The entire simulation-based optimization takes about 7s on an 2.4GHz CPU with 30 collocation points.

Figure 2.2 and Fig. 2.3 depict the results for problem (2.25). With $I_{max} = 2C$, the charging strategy in Figure 2.2 can be divided into 3 stages. First, the input current constraint is active, meaning that the input current equals the maximum value at the beginning of the optimal charging trajectory. At the second stage,

the side reaction overpotential constraint (2.18) becomes active, which forces the charging current to decrease until the SOC reaches the target value. At the last stage, the battery reaches the desired SOC value and the input currents further decreases to avoid overcharging. The nature of the solution is slightly different for the case with $I_{\max} = 4C$ in Figure 2.2. Due to the side reaction constraint, the upper limit on charging current is not reached at the beginning of charging process. This can prevent the battery from excessive degradation even given a high current limit, which demonstrates the advantages of adopting the physics-based constraint.

It is necessary to emphasize that the number of collocation points is highly related to the computational speed. Additionally, it is important to choose a proper number of collocation points to get accurate and efficient results. The choice of the number of collocation points is a case-by-case decision which depends on both optimization duration and system dynamics.

2.6.2 Standard Charging Strategy

The standard CCCV charging strategy adopts only voltage and current limits instead of physics-based constraints. The problem can be defined as

$$
\begin{aligned}
&\min_{u(t)} \; J = \int_{t_0}^{t_f} \left(SOC_{cell}(t) - SOC_{ref}\right)^2 dt \\
&\quad \text{s.t:} \\
&\qquad SOC_{cell} = \frac{SOC_n(t) - \theta_{n,0}}{\theta_{n,100} - \theta_{n,0}} \\
&\qquad SOC_n(t) = \frac{c_{s,n,avg}(t)}{c_{s,n,max}} \\
&\qquad SOC_n^{surf}(t) = \frac{c_{s,n}^{surf}(t)}{c_{s,n,max}} \\
&\qquad c_{s,n,avg}(t) = \int_0^{R_n} c_{s,n} dr \\
&\qquad c_n(r,t) \approx \sum_{i=0}^{M} \beta_{n,i}(t) P_i(r) \\
&\qquad J_n(t) = i_{0,n}(t) \left[\exp\left(\frac{\alpha_a F}{RT}\eta_n(t)\right) - \exp\left(-\frac{\alpha_c F}{RT}\eta_n(t)\right)\right] \\
&\qquad \eta_j(t) = \phi_{1,j}(t) - \phi_{2,j}(t) - U_j(SOC_j^{surf}(t)) \\
&\qquad \phi_{2,p}(t) - \phi_{2,n}(t) = I(t) R_{cell} \\
&\qquad V_{cell}(t) = \phi_{1,p}(t) - \phi_{1,n}(t) \\
&\qquad \eta_{sr}(t) = \eta_n + U_n(SOC_n^{surf}(t)) \geq 0 \\
&\qquad 0 \leq I(t) \leq I_{\max} \\
&\qquad V_{cell}(t) \leq V_{\max} \\
&\qquad SOC_{cell}(0) = SOC_{ini}
\end{aligned}
\tag{2.51}
$$

where $V_{\max}$ is the cell voltage upper bound used in the CCCV strategy.

The results of problem (2.51) are shown in Figure 2.4 and Figure 2.5. Note that while the side reaction overpotential is shown in Figure 2.4 and 2.4, it is not constrained in this problem. The input profiles first charge the battery with the maximum charging rate until the maximum voltage is reached. Then the voltage is held constant, and the remainder of the battery charging process proceeds at that constant voltage. Therefore, the optimal charging profiles are basically the

CCCV strategy, as one would expect given the optimization problem formulation with only current and voltage constraints (2.51).

Comparing the results of problem (2.25) and (2.51) confirms the established fact from the literature that model-based control is superior to CCCV charging: it is able to charge the battery while avoiding lithium plating. The input profiles in Figure 2.4 and Figure 2.5 can be damaging for batteries due to the fact that the side reaction overpotential is negative for substantial durations of time for both $I_{\max} = 2C$ and $I_{\max} = 4C$ cases. This makes the battery lose lithium ions irreversibly, which can induce some capacity loss - not to mention the safety hazard that results from the fact that these ions can precipitate dendritically, potentially piercing the battery's separator and inducing internal short circuits [10, 76]. The resulting input trajectories in problem (2.25), however, are grounded in physics-based constraint and are better in the sense of degradation.

Please note that the health-conscious optimal charging strategy requires a battery model: side reaction overpotentials cannot be measured directly, and therefore cannot be constrained using simple current/voltage sensor measurements. The degree to which model-based battery management is robust to battery modeling and parameter estimation errors is an interesting research topic, which is not addressed in this chapter and is addressed in other work by the author [77].

2.6.3 GPM Vs. Flatness-Based GPM

To further show the efficiency of the proposed framework, we also solve problem (2.25) using the GPM without exploiting differential flatness. The computational time for applying two methods is recorded with a different number of collocation points. While the GPM is known for its computational advantages [61], Figure 2.6 shows that the proposed flatness-based GPM is much more efficient than the traditional GPM. The difference in computational efficiency is more substantial with a larger number of collocation points.

The computational benefits of exploiting differential flatness for battery trajectory optimization are twofold. First, when using pseudospectral optimization alone - without exploiting differential flatness - one must translate the state equations governing the battery model into equality constraints. The same pseudospectral optimization problem, formulated using differential flatness,eliminates these equality

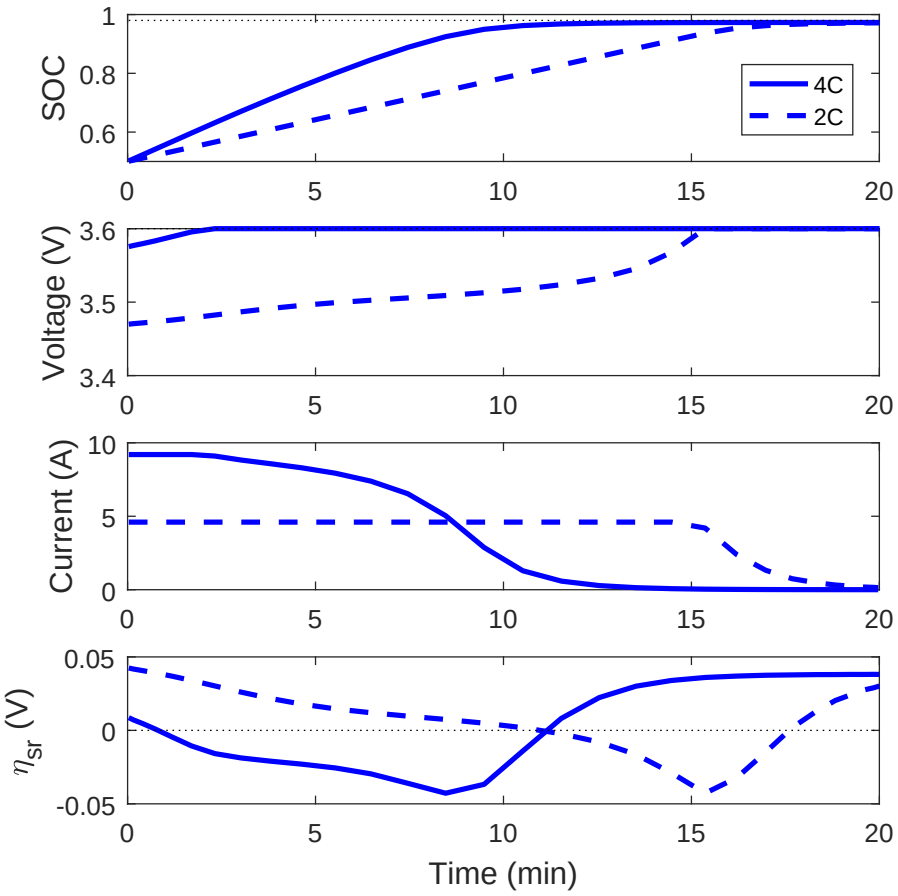

Figure 2.4: Simulation results for problem (2.51) applying the flatness-based GPM for two current upper limits: $I_{\max} = 9.2A$ (4C) (solid lines) and $I_{\max} = 4.6A$ (2C) (dashed lines). The initial SOC is 0.5 and voltage upper bound is 3.6V

constraints. State and input trajectories are expressed directly in terms of the flat output's trajectory, and can be derived from it through post-processing, after the optimization is complete. Second, with the differential flatness approach there are fewer optimization variables. For classical pseudospectral methods, each dimension of state space x and input space u has to be parameterized, which produces an NLP problem with $N(n+m)$ (i.e., $4N$ in problem (2.25)) optimization variables, where n and m are the number of state and input variables. This can lead to high-dimension optimization problems and can be computationally expensive, especially for high order systems or with a large number of collocation points. However, since battery electrode dynamics can be shown to be differentially flat, the only trajectory that needs to be parameterized is the trajectory of the flat output z. Thus for a flat

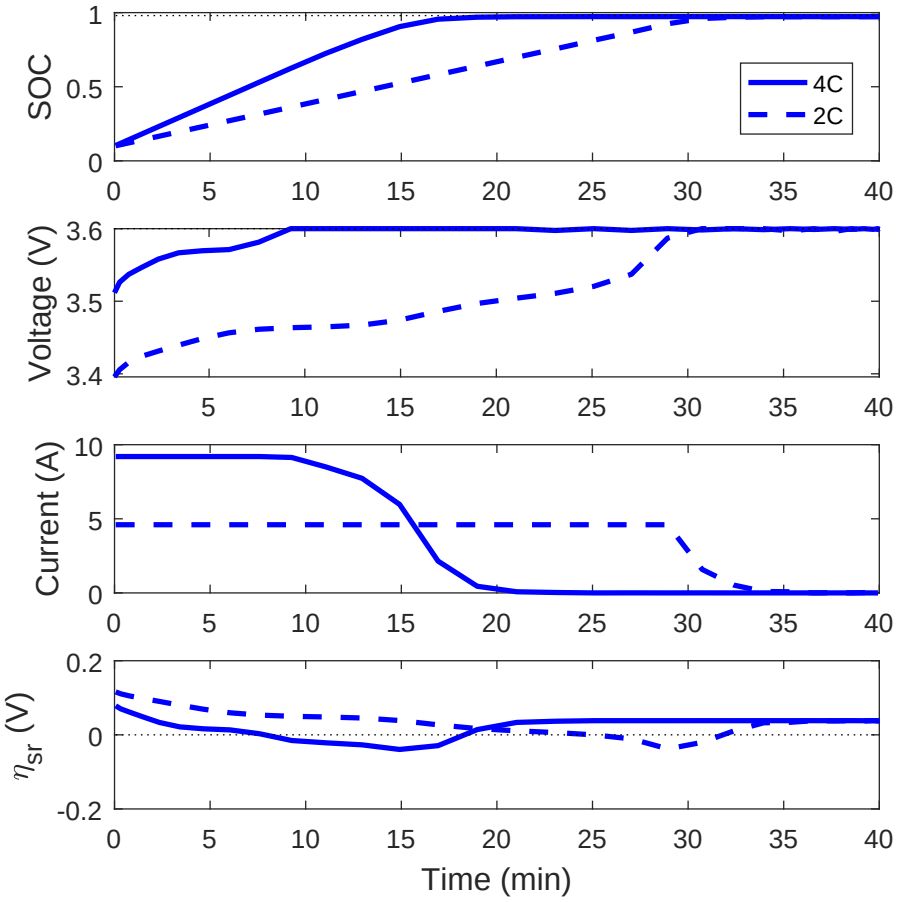

Figure 2.5: Simulation results for problem (2.51) applying the flatness-based GPM for two current upper limits: $I_{\max} = 9.2A$ (4C) (solid lines) and $I_{\max} = 4.6A$ (2C) (dashed lines). The initial SOC is 0.1and voltage upper bound is 3.6V

system, the resulting NLP problem has only N optimization variables instead of $4N$.

2.7 Conclusions

This chapter proposes a framework for the more efficient solution of battery charge/discharge trajectory optimization problems. This framework achieves this by combining four key tools: time-scale separation, orthogonal projection, differential flatness, and pseudospectral methods. The efficiency of this framework is mainly due to two facts: (i) the number of optimization variables is decreased to N, where N is the number of collocation points and (ii) there are no explicit dynamic equality

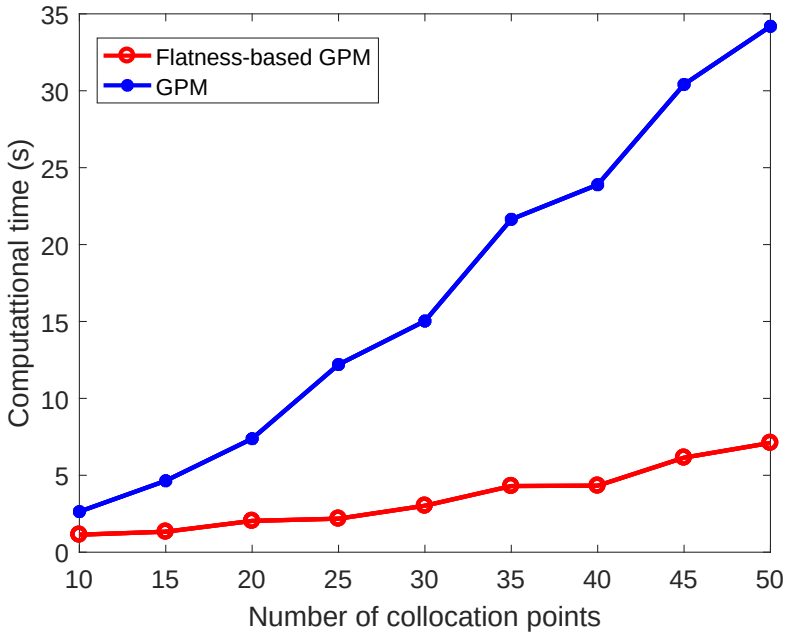

Figure 2.6: Computational time of the flatness-based GPM and the GPM versus the number of collocation points

constraints in the resulting NLP.

While the proposed framework can be adopted for general battery control, it is demonstrated in this chapter via two lithium-ion battery optimal charging problems. The first one includes physics-based constraints to prevent lithium plating and the second problem is the standard CCCV charging problem. The results clearly show the advantages of using model-based control with physics-based constraint. In addition, to further show the efficiency of the proposed method, we solve problem (2.25) using two methods: the traditional Gauss pseudospectral method (i.e., without using the flatness) and a flatness-based Gauss pseudospectral method. The computational time of two methods is compared and the computational speed applying the proposed framework can be improved by a factor of 5 compared to using the GPM alone.

The work in this chapter serves as a foundation for much of this dissertation. However, this chapter is limited by the assumption that there exists a significant difference in diffusion time scale between the battery's positive and negative electrodes. Subsequent chapters extend the work from this chapter by removing this assumption.

Chapter 3
Health-Conscious Nonlinear Model Predictive Control of Lithium-Ion Batteries

3.1 Introduction

This chapter proposes a computationally efficient nonlinear model predictive control (NMPC) framework for health-conscious lithium-ion battery management. [1]. The chapter extends the work shown in chapter 2 where battery electrode dynamics are shown to be differential flat, and this flatness property is exploited for efficient trajectory optimization. The chapter's main contributions compared to that work are twofold. First, the chapter represents the charge dynamics of a full battery cell using a single flat output variable, rather than one flat output variable per electrode. Second, instead of an electrochemistry-based single particle model (SPM), this chapter adopts an electrochemical-thermal SPM with temperature dynamics (SPM-T), where the diffusion and thermal dynamics are nonlinear and coupled. The flat output trajectory is optimized using a pseudospectral method. The use of NMPC can compensate for unmodeled effects [66], which is attractive compared to the implementation of charge/discharge trajectories optimized offline.

The degradation mechanism emphasized in this chapter is lithium plating.

[1] This chapter is based on a peer-reviewed publication by the dissertation's author. The publication has already appeared in the IEEE Transactions on Control System Technology [59]. The chapter extends the above publication by incorporating temperature dynamics into the publication's NMPC framework

Unlike the CCCV strategy with a fixed voltage constraint, we constrain the physics-based overpotential governing the lithium plating side reaction. We also constrain cell temperature which protects from overheating and thermal runaway. This leads to optimized input protocols that can increase battery life and safety by protecting batteries from overheating, lithium plating, and dendrite growth due to plating. The NMPC strategy improves the robustness of the optimized input protocols to uncertainties, such as unmodeled dynamics, battery model parameter uncertainty, and sensor noise.

The control literature offers a fundamental tool that makes battery trajectory optimization problems significantly more tractable, namely, *differential flatness* [52]. Solid-phase battery diffusion dynamics are governed by Fick's second law of diffusion in each electrode. Fick's law is known to be differentially flat [1, 58]. This concept makes it possible to capture all of the diffusion dynamics in each electrode using one trajectory of a single *flat output* variable instead of all of the state and input variables. Chapter 2 demonstrates the computational benefits of exploiting differential flatness for battery trajectory optimization. However, one major drawback remains: the dynamics of a full electrochemical battery model are not differentially flat. One way to solve this issue is to exploit time-scale separation by using a battery model which only models the electrode with slower diffusion dynamics and neglects the faster dynamics in the other electrode, as shown in chapter 2. This is not always desirable, since the single-electrode model fails to capture full battery transient dynamics accurately.

This chapter's novel and unique contribution is the development of an "extendedâĂŸâĂŹ differential flatness approach for optimal lithium-ion battery charging and discharging. The approach recovers differential flatness by expressing the flat output trajectory of one battery electrode explicitly as a function of the other electrode's flat output. We optimize the flat output trajectories using a computationally efficient pseudospectral method [61]. We perform the optimization within an NMPC framework and demonstrate framework's performance in the presence of parameter uncertainties.

The remainder of this chapter is organized as follows. Section 3.2 presents the governing equations and model reduction for the SPM-T model. Section 3.3.1 formulates the health-conscious battery optimal charging problem. Section 3.3.2 introduces the differential flatness property. In addition, the proposed differential

flatness-based Gauss pseudospectral method is introduced in Section 3.3.3. Section 3.3.4 shows the results of battery optimal control problem and compares them to an optimized benchmark CCCV protocol. Additionally, the sensitivity of the proposed NMPC framework to parameter uncertainties is studied. Section 3.4 presents the optimal charging protocol using the SPM-T model. Finally, section 3.5 concludes the chapter.

3.2 SPM-T Model

3.2.1 Thermal Sub-Model

In this section, the governing equations of the thermal model of the SPM-T are briefly introduced. The SPM-T model shares the same electrochemical dynamics with the SPM, i.e., Eq. (2.1)-Eq. (2.17), except that in the SPM-T model the diffusion coefficient $D_{s,j}$, reaction rate constant k_j, and effective resistance R_{cell} are temperature-dependent. The electrochemical parameters of the SPM-T used in this chapter are obtained from [3] and the reference potential curves for both electrodes are from [2] for a commercial $LiFePO_4$ (LFP) 26650 2.3Ah cell. The parameters of the thermal submodel of the SPM-T model are obtained from [78].

The diffusion coefficient $D_{s,j}(t)$ and reaction rate constant $k_j(t)$ are updated through the Arrhenius equation as follows:

$$D_{s,j}(t) = D_{s,j}^{ref} \exp\left(\frac{Ea_{D,j}}{R}\left(\frac{1}{T(t)} - \frac{1}{T_{ref}}\right)\right) \tag{3.1}$$

$$k_j(t) = k_j^{ref} \exp\left(\frac{Ea_{k,j}}{R}\left(\frac{1}{T(t)} - \frac{1}{T_{ref}}\right)\right) \tag{3.2}$$

$$\tag{3.3}$$

where $D_{s,j}^{ref}$ and k_j^{ref} are the diffusion coefficient and reaction rate constant at the reference temperature T_{ref}. The symbols $Ea_{D,j}$ and $Ea_{k,j}$ are the activation energy of diffusivity and reaction rate constant.

The first-order lumped parameter thermal model is adopted in this chapter to describe the thermal behavior of lithium-ion batteries [71, 79]:

$$mC_p\dot{T}(t) = -hA(T(t) - T_{ref}(t)) + I(t)T(t)\mathrm{S} + I(t)(\eta_p(t) - \eta_n(t) + I(t)R_{cell}) \tag{3.4}$$

where battery entropy coefficient, S, is defined as

$$\mathrm{S} = \left(\frac{\partial U_p}{\partial T}(SOC_p^{surf}(t)) - \frac{\partial U_n}{\partial T}(SOC_n^{surf}(t)) \right) \tag{3.5}$$

The term $\partial U_j / \partial T(SOC_j^{surf})$ is the entropy coefficient for the electrode j and is a function of electrode surface SOC. The term mC_p is the thermal mass of the battery, h is the convection heat transfer coefficient, and A is the cell surface area. The first term on the right hand side of Eq. (3.4) is the convection heat transferred from the surface of the battery to the surroundings. The second term is the reversible or entropic heat generation term. The last term is the irreversible heat component due to ohmic losses.

3.2.2 Model Order Reduction

Since the electrochemical sub-model in the SPM-T model is governed by partial differential equations (PDE) , for control purposes, the PDE needs to be discretized in space into ordinary differential equations (ODE). The model order reduction process shown below is similar to the one shown in Section 2.2.2. The difference is that since the diffusion coefficient and reaction rate constant are temperature-dependent, the resulting ODEs representing electrochemical dynamics are also temperature-dependent. Therefore, the whole SPM-T model is nonlinear and coupled. The model order reduction process of the electrochemical sub-model in the SPM-T model is described as below.

We approximate the lithium ion concentration profile $c_j(r,t)$ along the particle radius using as a linear combination of some unknown coefficients $\beta_j(t)$ (as functions of time t) and known Legendre polynomials $P_{j,i}(r)$ with degree i (as a function of radius r)

$$c_j(r,t) \approx \sum_{i=0}^{M} \beta_{j,i}(t) P_{j,i}(r) \tag{3.6}$$

where M is the degree of Legendre polynomials and is an even integer to satisfy the boundary condition (2.2), $P_{j,i}$ is the i-th degree Legendre polynomial corresponding to the term c_j for electrode j, and $\beta_{j,i}(t)$ is the i-th unknown coefficient for electrode j.

The Legendre polynomials are normalized such that

$$\int_0^{R_j} P_{j,i}(r)P_{j,k}(r)dr = \begin{cases} 0 & \text{if } i \neq k \\ 1 & \text{if } i = k \end{cases} \tag{3.7}$$

where R_j is the radius of particles.

Substituting Eq. (3.6) into Eq. (2.1) gives

$$\begin{aligned} &\sum_{i=0}^{M} P_{j,i}(r)\dot{\beta}_{j,i}(t) \\ &= D_{s,j}(t)\left[\frac{2}{r}\sum_{i=0}^{M}\frac{dP_{j,i}(r)}{dr}\beta_{j,i}(t) + \sum_{i=0}^{M}\frac{d^2P_{j,i}(r)}{dr^2}\beta_{j,i}(t)\right] \end{aligned} \tag{3.8}$$

where $\dot{\beta}_{j,i}(t)$ is the derivative with respect to time. Note that in the SPM-T model the diffusion coefficient is temperature dependent.

Galerkin projection is used to get the unknown coefficients $\beta_{j,i}(t)$. This is achieved by multiplying both sides of (3.8) by $P_{j,i}(r)$ and integrating over the radial coordinate. This furnishes the dynamics of the coefficients $[\beta_{j,0}, \beta_{j,2}, \ldots, \beta_{j,M}]^T$.

The number of Legendre polynomials decides the accuracy and the efficiency of the model reduction method and we choose $M = 6$ in this chapter. The diffusion dynamics Eq. (2.1) in each electrode can then be expressed as follows

$$\begin{bmatrix} \dot{\beta}_{j,0}(t) \\ \dot{\beta}_{j,2}(t) \\ \dot{\beta}_{j,4}(t) \\ \dot{\beta}_{j,6}(t) \end{bmatrix} = \frac{D_{s,j}(t)}{R_j^2} \begin{bmatrix} 0, & 9\sqrt{5}, & 20, & 29.4\sqrt{13} \\ 0, & 0, & 35\sqrt{5}, & 16.8\sqrt{65} \\ 0, & 0, & 0, & 46.2\sqrt{13} \\ 0, & 0, & 0, & 0 \end{bmatrix} \begin{bmatrix} \beta_{j,0}(t) \\ \beta_{j,2}(t) \\ \beta_{j,4}(t) \\ \beta_{j,6}(t) \end{bmatrix} \tag{3.9}$$

Similarly, the boundary condition Eq. (2.3) can be expressed as

$$\begin{aligned} \frac{3}{R_j}\sqrt{\frac{5}{2R_j}}\beta_{j,2}(t) + \frac{10}{R_j}\sqrt{\frac{9}{2R_j}}\beta_{j,4}(t) + \frac{21}{R_j}\sqrt{\frac{13}{2R_j}}\beta_{j,6}(t) \\ = -\frac{J_j(t)}{D_{s,j}(t)a_j} \end{aligned} \tag{3.10}$$

From Eq. (3.9) and Eq. (3.10), it can be seen that the term $\beta_{j,6}$ does not have dynamics and can be expressed as a function of other unknown variables. Therefore, it is not considered as a state variable. As a result, we achieve a standard

state-space representation for the dynamics of the electrode j

$$\dot{x}_{d,j}(t) = A_j(T)x_j(t) + B_j(T)I(t) \tag{3.11}$$

where A_j and B_j are the state and input matrix for diffusion sub-model. The state vector for electrode j is

$$x_{d,j} = [\beta_{j,0}(t), \beta_{j,2}(t), \beta_{j,4}(t)]^T \tag{3.12}$$

where $x_{d,j} \in \mathbf{R}^{3\times 1}$ are the states describing diffusion dynamics for electrode j and the input current is I.

Note that in the SPM-T model the state matrix $A_{d,j}$ and input matrix $B_{d,j}$ are functions of temperature due to the temperature-dependent nature of the diffusion coefficient $D_{s,j}$ as in Eq. (3.11). For the SPM model without temperature dynamics in Eq. (2.24), the diffusion dynamics are linear time-invariant. In the SPM-T model, however, the diffusion dynamics in each electrode in the SPM are coupled with temperature dynamics. Therefore, the state space representation of diffusion sub-model in the SPM-T can be expressed as

$$\dot{x}_d(t) = A(T)x_d(t) + B(T)I(t) \tag{3.13}$$

The state variable describing the diffusion dynamics of full SPM model is defined as

$$\begin{aligned} x_d(t) &= [x_{d,n}^T(t), x_{d,p}^T(t)]^T \\ &= [\beta_{n,0}(t), \beta_{n,2}(t), \beta_{n,4}(t), \beta_{p,0}(t), \beta_{p,2}(t), \beta_{p,4}(t)]^T \end{aligned} \tag{3.14}$$

The state matrix in Eq. (3.13) corresponding diffusion dynamics is

$$A(t) = \begin{bmatrix} A_n(T) & \mathbf{0} \\ \mathbf{0} & A_p(T) \end{bmatrix} \tag{3.15}$$

where $\mathbf{0}$ is a 3×3 zero matrix and the input matrix is

$$B(t) = \begin{bmatrix} B_n(T) \\ B_p(T) \end{bmatrix} \tag{3.16}$$

Additionally, one needs a state variable describing cell thermal dynamics. In this

chapter, this variable is bulk temperature, $T(t)$. The dynamics of this temperature can be found in Eq. (3.4).

Therefore, the state vector of the entire SPM-T model can be expressed as below:

$$x(t) = \begin{bmatrix} x_d(t) \\ T(t) \end{bmatrix} \tag{3.17}$$

The input vector can be defined as

$$u(t) = \begin{bmatrix} I(t) \\ T_{ref}(t) \end{bmatrix} \tag{3.18}$$

The output vector is defined as

$$y(t) = \begin{bmatrix} V_{cell}(t) \\ T(t) \end{bmatrix} \tag{3.19}$$

The state space representation of the full SPM-T model is

$$\dot{x}(t) = f(x(t), u(t)) \tag{3.20}$$

$$y = g(x(t), u(t)) \tag{3.21}$$

where $x \in R^{n_x}$, $y \in R^{n_y}$ and $u \in R^{n_u}$ with $n_x = 7$, $n_y = 2$, and $n_u = 2$ in this chapter.

3.3 Online Optimal Charging with SPM Model

3.3.1 Problem Formulation

The proposed NMPC framework can be applied to solve general battery trajectory optimization problems, such as optimal charging and discharging in the presence of different aging and degradation constraints. In the remainder of this chapter, we focus on optimal charging in the presence of a lithium plating side reaction constraint as an illustrative example, and our focus on charging (rather than

discharging) is justified by the fact that plating is more likely to occur during charging.

The problem is formulated as follows

$$
\begin{aligned}
&\min_{u(t)} \; J = \int_{t_0}^{t_f} \left(SOC_{cell}(t) - SOC_{ref}\right)^2 dt \\
&\quad \text{s.t:} \\
&\qquad \dot{x}(t) = Ax(t) + Bu(t) \\
&\qquad SOC_{cell} = \frac{SOC_n(t) - \theta_{n,0}}{\theta_{n,100} - \theta_{n,0}} \\
&\qquad SOC_j(t) = \frac{c_{s,n,avg}(t)}{c_{s,n,max}} \\
&\qquad SOC_j^{surf}(t) = \frac{c_{s,j}^{surf}(t)}{c_{s,j,max}} \\
&\qquad c_{s,j,avg}(t) = \int_0^{R_j} c_{s,j} dr \\
&\qquad c_j(r,t) \approx \sum_{i=0}^{M} \beta_{j,i}(t) P_{j,i}(r) \\
&\qquad J_j(t) = i_{0,j}(t) \left[\exp\left(\frac{\alpha_a F}{RT}\eta_j(t)\right) - \exp\left(-\frac{\alpha_c F}{RT}\eta_j(t)\right)\right] \\
&\qquad \eta_{sr}(t) = \eta_n + U_n(SOC_n^{surf}(t)) \geq 0 \\
&\qquad 0 \leq I(t) \leq I_{\max} \\
&\qquad SOC_{cell}(0) = SOC_{ini}
\end{aligned}
\tag{3.22}
$$

The goal of this problem is to bring battery state of charge to a level as close as possible to some target, SOC_{ref}, given the initial SOC, SOC_{ini}, within the time duration $[t_0, t_f]$. This optimization problem is subject to constraints imposed by: battery dynamics, maximum and minimum current limitations, and the desire to avoid side reaction overpotentials conducive to lithium plating. The side reaction constraint Eq. (2.18) distinguishes the problem from the traditional CCCV strategy which charges batteries using pre-determined voltage and input constraints. Additionally, the side reaction overpotential η_{sr} in Eq. (2.18) is a nonlinear and nonconvex function with respect to x and u.

The NMPC strategy is used as the online optimization framework. The nonlinearity of the optimization problem is mainly due to the side reaction constraint

(2.18). The input charging trajectory is optimized at each sampling time and only the first value of this trajectory is utilized. The optimization is then repeated using the updated state variables at the next sampling time. The use of the NMPC strategy can compensate for uncertainties (e.g., parameter uncertainty) and noise by re-optimizing the problem at each sampling time, which is demonstrated in Section 3.3.4.1. Due to the complexity of the NMPC problem, stability analysis is beyond the scope of this chapter. Note that the optimization problem assumes that all SPM state variables are known. Battery parameter and state estimation is an interesting research topic that is already addressed extensively in the literature [80–83] and will be examined in Chapter 5-6 of this dissertation.

3.3.2 Differential Flatness of SPM Model

The concept of differential flatness is introduced in chapter 2. This section briefly introduces how one can use differential flatness to represent the SPM model and SPM-T model.

The flat output for the electrode j, z_j, is found by transforming the reformulated diffusion sub-model for each electrode into the controllable canonical form:

$$\dot{\bar{x}}_j(t) = \begin{bmatrix} 0 & 1 & 0 \\ 0 & 0 & 1 \\ -\alpha_{1,j} & -\alpha_{2,j} & -\alpha_{3,j} \end{bmatrix} \bar{x}_j(t) + \begin{bmatrix} 0 \\ 0 \\ 1 \end{bmatrix} u(t) \tag{3.23}$$

where $\alpha_{i,j}$ are the coefficients of characteristic equation for electrode j and $\bar{x}_j$ is transformed state vector for the electrode j, defined as

$$x_j(t) = M_j \bar{x}_j(t) \tag{3.24}$$

where the matrix M_j is the similarity transformation matrix. One can define the flat output as the first transformed state:

$$z_j(t) := \bar{x}_{j,1}(t) \tag{3.25}$$

where $\bar{x}_j$ is transformed state vector for the sub-model of electrode j.

The transformed state variables $\bar{x}_j$ can then be expressed using the flat output

and a finite number of its derivatives

$$\bar{x}_j(t) = \begin{bmatrix} 1 & 0 & 0 \\ 0 & 1 & 0 \\ 0 & 0 & 1 \end{bmatrix} \begin{bmatrix} z_{j,1}(t) \\ \dot{z}_{j,1}(t) \\ \ddot{z}_{j,1}(t) \end{bmatrix} \tag{3.26}$$

Therefore, the original state variables x_j can be expressed by

$$x_j(t) = f_x(z_j(t), \dot{z}_j(t), \ddot{z}_j(t)) = M_j \bar{x}_j(t) \tag{3.27}$$

where M_j is the transformation matrix for the controllable canonical form. The input can be expressed similarly as well

$$\begin{aligned} u_j(t) &= f_{u_j}(z_j(t), \dot{z}_j(t), \ddot{z}_j(t), \dddot{z}_j(t)) \\ &= [-\alpha_{j,1}, -\alpha_{j,2}, -\alpha_{j,3}, 1] \begin{bmatrix} z_j(t) \\ \dot{z}_j(t) \\ \ddot{z}_j(t) \\ \dddot{z}_j(t) \end{bmatrix} \end{aligned} \tag{3.28}$$

where $\alpha_{j,i}$ are the coefficients of characteristic equation of the state matrix A_j in Eq. (3.15).

The existence of one flat output per battery electrode creates a problem for both the SPM and SPM-T models. The law of conservation of charge imposes the constraint that the currents flowing through the two electrodes are always equal. For any given temperature, T, at any given time instant, t, this constraint creates an affine relationship between the two electrodes' flat outputs. Thus, the full SPM model, and also the electrochemical component of the SPM-T model, is not differentially flat, even when the individual electrode diffusion dynamics are flat. For the SPM-T model, temperature, T, serves as a flat output, but the challenge remains that the underlying diffusion dynamics of the two battery electrode are not flat. The following section examines two different approaches for handling this difficulty.

3.3.3 Flatness-Based Gauss Pseudospectral Method

This section examines the problem of health-conscious battery trajectory optimization for a single-particle battery model (SPM) where one cannot assume significant time-scale separation between the two battery electrodes. As indicated above, this problem suffers from the fact that while each electrode's dynamics are individually differentially flat, the overall battery dynamics are not flat, because the conservation of charge creates a redundancy between the two electrodes' flat outputs. We address this challenge using two different methods. The first, perhaps more straightforward method, is to perform trajectory optimization with respect to the two flat outputs simultaneously, while using the law of conservation of charge to impose an additional equality constraint linking the two flat output trajectories. We refer to this as the "redundant flat output" approach. The second approach is to explicitly solve for one flat output trajectory a priori in terms of the other flat output trajectory, essentially be inverting the constraint created by the law of conservation of charge. The resulting nonlinear programming (NLP) problem will therefore be expressed in terms of only one flat output, and the differential flatness of battery diffusion dynamics will therefore be recovered. We refer to this as the "extended differential flatness" approach.

3.3.3.1 Redundant Flat Output Approach

Using the proposed framework in chapter 2, two flat outputs are required for the optimization problem (3.22). The resulting optimization problem with the

application of differential flatness is shown as follows

$$
\begin{aligned}
\min_{z_n(\tau_i), z_p(\tau_i)} \; & J = \frac{t_f - t_0}{2} \sum_{i=1}^{N} \omega_i \left(SOC_{cell}(\tau_i) - SOC_{ref} \right)^2 \\
\text{s.t:} \quad & \\
& x_j = f_x(z_j(\tau_i), \dot{z}_j(\tau_i), \ldots, z_j^{(\alpha)}(\tau_i)) \\
& u_j = f_u(z_j(\tau_i), \dot{z}_j(\tau_i), \ldots, z_j^{(\beta)}(\tau_i)) \\
& z_j = f_{z_j}(x_j, u_j, \dot{u}_j, \ldots, u_j^{(\gamma)}) \\
& u_n(\tau_i) = u_p(\tau_i) \\
& SOC_{cell} = \frac{SOC_n(\tau_i) - \theta_{n,0}}{\theta_{n,100} - \theta_{n,0}} \\
& SOC_n(\tau_i) = \frac{c_{s,n,avg}(\tau_i)}{c_{s,n,max}} \\
& SOC_j^{surf}(\tau_i) = \frac{c_{s,j}^{surf}(\tau_i)}{c_{s,j,max}} \\
& c_{s,j,avg}(\tau_i) = \int_0^{R_j} c_{s,j} dr \\
& c_j(r, \tau_i) \approx \sum_{i=0}^{M} \beta_{j,i}(\tau_i) P_{j,i}(r) \\
& J_j(\tau_i) = i_{0,j}(\tau_i) \left[\exp\left(\frac{\alpha_a F}{RT} \eta_j(\tau_i) \right) - \exp\left(-\frac{\alpha_c F}{RT} \eta_j(\tau_i) \right) \right] \\
& \eta_{sr}(\tau_i) = \eta_n + U_n(SOC_n^{surf}(t)) \geq 0 \\
& 0 \leq u(\tau_i) \leq u_{\max} \\
& \eta_{sr}(\tau_i) \geq 0 \\
& SOC_{cell}(\tau_0) = SOC_{ini} \\
& \text{where } i = 1, 2, \cdots, N
\end{aligned}
\tag{3.29}
$$

This problem formulation explicitly optimizes the trajectories of both z_n and z_p, subject to model dynamics and inequality constraints. The term N is the number of collocation points in the prediction horizon. Additionally, unlike the formulation in problem (3.22), there is no explicit model dynamic constraint Eq. (3.13). This is because model dynamics are automatically satisfied by exploiting the flatness property using Eq. (3.27) and Eq. (3.28). Note that there is an extra equality constraint on the current in each electrode, which is required to satisfy the

conservation of charge.

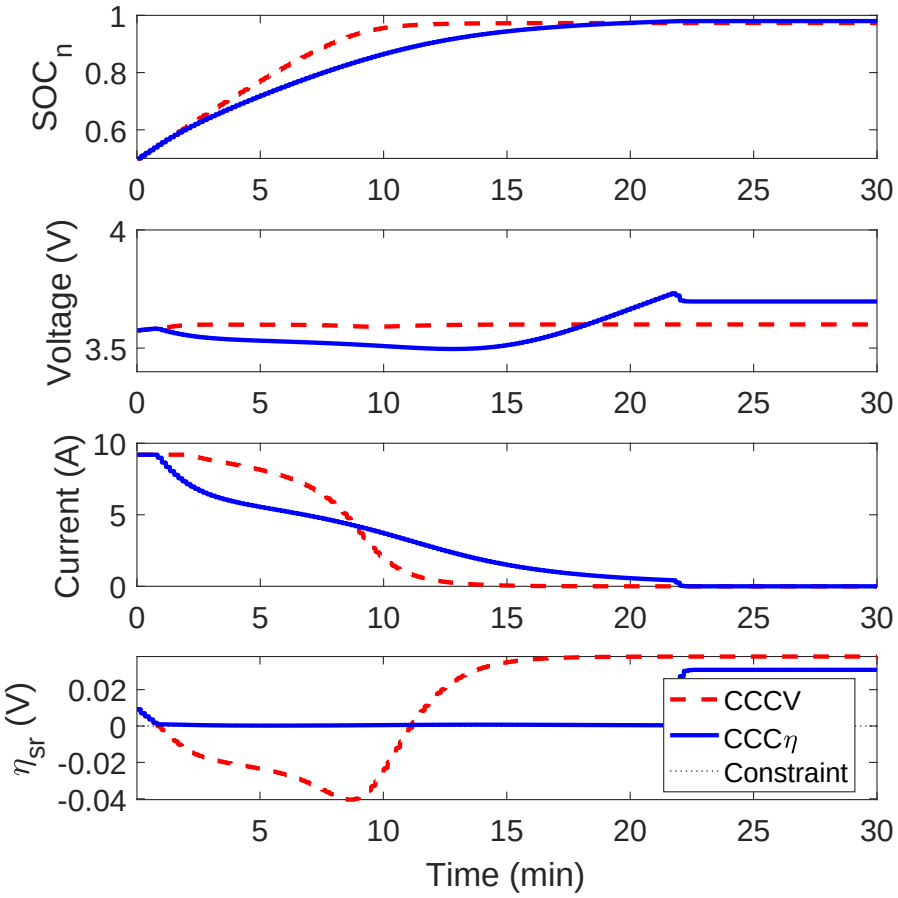

Figure 3.1: Comparison of two charging strategies: health-conscious optimal charging pattern (CCCη) from problem (3.22) versus CCCV charging pattern from problem (3.33). $u_{\max} = 4.6A$ (2C).

3.3.3.2 Extended Differential Flatness Approach

While the approach described above is efficient, it is necessary to use two trajectories of the flat outputs, $z_n(t)$ and $z_p(t)$, to represent full battery dynamics. This doubles the number of optimization variables needed for determining the optimal battery trajectory, and also introduces linear equality constraints between these variables. In contrast, this chapter shows that the dynamics of the entire battery can be forced to be differentially flat by eliminating one of the redundant flat outputs. Typically, the battery only has one input, i.e., the input current, and hence one flat output variable is enough to represent the dynamics of the entire SPM. We achieve

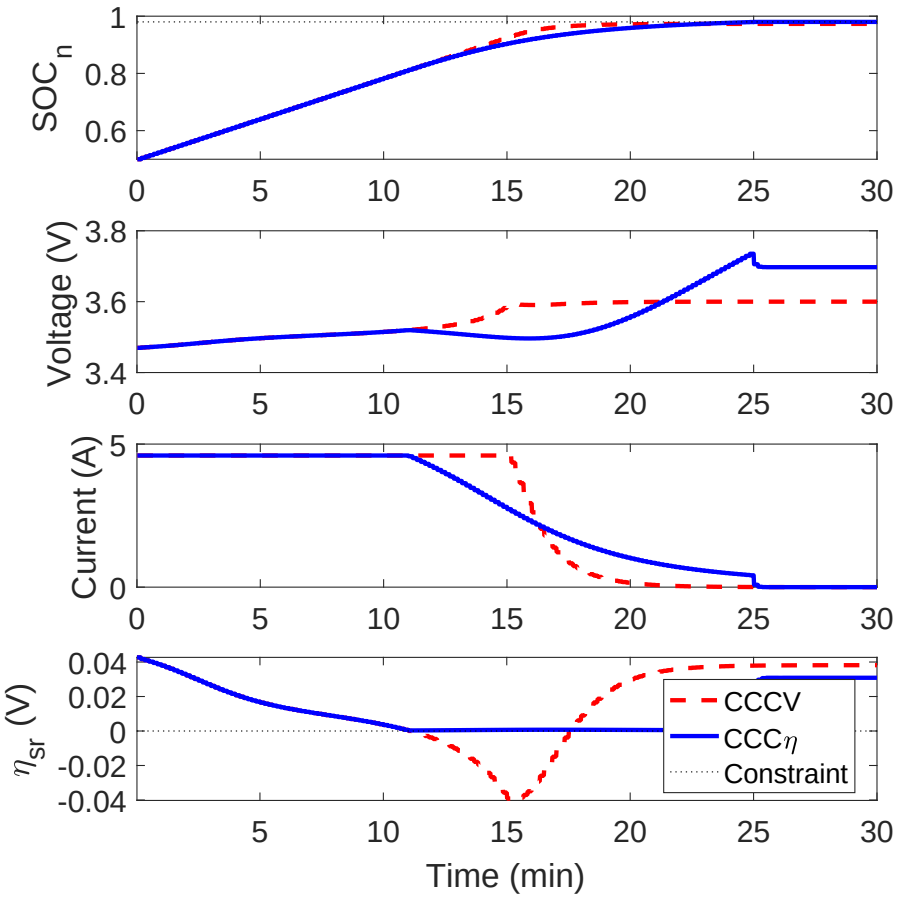

Figure 3.2: Comparison of two charging strategies: health-conscious optimal charging pattern (CCCη) from problem (3.22) versus CCCV charging pattern from problem (3.33). $u_{\max} = 9.2A$ (4C).

this using the law of conservation of charge: the amount of charge transferring through each electrode per unit time is the same, and therefore the current through both electrodes is the same

$$u_n(t) = u_p(t) \tag{3.30}$$

Equations (2.47) and (3.30) give the relationship between the flat outputs Z_p and Z_n

$$\begin{aligned} Z_p = &\left(-\alpha_{p,1} I_N - \alpha_{p,2} D_1 - \alpha_{p,2} D_2 - \alpha_{p,3} D_3\right)^{-1} \\ &\left(-\alpha_{n,1} I_N - \alpha_{n,2} D_1 - \alpha_{n,2} D_2 - \alpha_{n,3} D_3\right) Z_n \end{aligned} \tag{3.31}$$

where I_N is an identity matrix, $I_N \in \mathbf{R}^{N \times N}$. Therefore, the trajectory of $z_p(t)$ can

be expressed using an affine function of the trajectory of $z_n(t)$.

While the matrix inversion in Eq. (3.31) takes some computational time, this matrix inversion can be performed offline a priori, and does not affect the computational burden of online MPC. As a result, the problem (3.22) can be formulated and solved in a more efficient way

$$
\begin{aligned}
&\min_{z_n(\tau_i)} J = \int_{t_0}^{t_f} \frac{t_f - t_0}{2} \sum_{i=1}^{N} \omega_i \left(SOC_{cell}(\tau_i) - SOC_{ref}\right)^2 \\
&\quad \text{s.t:} \\
&\qquad x_j = f_x(z_j(\tau_i), \dot{z}_j(\tau_i), \ldots, z_j^{(\alpha)}(\tau_i)) \\
&\qquad u_j = f_u(z_j(\tau_i), \dot{z}_j(\tau_i), \ldots, z_j^{(\beta)}(\tau_i)) \\
&\qquad z_j = f_{z_j}(x_j, u_j, \dot{u}_j, \ldots, u_j^{(\gamma)}) \\
&\qquad Z_p = \left(-\alpha_{p,1} I_N - \alpha_{p,2} D_1 - \alpha_{p,2} D_2 - \alpha_{p,3} D_3\right)^{-1} \\
&\qquad \left(-\alpha_{n,1} I_N - \alpha_{n,2} D_1 - \alpha_{n,2} D_2 - \alpha_{n,3} D_3\right) Z_n \\
&\qquad SOC_{cell} = \frac{SOC_n(\tau_i) - \theta_{n,0}}{\theta_{n,100} - \theta_{n,0}} \\
&\qquad SOC_n(\tau_i) = \frac{c_{s,n,avg}(\tau_i)}{c_{s,n,max}} \\
&\qquad SOC_j^{surf}(\tau_i) = \frac{c_{s,j}^{surf}(\tau_i)}{c_{s,j,max}} \\
&\qquad c_{s,j,avg}(\tau_i) = \int_0^{R_j} c_{s,j} dr \\
&\qquad c_j(r, \tau_i) \approx \sum_{i=0}^{M} \beta_{j,i}(\tau_i) P_{j,i}(r) \\
&\qquad J_j(\tau_i) = i_{0,j}(\tau_i) \left[\exp\left(\frac{\alpha_a F}{RT} \eta_j(\tau_i)\right) - \exp\left(-\frac{\alpha_c F}{RT} \eta_j(\tau_i)\right)\right] \\
&\qquad \eta_{sr}(\tau_i) = \eta_n + U_n(SOC_n^{surf}(t)) \geq 0 \\
&\qquad 0 \leq u(\tau_i) \leq u_{\max} \\
&\qquad \eta_{sr}(\tau_i) \geq 0 \\
&\qquad SOC_{cell}(\tau_0) = SOC_{ini} \\
&\qquad \text{where } i = 1, 2, \cdots, N
\end{aligned}
\tag{3.32}
$$

This problem formulation only requires the optimization of Z_n, the flat output variable z_n evaluated at each collocation point. Therefore, the resulting optimization

problem using the extended approach only needs half of the optimization variables and no equality constraints compared to the NLP in Eq. (3.29). This makes the proposed framework computationally very efficient.

3.3.4 Results and Discussion

Problem (3.22) is set to start at $t_0 = 0$ with the initial SOC as 0.5 and with the sampling time as 10s (i.e., $\Delta t = 10s$). The sampling time is chosen such that it is about 5 times faster than the fastest time constant (about 60s) of battery diffusion dynamics. But the sampling time can be smaller. The prediction horizon is $T_p = 100s$ and at each time step the optimization problem is solved with 4 collocation points, i.e., $N = 4$. Due to the computational benefits, the proposed NMPC framework is able to solve the problem during each sampling time. The optimization is solved at each sampling time and the battery cell is then charged using the first optimized input trajectory. The optimization is repeated at next sampling time until the final time is reached. The hot-start strategy is used: the solution of previous sampling instance is used as the starting point (i.e., initial guess) for the current problem. All of simulations are solved in MATLAB using the Fmincon function on a laptop with a 2.4GHz CPU.

Figure 3.2 and Fig. 3.1 depict the results of problem (3.22) using two current upper bounds, 2C and 4C (1C corresponds to 2.3A current). Focusing on Fig. 3.2, i.e., the trajectory with $u_{\max} = 9.2A$, one can see the input trajectory first charges the battery with the maximum rate, because when a cell has low SOC the overpotential of lithium plating (2.18) can be positive even with high current. This is due to the fact that batteries at low SOC tend to have high positive electrode reference potentials. Once the side reaction constraint reaches zero, the charging current is tapered to satisfy the side reaction constraint. This charging process terminates when the battery SOC reaches the desired SOC. From the results, one can see the charging profiles have the following pattern: batteries are charged first with constant maximum current rate and then the current is decreased to keep constant overpotential. We call this charging profile as constant current constant overpotential (CCCη) strategy. The other trajectory shown in Fig. 3.1 demonstrates a similar pattern as described above.

To compare with the health-conscious optimal charging results, this chapter

also solves a standard CCCV charging problem with only voltage and current limits

$$\begin{aligned}
&\min_u J = \int_{t_0}^{t_f} \left(SOC_{cell}(t) - SOC_{ref}\right)^2 dt \\
&\text{s.t:} \\
&\qquad \dot{x}(t) = Ax(t) + Bu(t) \\
&\qquad y(t) = g(x(t), u(t)) \\
&\qquad 0 \leq u(t) \leq u_{\max} \\
&\qquad y(t) \leq y_{\max}
\end{aligned} \tag{3.33}$$

where this problem has the same SOC reference and current limits as problem (3.22) and $y_{\max}$ is voltage limit. The problem is solved using the proposed NMPC framework with the moving horizon $T_p = 100s$, sampling time $\Delta t = 10s$, $y_{\max} = 3.6V$ and the number of collocation points $N = 4$.

The dashed lines in Fig. 3.2 and Fig. 3.1 depict the simulation results of problem (3.33): the traditional CCCV strategy. The CCCV protocol first charges the battery with the constant maximum charging rate until the voltage upper limit is reached. Then voltage is kept constant by charging the battery using reduced current. Note that while the side reaction overpotential is shown in Fig. 3.2 and Fig. 3.1, it is not considered as a constraint in the optimization.

The benefits of health-conscious battery optimal charging can be seen by comparing two charging trajectories in either Fig. 3.1 or Fig. 3.2. The side reaction overpotentials are negative for substantial durations of time for CCCV charging. Therefore, CCCV charging can lead to excessive lithium-ion loss through lithium plating. The charging patterns in problem (3.22), i.e., the CCCη charging, however, can charge the battery without excessive degradation and reach the targeted charge capacity at the same time, even if the current upper limit is set to be aggressive.

This section also compares the charging time using the optimal charing and the traditional CCCV charging. Figure 3.3 depicts the trade-off between the charging time and battery degradation (i.e., the overpotential governing lithium plating in this study) . From the Pareto front of CCCV charing, it shows that faster charging leads to faster degradation due to larger side redaction overpotential. For the specific battery model and parameters used in this study, for the charging

current rate larger than 7C can not increase the charging time significantly. This is because that the high C-rate can lead to high voltage across the internal resistance and hence cell voltage can reach the constant voltage the beginning of charging. Moreover, the optimal charing solution can achieve comparable charging time with about 5C but without any degradation. This demonstrates the benefits of using the proposed optimal charging protocol, i.e., it can charge the cell (i) fast and (ii) does not introduce lithium plating degradation.

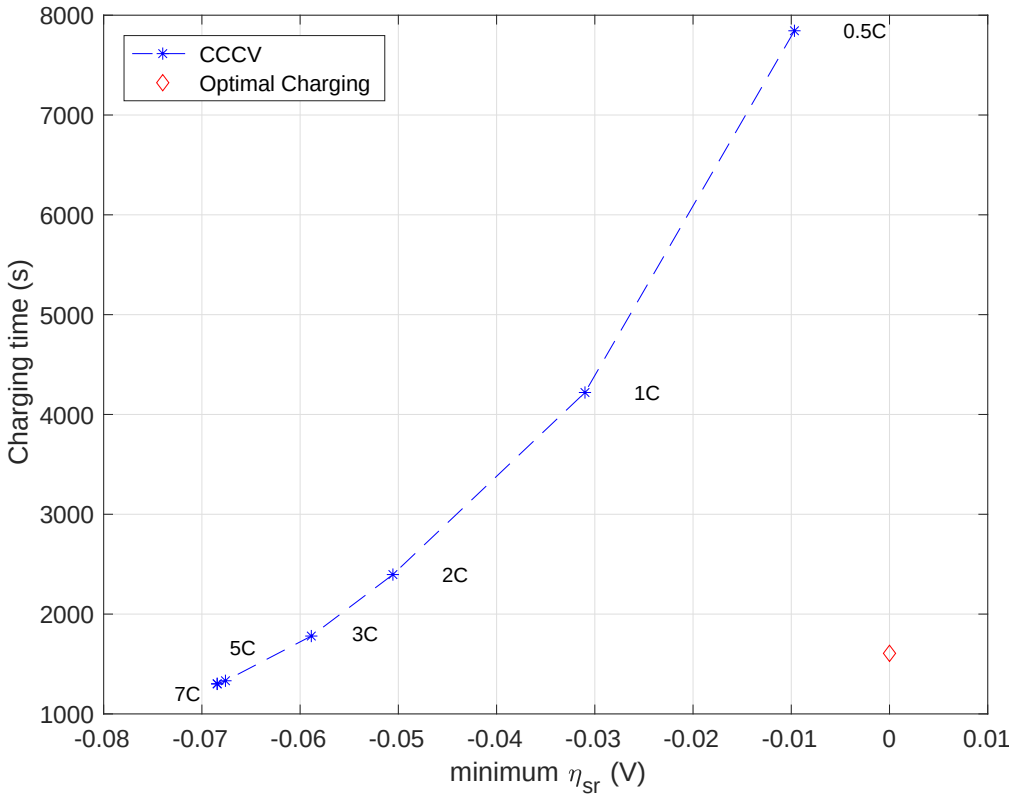

Figure 3.3: Pareto front between charging time and battery degradation. The optimal charging can achieve high charging C-rate and does not introduce degradation.

3.3.4.1 NMPC Sensitivity to Parameter Uncertainties

This section demonstrates the robustness of the proposed NMPC framework with respect to SOH parameters by comparing with an offline optimal charging solution. The volume fraction of the active material ε_j in Eq. (2.4) is one of the SOH parameters relating to electrode capacity in SPM and hence cell capacity, which changes with aging for a given battery [77]. Suppose the controller assumes each

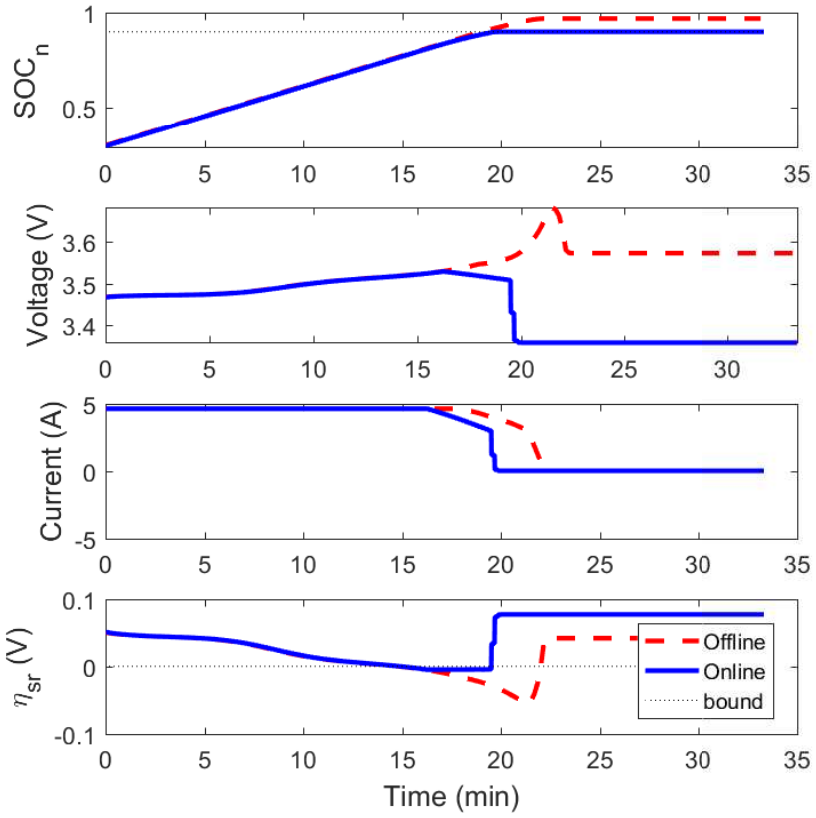

Figure 3.4: The NMPC framework is more robust than offline framework.

electrode has its original capacity, while the actual capacity is only 90% of the original due to aging.

Fig. 3.4 demonstrates the robustness of the NMPC framework. Both online and offline solutions do violate lithium plating overpotential constraints due to the uncertain SOH parameter ε_j. However, the online solution has much smaller lithium plating overpotential violation over a shorter duration and therefore exhibits less lithium plating. This is because the NMPC framework updates the optimal trajectory at every sampling time based on the updated state variables.

3.3.4.2 Comparison of Three NMPC Frameworks

The efficiency of the proposed framework in this chapter is demonstrated by solving problem (3.22) online using 3 approaches: i) the GPM, ii) the flatness-based GPM with two redundant flat outputs shown in problem (3.29) (differential flatness only

Table 3.1: Comparison of 3 NMPC frameworks: The proposed framework is the most efficient.

NMPC Framework	Optimization variables	Equality constraints
GPM	$(n_x + n_u) \times N = 7N$	$n_x \times N = 6N$
Two flat outputs GPM	$2n_u \times N = 2N$	$n_u \times N = N$
One flat output GPM	$n_u \times N = N$	0

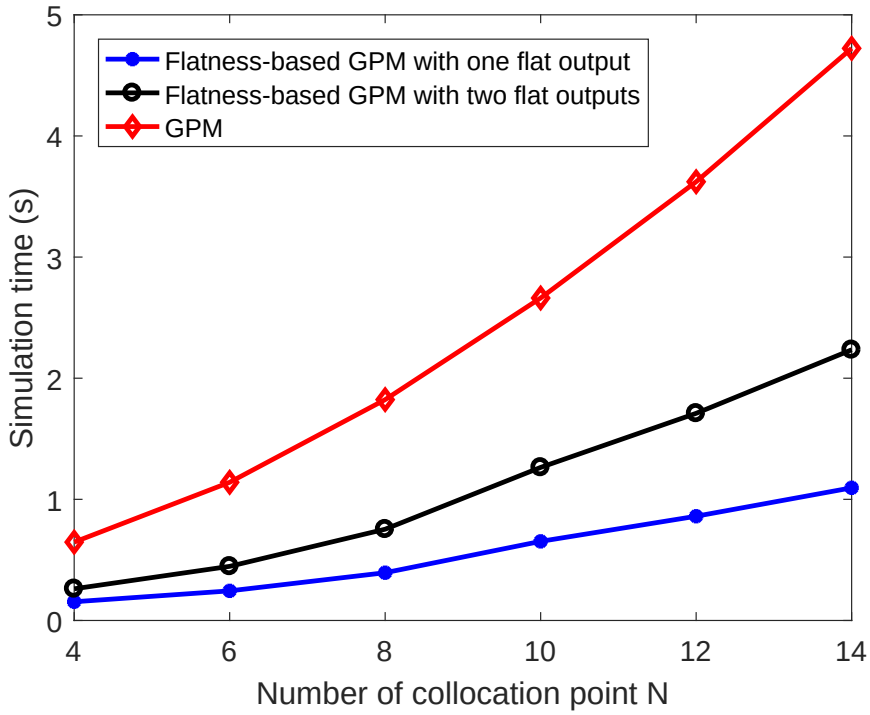

Figure 3.5: Average simulation time for each time step. The proposed extended flatness approach is more efficient than the flatness-based GPM with two flat outputs proposed in [1].

applies to each electrode but not the entire battery), and iii) the flatness-based GPM with one flat output in problem (3.32) (the approach proposed in this chapter). All three simulations are conducted using the same set of parameters (i.e., $\Delta t = 5s$, $T_p = 400s$, $SOC(t_0) = 0.4$, $t_0 = 0s$, and $t_f = 2100s$). Fig. 3.5 depicts the average simulation time for one time step as a function of the number of collocation points. The average simulation time is calculated by dividing the simulation time for the entire optimization by the number of time steps. While all three approaches produce the same charging profile, the extended flatness-based approach proposed

in this paper can reduce the computational time by a factor of 5 compared to online pseudospectral optimization alone.

The proposed NMPC framework is computationally efficient mainly for two reasons. First, by using the differential flatness property, it automatically satisfies system dynamic constraints. Therefore the resulting NLP problem does not have any explicit dynamic constraints. This holds for both methods using differential flatness. Second, the proposed extended flatness-based method reduces the number of optimization variables significantly. Specifically, the proposed extended flatness-based method only requires N optimization variables, since the differential flatness for the full SPM is recovered.

3.4 Online Optimal Charging with SPM-T Model

3.4.1 Problem Formulation

Instead of using the SPM model, this chapter also extends the problem proposed in problem 3.22 by using the SPM-T model. The added thermal model enables the controller to protect the cell from overheating or thermal runaway, which can happen during fast charging. Additionally, it can model the dynamics of battery

more accurately. The problem is formulated as follows:

$$
\begin{aligned}
&\min_{u(t)} \; J = \int_{t_0}^{t_f} \left(SOC_{cell}(t) - SOC_{ref}\right)^2 dt \\
&\quad \text{s.t:} \\
&\qquad \dot{x}(t) = f(x(t), u(t)) \\
&\qquad SOC_{cell} = \frac{SOC_n(t) - \theta_{n,0}}{\theta_{n,100} - \theta_{n,0}} \\
&\qquad SOC_j(t) = \frac{c_{s,n,avg}(t)}{c_{s,n,max}} \\
&\qquad SOC_j^{surf}(t) = \frac{c_{s,j}^{surf}(t)}{c_{s,j,max}} \\
&\qquad c_{s,j,avg}(t) = \int_0^{R_j} c_{s,j} dr \\
&\qquad c_j(r,t) \approx \sum_{i=0}^{M} \beta_{j,i}(t) P_{j,i}(r) \\
&\qquad J_j(t) = i_{0,j}(t) \left[\exp\left(\frac{\alpha_a F}{RT}\eta_j(t)\right) - \exp\left(-\frac{\alpha_c F}{RT}\eta_j(t)\right)\right] \\
&\qquad \eta_{sr}(t) = \eta_n(T) + U_n(SOC_n^{surf}(t)) \geq 0 \\
&\qquad 0 \leq I(t) \leq I_{\max} \\
&\qquad T_{\min} \leq T(t) \leq T_{\max} \\
&\qquad SOC_{cell}(0) = SOC_{ini}
\end{aligned}
\tag{3.34}
$$

Compared to the problem formulated in problem 3.22, the SPM-T model makes it possible to constrain temperature in addition to the side reaction exponential and current constraints in problem 3.22.

3.4.2 Differential Flatness of SPM-T Model

The details on the exploitation of the differentially flat nature of the SPM-T model are briefly introduced as below. First, one needs to identify the flat output vector. One needs two flat outputs to fully represent the electrochemical-thermal dynamics of the SPM-T model, according to the definition of the differential flatness, i.e., the number of flat outputs should be the same as the number of inputs. The two flat outputs can be chosen as: one representing the electrochemical dynamics, i.e., the variable used in Sec. 3.3.2 and another one representing thermal dynamics.

Note that the diffusion and thermal dynamics are coupled through temperature-dependent parameters. Due to the bi-directional coupled nature of the SPM-T model, one needs to identify two flat outputs together.

First, the flat output corresponding to the diffusion dynamics can be found using the same procedures shown in Sec. 3.3.2

$$z_1(t) := \bar{x}_{n,j,1}(t) \tag{3.35}$$

where $\bar{x}_{d,n}$ is transformed state vector for diffusion sub-model of electrode n.

Another independent flat output is needed to describe the dynamics of the bulk temperature T. The bulk temperature T can be chosen as the second flat output, i.e.,

$$z_2(t) = T(t) \tag{3.36}$$

Therefore, the flat output vector for the SPM-T model is defined as

$$z(t) = \begin{bmatrix} \bar{x}_{d,n,1}(t) \\ T(t) \end{bmatrix} \tag{3.37}$$

Second, the transformed diffusion-related state variables $\bar{x}_{d,j}$ can then be expressed using the flat output and a finite number of its derivatives.

$$\bar{x}_{d,j}(t) = \begin{bmatrix} 1 & 0 & 0 \\ 0 & 1 & 0 \\ 0 & 0 & 1 \end{bmatrix} \begin{bmatrix} z_1(t) \\ \dot{z}_1(t) \\ \ddot{z}_1(t) \end{bmatrix} \tag{3.38}$$

Therefore, the original state variables $x = [x_{d,j}^T, T]^T$ can be expressed by

$$\begin{aligned} \begin{bmatrix} x_{d,j}(t) \\ T(t) \end{bmatrix} =& f_x(z_{j,1}(t), \dot{z}_{j,1}(t), \ddot{z}_{j,1}(t), z_2(t)) \\ =& \begin{bmatrix} M_j\left(z_2(t)\right) \bar{x}_{d,j}(t) \\ z_2(t) \end{bmatrix} \end{aligned} \tag{3.39}$$

where $M_j(z_2(t))$ is the transformation matrix for the controllable canonical form. This matrix is a function of temperature $z_2(t)$, because the state matrix $A_d(t)$ is a function of temperature governed by Arrhenius equation Eq. (3.1).

Additionally, the input vector needs to be expressed using the flat output variables. In the SPM-T model, the input is a two dimensional vector, i.e., $u = [I, T_{ref}]^T$. The first element in the input vector corresponds to the input current and the second one is ambient temperature. The input current u_1, calculated from the diffusion sub-model of the electrode j, can be expressed as shown below

$$\begin{aligned} u_1(t) =& f_{u_1}(z_{j,1}(t), \dot{z}_{j,1}(t), \ddot{z}_{j,1}(t), \dddot{z}_{j,1}(t), z_2(t)) \\ &= [-\alpha_{j,1}(z_2(t)), -\alpha_{j,2}(z_2(t)), -\alpha_{j,3}(z_2(t)), 1] \begin{bmatrix} z_{j,1}(t) \\ \dot{z}_{j,1}(t) \\ \ddot{z}_{j,1}(t) \\ \dddot{z}_{j,1}(t) \end{bmatrix} \end{aligned} \tag{3.40}$$

where u_1 is the input current and, $\alpha_{j,i}(t)$ is the I^{th} coefficient of characteristic equation of the state matrix $A_j(t)$ in Eq. (3.11). Unlike the SPM model, the dynamics of the SPM-T model change with temperature and hence the coefficients of above equation $\alpha_{j,i}$ also change with temperature $z_2(t)$. The relationship is based on the Arrhenius equation. Thermal dynamics in Eq. (3.4) are used to derive the relation between u, and z

$$\begin{aligned} u_2(t) =& f_{u_2}(z(t), \dot{z}(t), \ddot{z}(t), \dddot{z}(t)) \\ =& \frac{1}{hA} \left(mC_p \dot{z}_2(t) - u_1(t)u_2(t)S(t) - u_1(t)(\eta_p(t) - \eta_n(t) - u_1(t)R_{cell})\right) \\ &+ z_2(t) \end{aligned} \tag{3.41}$$

where the entropy coefficient S and overpotential $\eta_j(t)$ are functions of state and input variables and therefore can be expressed using the output $z(t)$.

Similar to the flatness-based process shown in section 3.3, the health-conscious

optimal charging problem in Eq. (3.34) is transformed to the following form

$$\min_{z_n(\tau_i)} J = \int_{t_0}^{t_f} \frac{t_f - t_0}{2} \sum_{i=1}^{N} \omega_i \left(SOC_{cell}(\tau_i) - SOC_{ref}\right)^2$$

s.t:

$$\begin{aligned}
&x(\tau_i) = f_x(z(\tau_i), \dot{z}(\tau_i), \ldots, z^{(\alpha)}(\tau_i)) \\
&u(\tau_i) = f_u(z(\tau_i), \dot{z}(\tau_i), \ldots, z^{(\beta)}(\tau_i)) \\
&z(\tau_i) = f_z(x(\tau_i), u(\tau_i), \dot{u}(\tau_i), \cdots, u^{(\gamma)}(\tau_i)) \\
&Z_p = \left(-\alpha_{p,1}(t) I_N - \alpha_{p,2}(t) D_1 - \alpha_{p,2}(t) D_2 - \alpha_{p,3}(t) D_3\right)^{-1} \\
&\left(-\alpha_{n,1}(t) I_N - \alpha_{n,2}(t) D_1 - \alpha_{n,2}(t) D_2 - \alpha_{n,3}(t) D_3\right) Z_n \\
&SOC_{cell} = \frac{SOC_n(\tau_i) - \theta_{n,0}}{\theta_{n,100} - \theta_{n,0}} \\
&SOC_n(\tau_i) = \frac{c_{s,n,avg}(\tau_i)}{c_{s,n,max}} \\
&SOC_j^{surf}(\tau_i) = \frac{c_{s,j}^{surf}(\tau_i)}{c_{s,j,max}} \\
&c_{s,j,avg}(\tau_i) = \int_0^{R_j} c_{s,j} dr \\
&c_j(r, \tau_i) \approx \sum_{i=0}^{M} \beta_{j,i}(\tau_i) P_{j,i}(r) \\
&J_j(\tau_i) = i_{0,j}(\tau_i) \left[\exp\left(\frac{\alpha_a F}{RT} \eta_j(\tau_i)\right) - \exp\left(-\frac{\alpha_c F}{RT} \eta_j(\tau_i)\right)\right] \\
&\eta_{sr}(\tau_i) = \eta_n + U_n(SOC_n^{surf}(t)) \geq 0 \\
&0 \leq u(\tau_i) \leq u_{\max} \\
&T_{\min} \leq T(t) \leq T_{\max} \\
&\eta_{sr}(\tau_i) \geq 0 \\
&SOC_{cell}(\tau_0) = SOC_{ini} \\
&\text{where } i = 1, 2, \cdots, N
\end{aligned} \tag{3.42}$$

3.4.3 Results and Discussion

Figure 3.6 and Fig. 3.7 present the results of health-conscious charging using the SPM-T model. For this case study, two comparison are made. First, Fig. 3.6

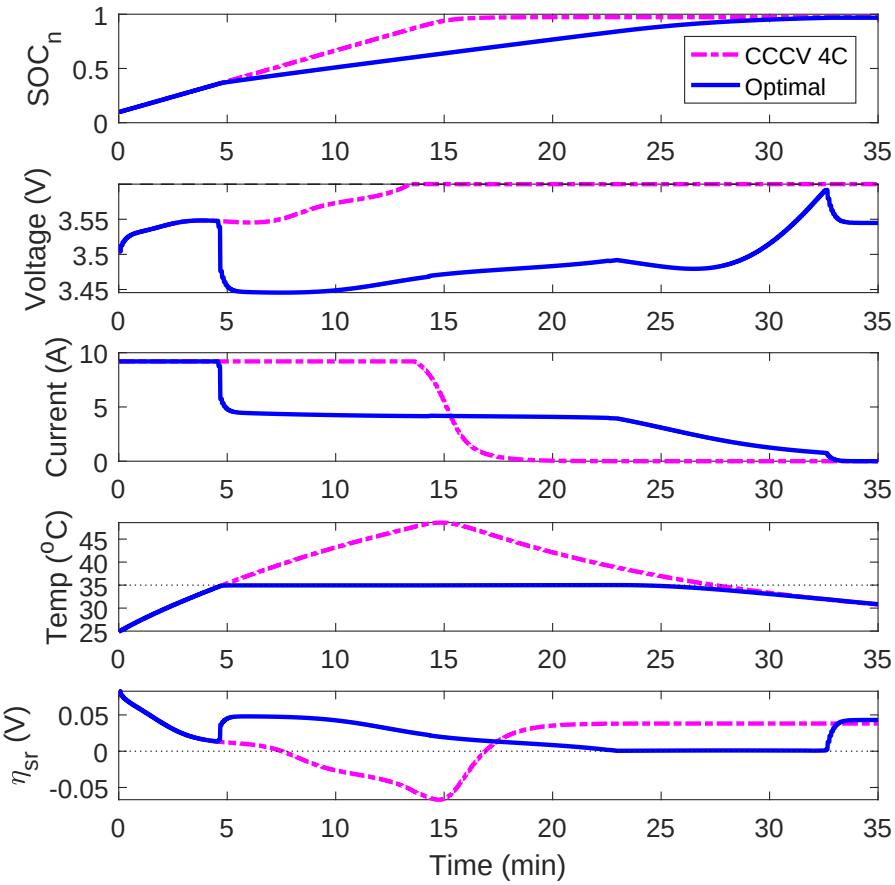

Figure 3.6: Comparison between online optimal charging trajectory with CCCV charging patterns with $u_{\max} = 4C$

depicts the online optimal charging strategy using the SPM-T model with 4C maximum current versus the CCCV charging strategy with 4C maximum current limit. Second, Fig. 3.7 presents the online optimal charging strategy using the SPM-T model with 4C maximum current versus CCCV charging strategy with 2C maximum current limit.

In Fig. 3.6, one can see the optimal charging trajectory (solid lines) first charges the cell with the maximum current rate. This is due to the fact that when a cell has low SOC the overpotential of lithium plating (2.18) can be positive even with high current and the cell temperature is near room temperature. Once cell temperature reaches the temperature bound, the input current is decreased to about 2C to satisfy the bound. After about 20 minutes, the side reaction constraint reaches zero and the charging current is tapered again to satisfy the side reaction constraint.

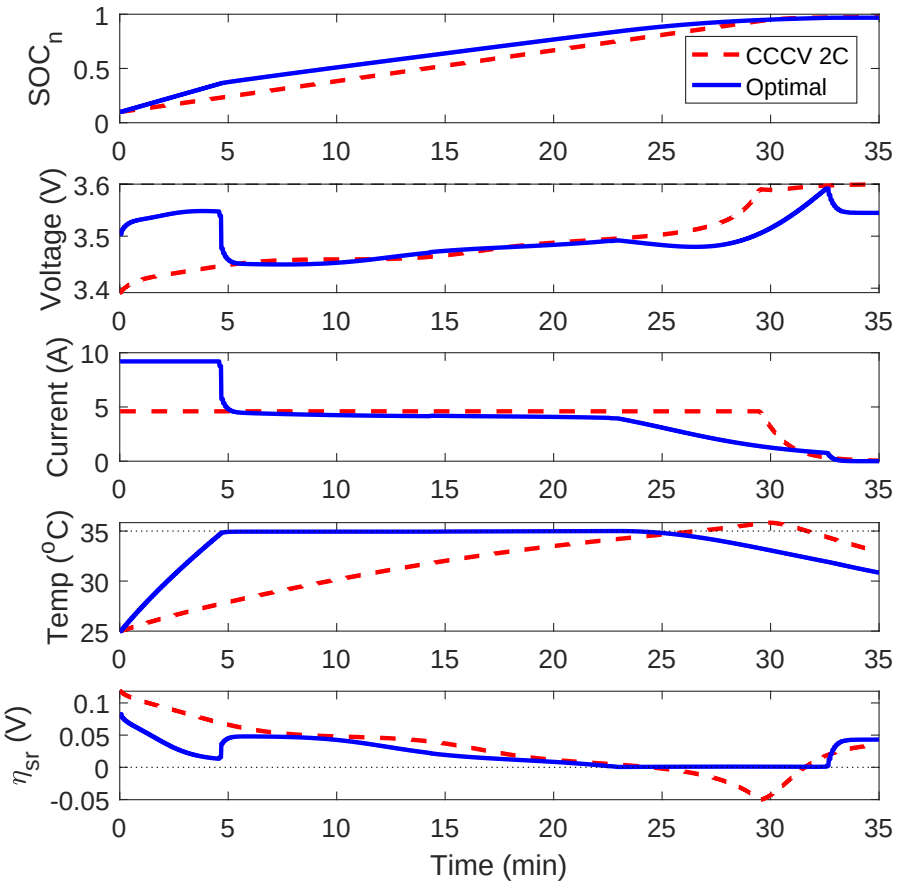

Figure 3.7: Comparison between online optimal charging trajectory $u_{\max} = 4C$ with CCCV charging patterns with $u_{\max} = 2C$

This charging process terminates when the battery SOC reaches the desired SOC. From the results, one can see the charging profiles have the following pattern: the cell is charged first with constant maximum current rate and then the current is decreased to keep constant temperature and then is further decreased to keep constant zero side reaction overpotential.

Figure 3.8 depicts the results with 20C as the current upper bound without adding temperature constraint. Although the SPM-T model may not be accurate with large current, the results can provide some insights. Even given a large current bound and even without temperature constraint, the optimal charging trajectory does not reach the bound due to the fact that at the beginning of the charging process, the overpotential constraint is active. Therefore, the proposed framework can still provide health-conscious charging protocol even given large current bound.

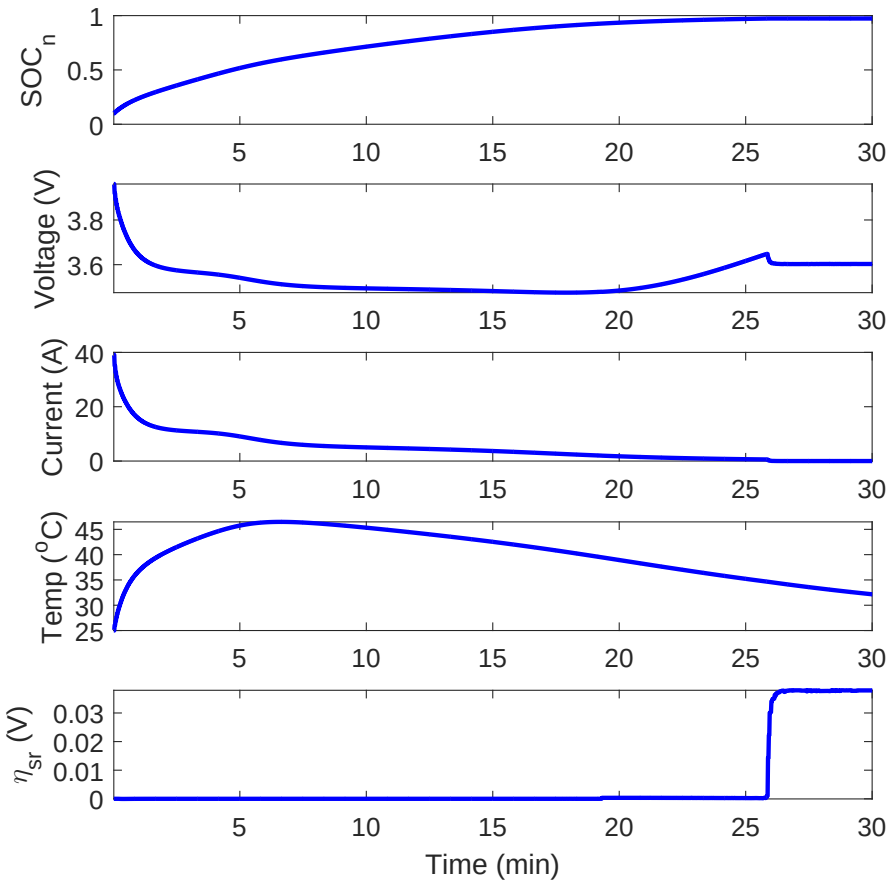

Figure 3.8: Optimal online optimal charging trajectory with $u_{\max} = 20C$ without temperature constraint

The charging power density can be seen by comparing Fig. 3.6 and Fig. 3.7. At the beginning, the optimal charing strategy and the CCCV pattern with 4C share the same charging power density, since both of them reach the maximum current rate. However, due to the temperature and overpotential constraints, the charging power density has to decrease. Therefore, among the three strategies: (i)optimal charging, (ii) CCCV with 4C current, and (iii) CCCV with 2C current, the optimal charging pattern is not the fastest and has similar charing power density with CCCV charging with 2C current. A key advantage, however, is that the optimal charging strategy does not violate battery safety constraints, where as both CCCV strategies do.

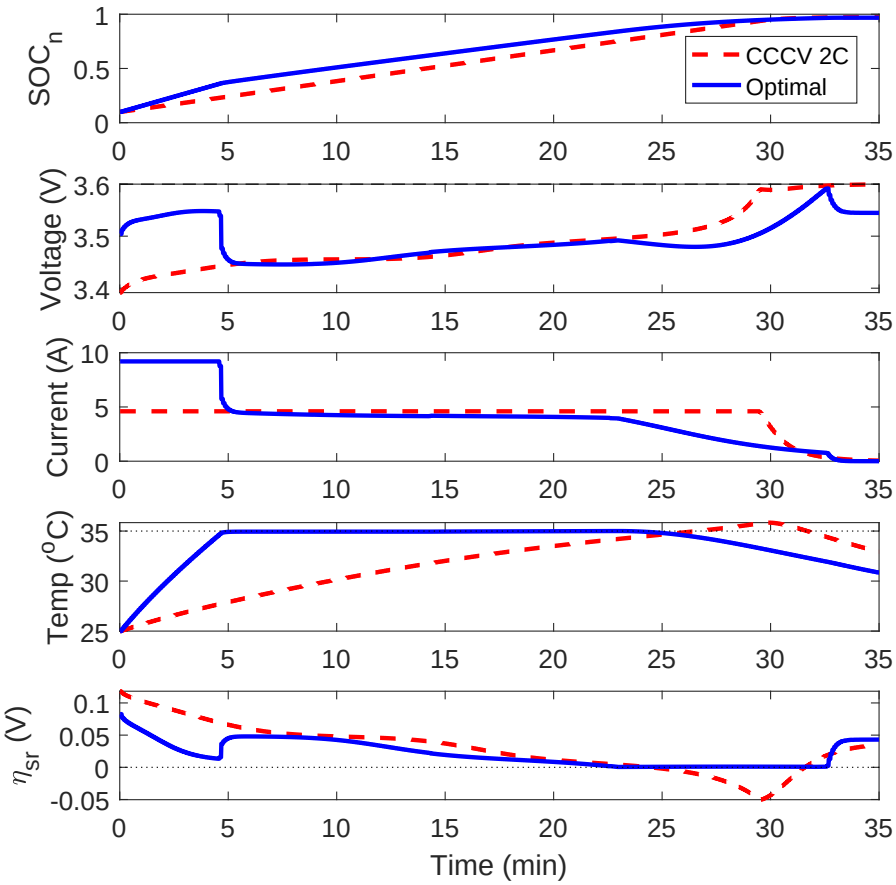

Figure 3.9: Comparison between online optimal charging trajectory $u_{\max} = 4C$ with CCCV charging patterns with $u_{\max} = 2C$

3.5 Conclusions

This chapter proposes a computationally efficient nonlinear model predictive control (NMPC) framework to solve battery trajectory optimization problems online. This framework extends the differential flatness approach in chapter 2 to recover the flatness of the SPM and SPM-T model, respectively, which makes it possible to represent the dynamics of the entire battery using only one flat output (for diffusion dynamics). The trajectory of the resulting flat output is optimized using pseudospectral methods. This chapter demonstrates the proposed NMPC framework by applying it to solve an online health-conscious battery optimal charging problem with a temperature constraint and a physics-based side reaction constraint. The robustness of the NMPC framework is demonstrated for specific SOH parameter

uncertainties. The proposed framework improves computational efficiency by a factor of 5 compared to pseudospectral optimization alone.

Chapter 4
Efficient Total Least Squares State and Parameter Estimation for Differentially Flat Systems

4.1 Introduction

To fully achieve the benefits of model-based battery control, one must be able to estimate the state variables of the underlying battery models accurately. This chapter presents a framework for flatness-based pseudospectral combined state and parameter estimation in lumped-parameter nonlinear systems. This framework enables computationally-efficient total least squares (TLS) estimation for lumped-parameter nonlinear systems. This is quite relevant to practical lithium-ion battery systems, where both battery input and output measurements can be quite noisy. Instead of using battery examples, this chapter adopts a classical nonlinear mass-spring-damper system to demonstrate the proposed framework. The proposed framework is applied to battery state estimation in chapter 5. [1]

Least squares methods are widely used in the literature for solving problems including curve fitting, state estimation, and system identification [77,85–87]. There are two categories of least squares problems: ordinary least squares (OLS) and TLS. The OLS problem assumes that only the output variables of a given system are corrupted by noise, while true input values are known. The TLS problem, in

[1] The work in this chapter has appeared in a peer-reviewed American Control Conference paper by the dissertation's author [84].

contrast, assumes both input and output measurements to be noisy.

Linear TLS problems can be solved using well-developed singular value decomposition (SVD) approaches [87, 88]. Additionally, in the control literature many researchers formulate linear system identification problems as TLS problems, which can be solved using tools such as Hankel matrix and subspace identification [89, 90].

It is challenging to solve TLS estimation problems for nonlinear systems [91]. Since both the input and output measurements in these problems are assumed to be noisy, one must optimize both of these trajectories, rather than treating the inputs as known. This can easily furnish nonlinear optimization problems with hundreds of decision variables, quickly compromising computational tractability. Moreover, the underlying system dynamics translate to equality constraints in nonlinear TLS estimation.

Given the above challenges, the overall goal of this chapter is to solve TLS estimation problems for differentially flat systems in an efficient manner. The concept of differential flatness was first introduced by Fliess *et al.* [52]. A system is differentially flat if it possesses flat output variables, equal in number to its input variables, such that the state and input variables can be expressed in terms of the flat outputs and a finite number of their derivatives, and the flat outputs can be expressed in terms of the state and input variables and a finite number of their derivatives. Differential flatness is attractive because it makes it possible to express all system state, input, and output trajectories in terms of time histories of the flat output variables. This simplifies trajectory optimization problems significantly: a fact that can be very beneficial in optimal control applications [1, 92].

This chapter solves TLS problems for flat systems using a pseudospectral approach. The chapter examines the TLS estimation of both system trajectory variables and constant parameters. We use a pseudospectral method to express the trajectory variables (i.e., the state, input, and output variables) in terms of the values of a flat output trajectory at specific collocation points. This transforms the TLS problem into a nonlinear programming (NLP) problem, which can be solved using well-developed NLP algorithms [1, 63]. The choice of collocation points has significant computational advantages compared to the use of evenly distributed discretization points in the time domain [63].

State and parameter estimation problems for nonlinear systems are widely studied in the literature. Extended Kalman filters (EKF), Unscented Kalman

filters (UKF), and nonlinear observers are widely used [7, 93]. The fact that our estimation approach relies on nonlinear programming rather than classical feedback-based state and parameter estimation makes it possible to account for physical constraints on the estimated state variables, input variables, and parameters. This can potentially improve estimation accuracy and convergence for systems exhibiting such constraints [67].

The literature already examines the use of pseudospectral methods and differential flatness for estimation. Gong *et al.*, for instance, build a state observer for nonlinear systems using pseudospectral methods [64]. Moreover, both Fliess *et al.* and Mahadevan *et al.* exploit differential flatness for OLS state estimation problems [94, 95]. Compared to the above work, this chapter's focus is on total (rather than ordinary) nonlinear least squares state and parameter estimation for differentially flat systems using pseudospectral methods. We demonstrate the proposed estimation framework using a nonlinear mass-spring-damper state and parameter estimation example. The results of this simple demonstration study are very encouraging: the proposed framework converges to accurate state and parameter estimates with very low computational cost.

The remainder of this chapter is organized as follows. Section 2 introduces general total least squares problems. Section 3 reviews the concept of a differentially flat system. The Legendre pseudospectral method (LPM) combined with the differential flatness property is introduced in Section 4, and serves as a foundation for the computationally efficient TLS state and parameter estimation framework presented in this chapter. The chapter demonstrates this framework on a nonlinear mass-spring-damper TLS state and parameter estimation problem in Section 5. Finally, Section 6 concludes the chapter and summarizes its contributions.

4.2 Total Least Squares Estimation

This section introduces TLS estimation, and formulates a generic TLS state and parameter estimation problem. The problem assumes that the input and output noise processes are both independent, identically distributed (i.i.d.). However, the overall contributions of this chapter can be easily extended to drop this assumption.

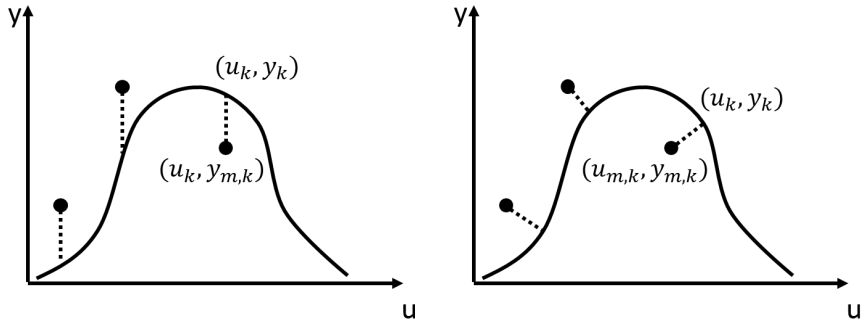

Figure 4.1: Comparison between OLS and TLS estimation.

Consider a general continuous-time dynamic system:

$$\begin{aligned} \dot{x} &= f(x, u, \theta), \\ y &= g(x, u, \theta) \end{aligned} \tag{4.1}$$

where $x \in \mathbb{R}^{n_x}$, $u \in \mathbb{R}^{n_u}$, $y \in \mathbb{R}^{n_y}$, and $\theta \in \mathbb{R}^{n_\theta}$ are the state, input, output, and unknown parameter vectors, respectively, so that $f : \mathbb{R}^{n_x} \times \mathbb{R}^{n_u} \mapsto \mathbb{R}^{n_x}$ and $g : \mathbb{R}^{n_x} \times \mathbb{R}^{n_u} \mapsto \mathbb{R}^{n_y}$.

Our goal is to estimate the parameters θ and state trajectories $x(t)$ including the initial states, given measurements of the inputs and outputs. This problem can be formulated as an OLS or TLS problem. The difference between the OLS and TLS formulations is highlighted in in Fig. 4.1: OLS problems assume that only the output variables are corrupted by noise, and treat the input variables as known exactly. In contrast, TLS problems assume that both the input and output measurements are noisy. Therefore, TLS estimation attempts to minimize the "orthogonal distance" (rather than vertical distance) between the estimated system trajectory and the input-output measurement pairs.

Suppose that the dynamics of the system in Eq. (4.1) are discretized in time, to furnish a model of the form:

$$\begin{aligned} x_{k+1} &= f(x_k, u_k + w_k, \theta) \\ y_{m,k} &= g(x_k, u_k, \theta) + v_k \end{aligned} \tag{4.2}$$

where $k = 1, 2, \ldots, n$, n is the number of data points, $w_k \in \mathcal{W}$ is the input noise,

and $v_k \in \mathcal{V}$ is output measurement noise, respectively. The noise processes are assumed to be zero-mean and Gaussian.

If we assume that the input measurement is accurate (i.e., $w_k = 0$) and the output noise is iid, this furnishes the OLS problem. It minimizes the sum of squared vertical distances from each data point to the estimated curve as shown in Fig. 4.1. The OLS problem can be formulated as

$$\begin{aligned} \min_{\hat{x}_k, \hat{\theta}} J &= \sum_{k=1}^{n} \|\hat{y}_k - y_{m,k}\|_2^2 \\ \text{subject to: } \hat{x}_{k+1} &= f(\hat{x}_k, u_k, \hat{\theta}) \\ \hat{y}_k &= g(\hat{x}_k, u_k, \hat{\theta}) \end{aligned} \tag{4.3}$$

where $\|\cdot\|_2$ represents the $\mathcal{L}_2$ norm of the corresponding vector and $\hat{\cdot}$ is the estimated value.

In contrast, the TLS problem assumes that neither the input nor output variables can be measured perfectly and there are noise signals associated with these variables. The measured input $u_{m,k}$ consists of the true but unknown input u_k corrupted with noise. TLS minimizes the sum of orthogonal squared distance from data points to the estimated curve, as shown in Fig. 4.1. Mathematically, this translates to:

$$\begin{aligned} \min_{\hat{x}_k, \hat{u}_k, \hat{\theta}} J &= \sum_{k=1}^{n} \left(Q\|\hat{y}_k - y_{m,k}\|_2^2 + R\|\hat{u}_k - u_{m,k}\|_2^2 \right) \\ \text{subject to: } \hat{x}_{k+1} &= f(\hat{x}_k, \hat{u}_k + w_k, \hat{\theta}) \\ \hat{y}_k &= g(\hat{x}_k, \hat{u}_k, \hat{\theta}) + v_k \end{aligned} \tag{4.4}$$

The cost function J has two weighted squared errors: (i) the difference between the estimated output y_k and the measured output $y_{m,k}$ (ii) the difference between true but unknown input u_k and the measured input $u_{m,k}$. The weights Q and R represent the confidence the estimator puts on input and output data and can be chosen according to the variance of measurement noise.

There are two challenges when one solves the estimation problem in Eq. (4.4). First, the number of optimization variables can be very large, especially when the number of measurements n is large. More specifically, the set of optimization variables includes all of the input values u_k and state variable values x_k at each sampling time, which results an optimization problem with $n \times (n_u + n_x)$ variables.

This can quickly lead to intractability. Second, the dynamic equality constraint Eq. (4.2) makes the problem more difficult to solve, especially for nonlinear systems. The proposed framework can transform the TLS estimation problem (4.4) into an unconstrained optimization problem with only $N \times n_u$ variables, where N is the number of collocation points and is typically much smaller than the number of data points.

4.3 Flatness-Based Pseudospectral Methods

The concept of differential flatness is widely used in different fields [1, 56, 92, 96]. The details on differential flatness can be found in chapter 2. The flatness-based Legendre pseudospectral method is briefly introduced as below.

This chapter uses pseudospectral methods to optimize the trajectory of the flat output z, which furnishes an efficient parameterization method compared to traditional methods using evenly distributed discretization points. This section briefly introduces the implementation of the Legendre pseudospectral method (LPM) for differentially flat systems.

The LPM uses Legendre-Gauss-Lobatto (LGL) points as collocation points. These are the roots of the first derivative of $(N-1)^{\text{th}}$ degree of Legendre polynomial, P_{N-1} [63], where N is the number of discretization points (which are the same as collocation points). The LGL points are located in the range $[-1, 1]$ in a transformed temporal domain. Thus, to use this set of collocation points as discretization points, time should be mapped from $t \in [t_0, t_f]$ to $\tau \in [-1, 1]$ with $\tau_1 = -1$ and $\tau_N = 1$

$$t = \frac{(t_f - t_0)\tau + (t_f + t_0)}{2} \tag{4.5}$$

where t_0 and t_f are the initial time and final time of the optimization.

The flat output trajectory $z(\tau)$ is approximated by a basis of N Lagrange polynomials based on the N collocation points

$$z(\tau) \approx \mathbf{z}(\tau) = \sum_{j=1}^{N} L_j(\tau) z(\tau_j) \tag{4.6}$$

where $\mathbf{z}$ is the interpolated flat output trajectory and the Lagrange polynomial

bases are

$$L_j(\tau) = \prod_{\substack{i=0 \\ i \neq j}}^{N} \frac{\tau - \tau_i}{\tau_j - \tau_i} \tag{4.7}$$

These Lagrange polynomials have the property

$$L_j(\tau_i) = \begin{cases} 1 & \text{if} \quad i = j \\ 0 & \text{if} \quad i \neq j \end{cases} \tag{4.8}$$

which gives accurate interpolated flat output at collocation points, i.e.,

$$\mathbf{z}(\tau_j) = z(\tau_j) \tag{4.9}$$

One benefit of pseudospectral methods is that time derivatives can be calculated analytically using the Lagrange polynomials. The first order derivation of flat output z, for instance, can be expressed as

$$\dot{\mathbf{z}}(\tau_i) = \sum_{j=1}^{N} \dot{L}_j(\tau_i)\mathbf{z}(\tau_j) = \sum_{j=1}^{N} D_1(i,j)\mathbf{z}(\tau_j) \tag{4.10}$$

where $D_1 \in \mathbb{R}^{N \times N}$ is the pseudospectral differentiation matrix defined as $D_1(i,j) = \dot{L}_j(\tau_i)$. The differentiation matrix can be calculated either using Eq. (4.7) or using the following formula

$$D_1(i,j) = \begin{cases} \frac{P_{N-1}(\tau_j)}{P_{N-1}(\tau_i)} \frac{1}{\tau_j - \tau_i} & \text{if} \quad k = i \\ -\frac{(N-1)N}{4} & \text{if} \quad k = i = 1 \\ \frac{(N-1)N}{4} & \text{if} \quad k = i = N \\ 0 & \text{otherwise} \end{cases} \tag{4.11}$$

The r^{th} order derivative of flat output z can be expressed as

$$\mathbf{z}^{(r)}(\tau_i) = \sum_{j=1}^{N} L_j^{(r)}(\tau_i)\mathbf{z}(\tau_j) = \sum_{j=1}^{N} D_r(i,j)\mathbf{z}(\tau_j) \tag{4.12}$$

where $D_r(i,j) = L_j^{(r)}(\tau_i)$. Therefore,

$$Z^{(r)} = D_r Z \tag{4.13}$$

$Z := [\mathbf{z}(\tau_1), \ldots, \mathbf{z}(\tau_N)]^T$ and $Z^{(r)} = [\mathbf{z}^{(r)}(\tau_1), \mathbf{z}^{(r)}(\tau_2), \cdots, \mathbf{z}^{(r)}(\tau_N)]$ is the vector of

r^{th} derivative of . It is shown that the high order differentiation matrix D_r can be expressed as the r^{th} power of D_1, i.e., $D_r = D_1^r$ [74].

Substituting Eq. (4.10) into Eq. (2.30) gives the mappings from z to x and u

$$x(\tau_i) = f_x(Z) \tag{4.14a}$$

$$u(\tau_i) = f_u(Z) \tag{4.14b}$$

The mappings are $\phi_{x,i} : \mathbb{R}^N \mapsto \mathbb{R}^{n_x}$ and $\phi_{u,i} : \mathbb{R}^N \mapsto \mathbb{R}^{n_u}$.

Moreover, the cost function is calculated. Traditional pseudospectral methods calculate the cost function using the quadrature rule at collocation points [61, 97]. This requires the values of input and output variables at collocation points. Typically, these values are available for optimal control problems because the state and input variables evaluated at collocation points are the optimization variables. For estimation problems, however, the measured input and output values are typically available at each sampling time. There are two ways to calculate the cost function in problem (4.4): (i) one can use interpolation to approximate the measured data at the collocation points [97]; (ii) one can calculate the summation of squared errors at each sampling time by interpolating the flat output $z(\tau_i)$ using collocation points following (4.6). This chapter chooses the second approach. This guarantees that the data used for cost function calculation represent real measurements without interpolation among these measurement.

Finally, the optimization problem (4.4) can be transformed into an unconstrained

NLP problem

$$
\begin{aligned}
\min_{\hat{Z},\hat{\theta}} J = & \sum_{k=1}^{n} \left(Q\|\hat{y}_k - y_{m,k}\|_2^2 + R\|\hat{u}_k - u_{m,k}\|_2^2 \right) \\
& \text{s.t:} \\
& \hat{x}(\tau_i) = f_x(\hat{Z}, \hat{\dot{Z}}, \cdots) \\
& \hat{u}(\tau_i) = f_u(\hat{Z}, \hat{\dot{Z}}, \cdots) \\
& \hat{y}_k = g(\hat{x}_k, \hat{u}_k, \hat{\theta}) + v_k \\
& \hat{x}_k \approx \sum_{j=1}^{N} L_j(\tau_k)\hat{x}(\tau_j) \\
& \hat{u}_k \approx \sum_{j=1}^{N} L_j(\tau_k)\hat{u}(\tau_j) \\
& Z^{(r)} = D_r Z
\end{aligned}
\tag{4.15}
$$

with optimization variable as $\hat{Z} \in \mathbb{R}^{Nn_u}$ and $\hat{\theta} \in \mathbb{R}^{Nn_\theta}$. System dynamics (4.1) are automatically satisfied by the exploitation of differential flatness using (2.30). If the problem (4.4) is solved using the traditional way (i.e., optimizing the state and input variables at each sampling time), the total number of optimization variables would be $n \times (n_u + n_x)$ where $n \gg N$, which is computationally very expensive.

Note that the proposed framework can solve the TLS problem with other constraints, such as the state and input constraints, although classical TLS estimation problems do not have these constraints. This has the potential to improve estimation accuracy for problems with physical constraints [67].

4.4 Estimation Example: Nonlinear Mass-Spring-Damper System

4.4.1 Estimation Problem Formulation

This chapter demonstrates the proposed flatness-based pseudospectral framework by solving a state and parameter estimation problem for a nonlinear second order mass-spring-damper system. The dynamics of the nonlinear mass-spring-damper

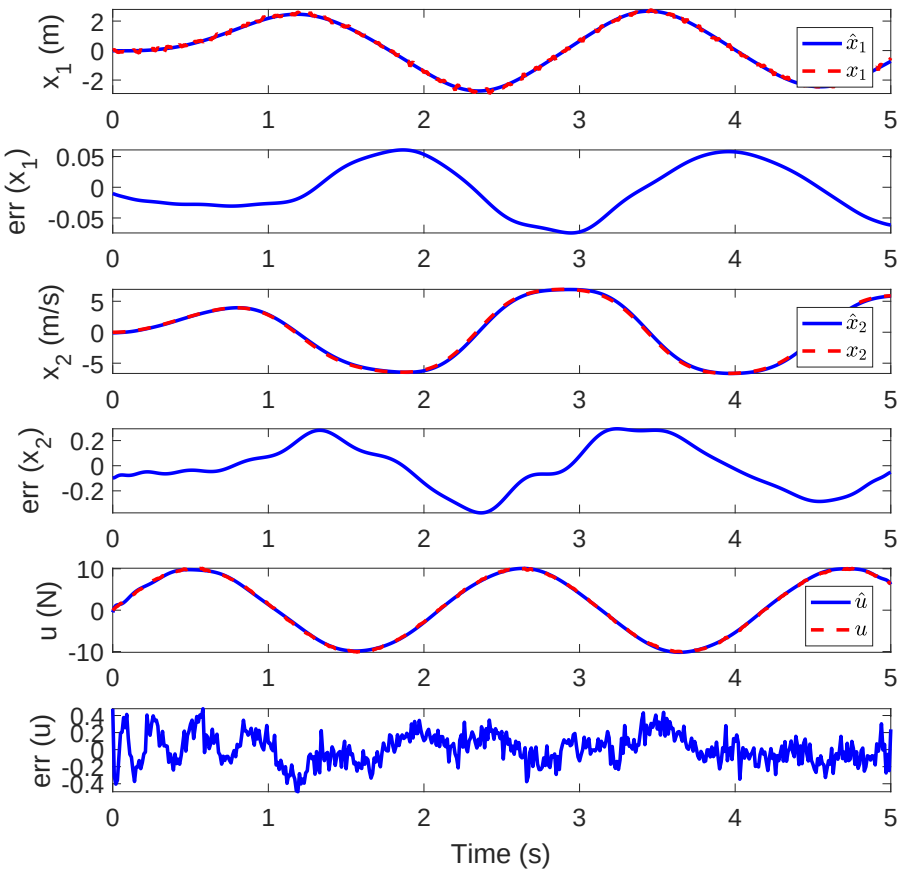

Figure 4.2: Estimation results using noisy input $u = 10sin3t$ with $\delta_u = 0.1$ and $\delta_y = 0.1$. The estimated parameters are: $\hat{\theta} = [0.96, 0.89, 0.99]^T$

system in state-space form are

$$\begin{aligned} \dot{x}_1 &= x_2 \\ \dot{x}_2 &= -\frac{k}{m}x_1^3 - \frac{c}{m}x_2 + \frac{1}{m}(u+w) \\ y_m &= x_1 + v \end{aligned} \tag{4.16}$$

where x_1 and x_2 are the displacement and velocity of the mass, respectively. The parameter vector $\theta = [k, c, m]^T$ comprises the mass $m = 1kg$, the spring constant $k = 1N/m$, and the damping coefficient $c = 1N \cdot s/m$. The input and output measurements are corrupted with additive Gaussian white noise $w \sim N(0, \sigma_u^2)$ and

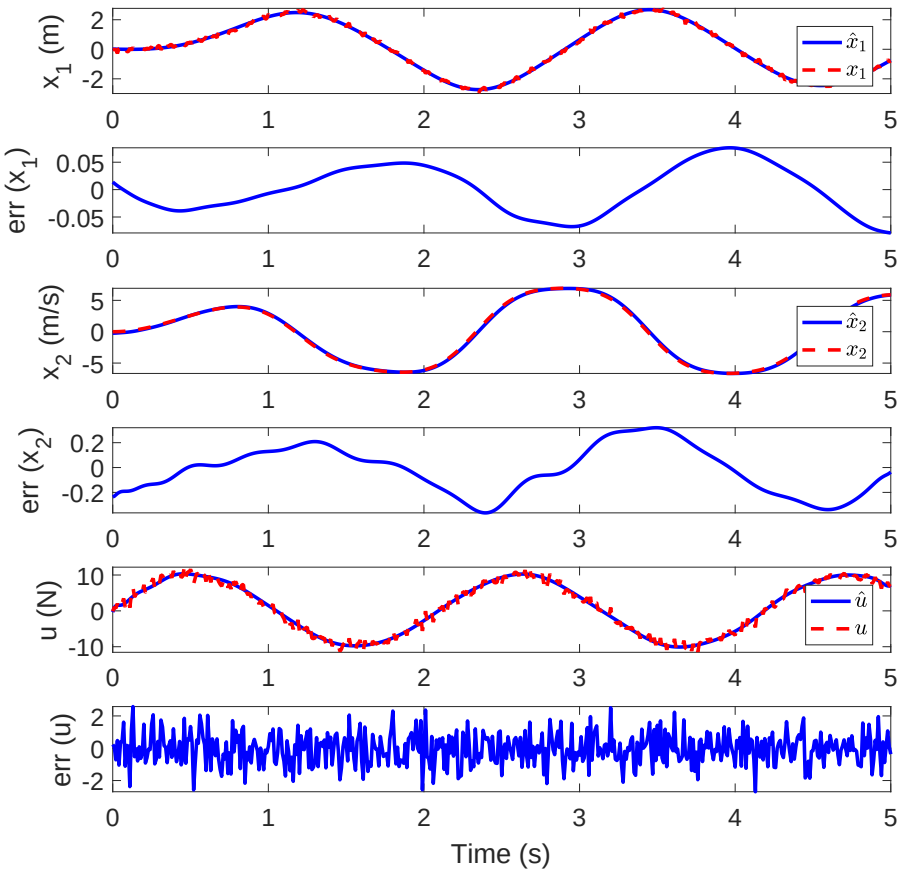

Figure 4.3: Estimation results using noisy input $u = 10sin3t$ with $\delta_u = 1$ and $\delta_y = 0.1$. The estimated parameters are: $\hat{\theta} = [0.96, 0.88, 1.00]^T$.

$v \sim N(0, \sigma_y^2)$, respectively.

The goal in this problem is to estimate the velocity x_2 and all parameters (i.e., k, c, and m) given noisy input measurement u_m and output measurement y_m. This problem has the same formulation as problem (4.4). To solve this estimation problem, the proposed flatness-based pseudospectral framework is adopted. The system (4.16) is differentially flat with the displacement i.e., $z = x_1$, serving as the flat output. The trajectory of the flat output z is optimized using the pseudospectral methods. The resulting NLP problem is solved using the Fmincon function in Matlab.

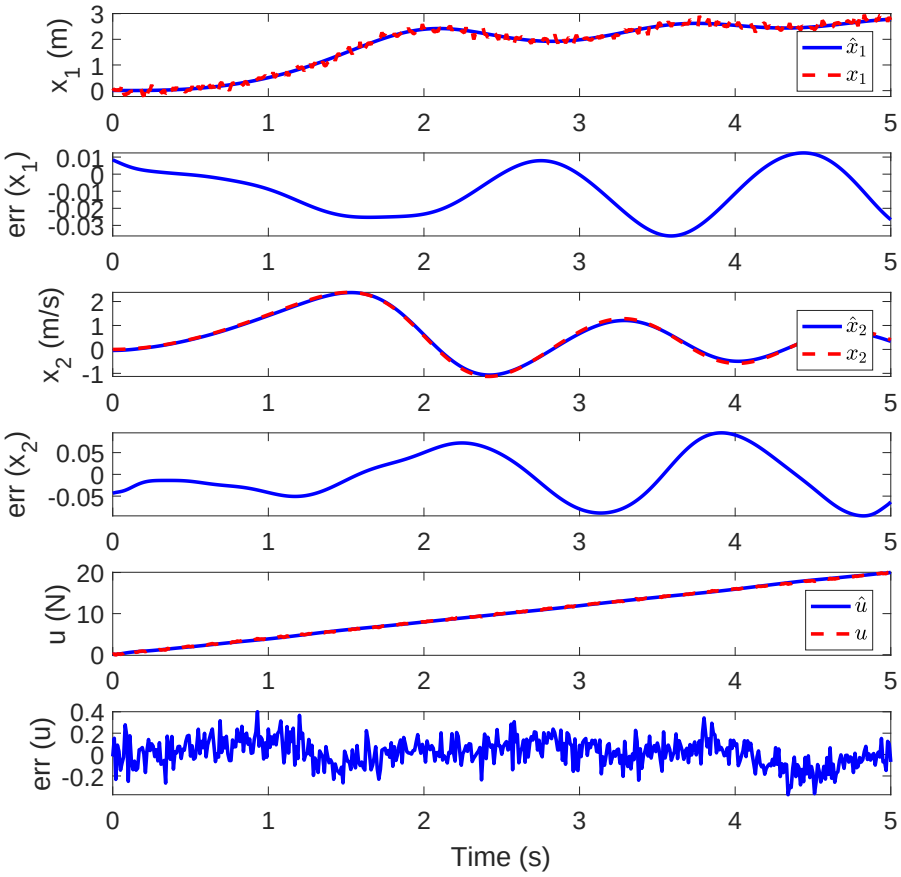

Figure 4.4: Estimation results using noisy input $u = 4t$ with $\delta_u = 0.1$ and $\delta_y = 0.1$. The estimated parameters are: $\hat{\theta} = [1.00, 0.94, 1.01]^T$

4.4.2 Results and Discussion

This chapter adopts two inputs to test the TLS estimator: a sine wave and a ramp input. The variables $\hat{x}_1, \hat{x}_2, \hat{u}$, and $\hat{\theta}$ are the estimated displacement, velocity, input, and parameters respectively. The duration of the problem is $t \in [0s, 5s]$ with the sampling rate $\Delta t = 0.01s$, which implies the number of sampling points $n = 500$. The number of collocation points is set to be $N = 30$. This example adopts the true initial condition as $x_1 = [0, 0]^T$ and the initial guess for TLS estimator to be $\hat{x}_1 = [-10, -10]^T$.

Two inputs are adopted to demonstrate the proposed framework. Figure 4.2

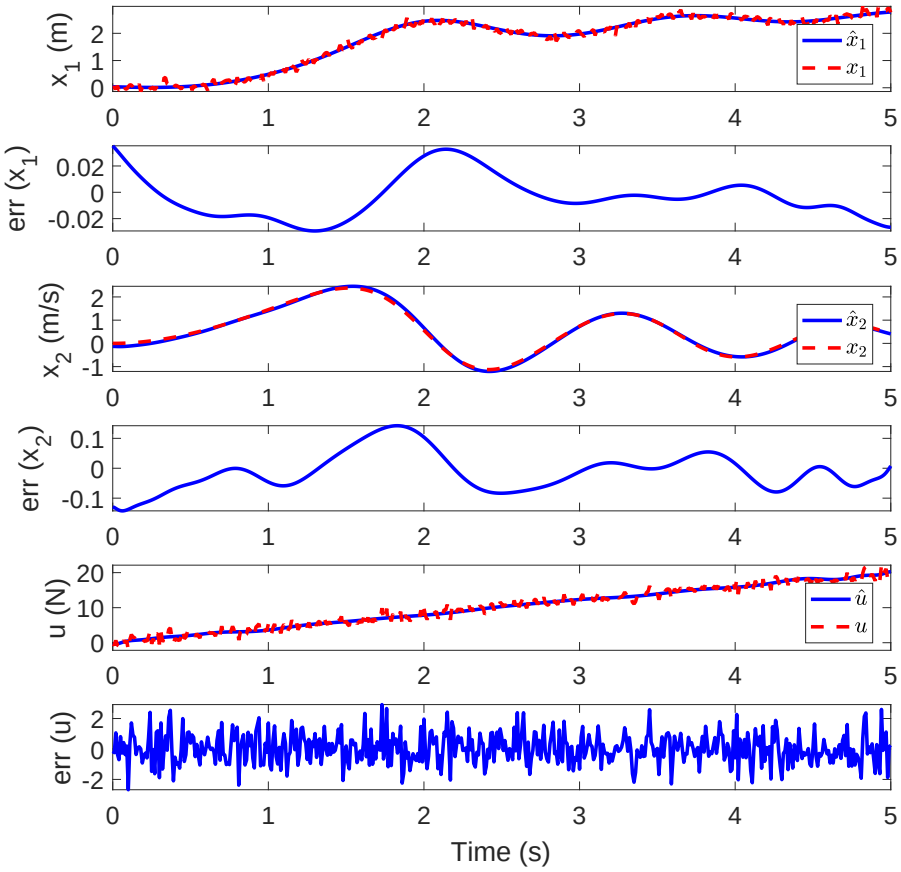

Figure 4.5: Estimation results using noisy input $u = 4t$ with $\delta_u = 1$ and $\delta_y = 0.1$. The estimated parameters are: $\hat{\theta} = [1.00, 0.95, 1.00]^T$.

and Fig. 4.3 use a sine wave as the input and Fig. 4.4 and Fig. 4.5 use a linear input. The term $err(\cdot)$ represents the estimation error, i.e., the difference between estimated value and the true value. Figure 4.3 and Fig. 4.5 have larger input sensor noise and therefore the estimated input has larger absolute error compared to Fig. 4.2 and Fig. 4.4. However, the estimated parameter $\hat{\theta}$ and velocity $\hat{x_2}$ are still very accurate.

Additionally, this chapter demonstrates the proposed framework for the TLS estimator using a Monte-Carlo simulation. We use the root-mean-square error (RMSE) and mean absolute error (MAE) as the metric for the accuracy of the TLS estimator. We simulate the estimator for 100 runs using the same set of parameters

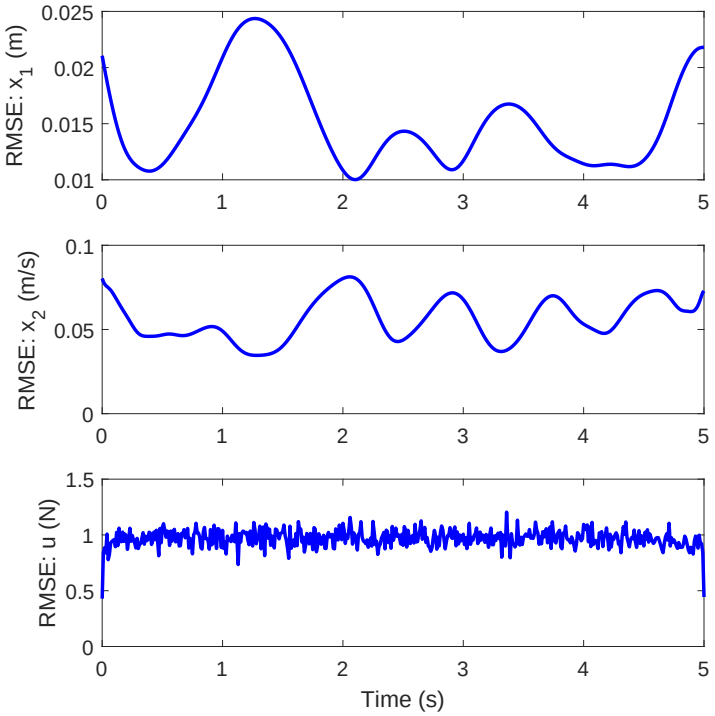

Figure 4.6: Monte Carlo simulation results with $\delta_u = 1$ and $\delta_y = 0.1$. The mean absolute error (MAE) for k, c, and m are 0.56%, 6.86%, and 1.29%, respectively.

as the one used in Fig. 4.2 The average simulation time for each run is 1.54s on a laptop with a 2.4GHz CPU. The results shown in Fig. 4.6 represent the RMSE of the estimator. The state estimation error of the velocity is within about 5% and the parameter estimation error is about 0.5% to 7%, even with a large input noise and moderate output noise.

It is computationally efficient to solve state and parameter estimation problems using the proposed framework for estimation problems. The resulting problem is an unconstrained NLP problem with N+3 = 33 optimization variables (including three parameters). If the problem is discretized using the finite difference method, it would result in a constrained nonlinear optimization problem with $n \times (n_u + n_x) + 3 = 1503$ optimization variables and $n \times n_x = 1000$ dynamical equality constraints.

4.5 Conclusions

This chapter proposes a general computationally efficient framework for total least squares (TLS) nonlinear state and parameter estimation for differentially flat dynamics systems. This framework transforms the original system into the flat output space by exploiting the differential flatness property. The trajectories of the resulting flat output variables are then optimized using pseudospectral methods. The end product is an unconstrained nonlinear programming (NLP) problem which is relatively easy to solve. This significantly reduces the number of optimization variables and eliminates explicit equality constraints to make TLS estimation problems more tractable. This chapter demonstrates the proposed framework by solving a nonlinear TLS state and parameter estimation problem with a nonlinear mass-spring-damper system. The results show the framework to be very efficient and accurate.

Chapter 5
Total Least Squares State of Charge Estimation for Lithium-Ion Batteries: An Efficient Moving Horizon Estimation Approach

5.1 Introduction

This chapter proposes a computationally efficient total least squares (TLS) framework for online state of charge (SOC) estimation with a moving horizon approach. [1] This chapter extends the TLS framework in chapter 4 by (i) adopting a moving horizon estimation approach which is practical for online implementation and (ii) applying the online differential flatness-based TLS framework to battery SOC estimation. The TLS framework in Chapter 4 performs state estimation for the entire trajectory of a dynamic system at once. This means that the framework's computational complexity will grow with time. In contrast, the work in this chapter modified the above framework to enable moving-horizon estimation.

This chapter is motivated by the need for accurate SOC estimation for model-based control. The literature shows that battery model-based control is critical for battery management system (BMS) in terms of safety and longevity [1, 36, 37]. However, to fully achieve the benefits of model-based control strategies, BMS

[1] The work in this chapter has been accepted by a peer-reviewed World Congress of the International Federation of Automatic Control (IFAC WC) paper by the dissertation's author [98]

requires accurate state of charge (SOC) estimation.

Battery SOC estimation problems are studied extensively in the battery control and estimation literature. The tools used for SOC estimation in the literature can be categorized into two classes: (i) open-loop estimation using coulomb counting and open circuit voltage (OCV) lookup table and (ii) closed-loop estimation [35]. The closed-loop SOC estimation techniques can be further classified into two categories: (i) model-based approaches: such as Luenberger observers [36, 37], backstepping observers [38], recursive least squares estimation [39], Kalman filters [40–42, 44–46], optimization-based estimators [47, 48], and (ii) data-driven estimators which may not need a battery model [99, 100]. All of above studies are valuable, in the sense that they contribute to a growing literature showing the challenges and benefits of accurate SOC estimation.

This chapter focuses on battery TLS SOC estimation using a moving horizon approach for the following two reasons. First, we adopt the TLS estimation framework since it explicitly assumes both input and output measurements are corrupted with noise, instead of assuming perfect input measurements and noisy output measurements. Although the TLS estimation for the cell capacity is studied in [101], there are few studies on nonlinear battery TLS SOC estimation. Second, our use of moving-horizon estimation makes it relatively straightforward to incorporate constraints into the estimation process. For example, while this is not done in this chapter, a moving-horizon estimator can constraint its estimates of internal charge concentration within a lithium-ion battery to always remain non-negative.

However, it is computationally challenging to solve the TLS SOC estimation problem online. First, the TLS estimation requires one to estimate all of the input, state, and output variables since both input and output measurements are noisy and therefore need to be estimated. Second, similar to the model predictive control (MPC) strategy, the MHE estimates the battery SOC at each sampling time with the data in the moving horizon. Therefore, the MHE requires the BMS to finish estimating battery SOC within a sampling instant.

Given the above challenges, the overall goal of this chapter is to solve battery TLS SOC estimation problem online in an efficient manner using the differential flatness property. Differential flatness has been adopted in battery online model-based control recently and is quite promising in terms of computational efficiency [1, 58]. Differential flatness makes it possible to express system dynamics using

algebraic equations consisting of only one variable, the *flat output*, without explicit integration [52]. It is true that there are other techniques (e.g., Carleman embedding as in [102, 103]) that can also increase the computational speed. However, the differential flatness property is the property of a system and the transformation using differential flatness is exact and does not involve approximation. Since battery dynamics are shown to be flat [1, 58], the battery SOC estimation problem can be transformed into a static optimization problem with fewer decision variables and no battery dynamics constraint. Recently, several studies adopt the MHE to estimate battery SOC with equivalent circuit models (ECM) [49–51]. However, none of these studies exploit the additional computational gains arising from of the differential flatness property. To the best of authors' knowledge, this work is the first to study battery online TLS SOC estimation problem with differential flatness.

The remainder of this chapter is organized as follows. Section 5.2 introduces a battery equivalent circuit model with thermal dynamics (ECM-T). Section 5.3 formulates the TLS SOC estimation problem and introduces the MHE approach. Additionally, the problem is further formulated using differential flatness. The SOC estimation results with the proposed framework are presented in Section 5.4. Additionally, Monte-Carlo simulation is used for comparing two estimators (i) a flatness-based MHE without constraints, and (ii) a benchmark UKF. Finally, Section 5.5 concludes the chapter and discusses related future work.

5.2 Equivalent Circuit Model with Thermal Dynamics (ECM-T)

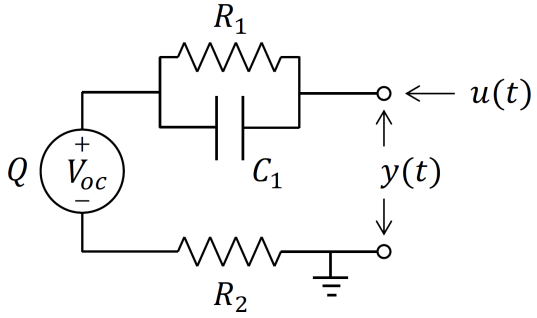

Figure 5.1: Second-order ECM Model

This section describes the governing equations of the ECM-T model used to represent battery thermal and electrochemical dynamics. The ECM-T model consists of an second-order equivalent circuit model (ECM) with first-order thermal dynamics. The battery parameters are identified using commercial A123 26650 lithium iron phosphate (LFP) batteries with 2.3 Ah nominal capacity. The parameters can be found in Table A.1 in Appendix A.

The governing equations for the ECM-T model are shown as below:

$$\dot{x}_1 = \frac{1}{Q}u_1 \tag{5.1a}$$

$$\dot{x}_2 = -\frac{1}{R_1C_1}x_2 + u_1 \tag{5.1b}$$

$$\dot{x}_3 = -\frac{hA}{mC_p}(x_3 - u_2) + \frac{1}{mC_p}u_1x_3\mathrm{S}(x_1) + \frac{1}{mC_p}u_1^2R_2 \tag{5.1c}$$

$$y = \begin{bmatrix} OCV(x_1) + \frac{1}{C_1}x_2 + R_2u_1 \\ x_3 \end{bmatrix} \tag{5.1d}$$

The ECM-T model is a unidirectional model: the diffusion dynamics Eq.(5.1a) and Eq.(5.1b) are not affected by the temperature x_3, but the temperature submodel Eq.(5.1c) is a function of x_1, x_2, and x_3. The state is $x \in \mathbb{R}^{3\times1}$ with x_1 as battery SOC, x_2 the amount of charge in the capacitor C_1, and x_3 cell bulk temperature. The term Q is battery charge capacity, and R_1C_1 is battery diffusion time constant representing battery diffusion dynamics. The term mC_p is the thermal mass of the battery, h is the convection heat transfer coefficient, A is cell surface area, and R_2 is the effective ohmic resistance of the battery. The resistance R_2 couples the electrochemical dynamics of the battery. The input $u \in \mathbb{R}^{2\times1}$ to this model are current u_1 and ambient temperature u_2, and the output, $y \in \mathbb{R}^{2\times1}$, includes the terminal voltage across the battery and bulk temperature. Battery terminal voltage y_1 consists of three components: OCV as a function of x_1, $OCV(x_1)$, the voltage from the RC pair, and the voltage from the internal resistance. The second output is battery bulk temperature.

The first-order lumped parameter thermal model is adopted in this chapter to describe the thermal behavior of lithium-ion batteries [71, 79, 104, 105]. The first term on the right hand side is the convection heat transferred from the surface of the battery to the surroundings. The second term is the reversible or entropic heat

generation term. The last term is the irreversible heat component due to ohmic losses.

The entropy coefficient in electrochemical model is a function of the SOCs in both electrodes [71]. However, this chapter approximates the overall battery entropy coefficient as a fourth-order polynomial as a function of bulk SOC x_1:

$$\mathrm{S}(x_1) = \theta_1 + \theta_2 x_1 + \theta_3 x_1^2 + \theta_4 x_1^3 + \theta_5 x_1^4 \tag{5.2}$$

The entropy coefficient curve (i.e., the θ_i) is identified using least squares estimation from voltage and temperature measurements using experimental data. The identified entropy coefficient curve matches the one from electrochemical model in [106] very well. Details on the identification of entropy coefficient curve can be found in [78].

5.3 Problem Formulation: Total Least Squares SOC Estimation

5.3.1 Moving Horizon Estimation

The MHE strategy is adopted for battery TLS SOC estimation. Although the full-information estimation includes all information using all of the past data as proposed in [84], the problem dimension grows with time. This may not be practical for online battery SOC estimation. Instead, in the literature, a moving horizon approach is adopted for online state estimation. Similar to the model predicative control (MPC) strategy, the MHE approach uses the measurements at each sampling instant within the horizon and implicitly incorporates the prior information. The state estimation problem at time k ($k > N$, where N is the length of the moving horizon) using the MHE strategy can be formulated as follows:

$$
\begin{aligned}
\min_{\{\hat{x}\}_{i=k-N}^{k},\{\hat{u}_1\}_{i=k-N}^{k}} \quad & J_k = \|\hat{x}_{k-N} - \bar{x}_{k-N}\|^2_{\Pi^{-1}} + \sum_{i=k-N}^{k} \|\hat{u}_{1,i} - u^m_{1,i}\|^2_{Q^{-1}} \\
& \quad + \sum_{i=k-N}^{k} \|\hat{y}_i - y^m_i\|^2_{R^{-1}} \\
\text{s.t.:} & \\
& \dot{\hat{x}}_1 = \frac{1}{Q}\hat{u}_1 \\
& \dot{\hat{x}}_2 = -\frac{1}{R_1 C_1}\hat{x}_2 + \hat{u}_1 \\
& \dot{\hat{x}}_3 = -\frac{hA}{mC_p}(\hat{x}_3 - \hat{u}_2) + \frac{1}{mC_p}\hat{u}_1\hat{x}_3 \mathrm{S}(\hat{x}_1) + \frac{1}{mC_p}\hat{u}_1^2 R_2 \\
& \hat{y}_k = \begin{bmatrix} OCV(\hat{x}_{1,k}) + \frac{1}{C_1}\hat{x}_{2,k} + R_2\hat{u}_{1,k} \\ \hat{x}_{3,k} \end{bmatrix} \\
& u_{2,i} = T_{ref}
\end{aligned}
\tag{5.3}
$$

where $\|\cdot\|$ represents the 2-norm. The input and output are corrupted with noise, i.e., $u_k = \hat{u} + w_k$ and output $y_k = \hat{y} + v_k$, where w_k is the input noise added to the input channel, and v_k is the output noise. In this chapter, the input noise w_k and output noise v_k are assumed to be independent and identically distributed (i.i.d.) zero-mean Gaussian noise, i.e., $w_k \in \mathbb{W}$, $v_k \in \mathbb{V}$.

The goal of the optimization is to minimize the estimation error in input and output channels by estimating the state and input trajectories, $\{\hat{x}\}_{i=k-N}^{T}$ and $\{\hat{u}\}_{i=k-N}^{T}$. The error is defined as the difference between the estimated values, $\hat{u_{1,i}}$ and $\hat{y}_i$, and the measured values, $u^m_{1,i}$ and y^m_i. Note that for simplicity, this chapter assumes that the ambient temperature u_2 is constant and known, T_{ref}. One can choose to estimate the ambient temperature by adding another term in the cost function to minimize the measured and estimated ambient temperature. Moreover, to incorporate the previous information that is not included in the moving horizon, the arrival cost is added. The first term in the cost function, $\|(\hat{x}_{i-N} - \bar{x}_{i-N})\|^2_{\Pi^{-1}}$, is the arrival cost. The arrival cost approximates prior information contained in the data outside of the moving horizon, i.e., the past information contained from time $i = 0$ to time $i = k - N - 1$. Specifically, in this chapter we adopt the "filter" update for the arrival cost: it penalizes the deviations of the initial estimate in the

horizon, $\hat{x}_{i-N}$, from an a priori estimate $\bar{x}_{i-N}$ [107].

The matrices Π, Q, R are tuning parameters with positive definite structures. These matrices represent the confidence for the initial guess, input measurements, and output measurements in the cost function J_k, respectively. The weight Π^{-1} for the arrival cost can be (i) a constant positive definite matrix as in [108, 109] or (ii) can be updated as the covariance matrix from the EKF [110]. When the weight Π^{-1} is a zero matrix, it means that the prior information is ignored completely. The inequality constraints can be used to incorporate more information, such as the bounds on the variables with physical values and the known statistical characteristics of the measurement noise [47, 67].

The MHE problem in Eq. (5.3) can be computationally expensive for TLS SOC estimation for two main reasons. First, due to the assumption of the TLS estimation problem that both input and output measurements are noisy, one needs to estimate all of the input, output, and state variables. This can lead to a high dimensional optimization problem. Second, battery SOC estimation problem in Eq. (5.3) is a nonlinear and nonconvex optimization problem. The nonlinearity is due to the nonlinear temperature dynamics in Eq. (5.1c) and the nonconvexity comes from the SOC-OCV curve and the entropy curve in Eq. (5.2). Note that the nonconvexity can lead to local minimum for the MHE problem. Therefore, the differential flatness property of the ECM-T model is exploited to increase the computational speed of battery TLS SOC estimation problem in Eq. (5.1).

5.3.2 Flatness-Based MHE

The dynamics of the ECM and ECM-T model are shown to be differentially flat [98, 111]. In this section, the details on how to identify the flat output vector of the ECM-T model is presented. In addition, the resulting MHE problem using differential flatness is formulated.

Similar to the SPM-T model, the ECM-T model needs two flat outputs as well, i.e., $z \in \mathbb{R}^{2\times 1}$, to represent the dynamics of the ECM-T model, since the model has two inputs, i.e., the input current u_1 and the ambient temperature u_2. The unidirectionally-coupled structure of the ECM-T model can help one to identify the flat output variable: battery electrical dynamics are decoupled from temperature dynamics. Intuitively, one can identify one flat output for battery

diffusion subsystem and second one for the temperature dynamics. Note that the choice of flat output vector may not be unique.

Note that the continuous system in Eq. (5.1) is first used to identify Eq. (2.30) and Eq. (2.31). The first flat output z_1 is chosen to be the first state after one transforms the subsystem of x_1 and x_2 into the controllable canonical form [1]. The state transformation has the following form:

$$\begin{bmatrix} x_1(t) \\ x_2(t) \end{bmatrix} = M \begin{bmatrix} \bar{x}_1(t) \\ \bar{x}_2(t) \end{bmatrix} \tag{5.4}$$

where $[\bar{x}_1, \bar{x}_2]^T$ are the transformed state variables and M is the transformation matrix for the controllable canonical form. For the subsystem of x_1 and x_2 describing the decoupled electrical dynamics of the battery, the flat output can be found to be the first state variable of the transformed state, i.e.,

$$z_1(t) = \bar{x}_1(t) \tag{5.5}$$

Since in the controllable canonical form the states are a chain of integrator except for the last state, the first two states of ECM-T model can be expressed as follows

$$\begin{bmatrix} x_1(t) \\ x_2(t) \end{bmatrix} = f_x(z(t), \dot{z}(t)) = M \left(\begin{bmatrix} 1 & 0 \\ 0 & 1 \end{bmatrix} \begin{bmatrix} z_1(t) \\ \dot{z_1}(t) \end{bmatrix} \right) \tag{5.6}$$

The second flat output needs to describe the dynamics of the bulk temperature and therefore the bulk temperature x_3 can be another flat output, i.e.,

$$z_2(t) = x_3(t) \tag{5.7}$$

Similarly, the input current u_1 can be expressed using the second flat output based on the subsystem of x_1 and x_2 as follows:

$$u_1(t) = [-\alpha_1, -\alpha_2, 1] \begin{bmatrix} z_1(t) \\ \dot{z}_1(t) \\ \ddot{z}_1(t) \end{bmatrix} \tag{5.8}$$

where α_i are the coefficients of the characteristic equation of the subsystem.

Additionally, the dynamics of the temperature x_3 can be expressed as an

algebraic function in terms of z and u_2. Therefore, the second input u_2, the ambient temperature, can be expressed as a function of z by solving the algebraic equation in terms of flat output vector z

$$u_2(t) = h(z(t), \dot{z}(t), \ddot{z}(t)) \tag{5.9}$$

Similarly, the battery output vector y can be expressed as

$$y = \begin{bmatrix} g_1(z(t), \dot{z}(t), \ddot{z}(t)) \\ z_2 \end{bmatrix} \tag{5.10}$$

where $g_1(\cdot)$ is the output equation for cell voltage.

Therefore, the online SOC estimation problem in Eq. (5.3) can be transformed into:

$$\begin{aligned}
\min_{\{\hat{z}_1\}_{i=k-N}^{k}} \quad & J_k = \|(\hat{x}_{k-N} - \bar{x}_{k-N})\|^2_{\Pi^{-1}} + \sum_{i=k-N}^{k} \|\hat{u}_{1,i} - u^m_{1,i}\|^2_{Q^{-1}} \\
& \quad + \sum_{i=k-N}^{k} \|\hat{y}_i - y^m_i\|^2_{R^{-1}} \\
\text{s.t.:} \quad & \\
& z_1(t) = \bar{x}_1(t) \\
& z_2(t) = x_3(t) \\
& x(t) = f_x(z(t), \dot{z}(t)) \\
& u_1(t) = [-\alpha_1, -\alpha_2, 1] \begin{bmatrix} z_1(t) \\ \dot{z}_1(t) \\ \ddot{z}_1(t) \end{bmatrix} \\
& u_2(t) = h(z(t), \dot{z}(t), \ddot{z}(t)) \\
& \hat{y}_k = \begin{bmatrix} g_1(\hat{z}_k, \hat{\dot{z}}_k, \hat{\ddot{z}}_k) \\ \hat{z}_{2,k} \end{bmatrix} \\
& u_{2,k} = T_{ref}
\end{aligned} \tag{5.11}$$

The estimated state at the beginning of the moving window $\hat{x}_{k-N}$, input and output noise are expressed as functions of the flat output trajectory and its derivatives. One benefit of using the flatness property is that the system dynamics Eq.

(5.1) are automatically satisfied by adopting Eq. (5.6), Eq. (5.8) - Eq. (5.10). Therefore, compared to the problem in Eq. (5.3), the transformed problem in Eq. (5.11) does not have battery dynamic equality constraints. Essentially, the battery TLS SOC estimation problem is now transformed into a static optimization problem in which one only needs to optimize the trajectory of the flat output.

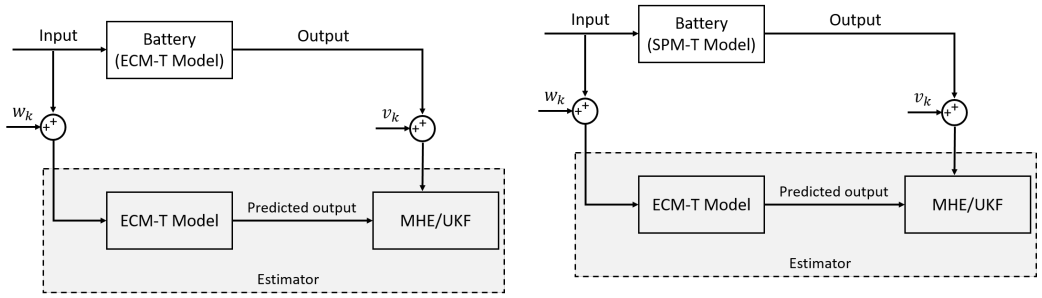

(a) Only include measurement uncertainties

(b) Include model and measurement uncertainties

Figure 5.2: Diagrams for estimators with uncertainties

To solve the problem in Eq. (5.11), the highest order derivative of the flat output is parameterized as a piecewise constant function over the moving horizon [55]. The flat output and its lower order derivatives are then calculated by integrating its highest order derivatives. For each integration, one introduces an integration constant which is treated as one of the decision variables. According to authors' experience and the literature, the integration procedure is numerically more stable than directly differentiating the flat output trajectory [95, 112].

5.4 Results and Discussion

This section demonstrates the proposed flatness-based MHE approach for battery SOC estimation. As shown in Fig. 5.2, two uncertainties are considered: i) measurement uncertainties and ii) model uncertainties. In the first section, only measurements uncertainties are considered as shown in Fig. 5.2a. The data used in the estimator is generated by simulating a ECM-T model and adding Gaussian noise to the measurements. In the section section, both model and measurement uncertainties are considered as illustrated in Fig. 5.2b. The SPM-T model is considered as the "true" battery which provides battery response. The ECM-T model is used in the estimator.

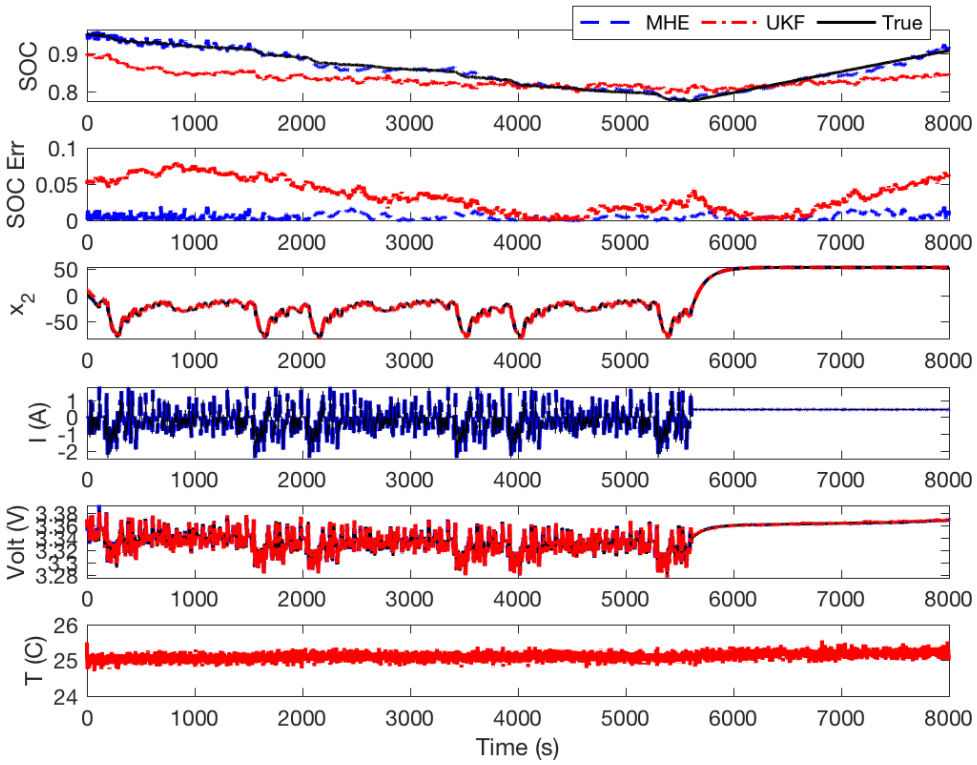

Figure 5.3: SOC estimation results comparison at high SOC region (starting from 95% SOC): MHE (blue dashed lines), UKF (red dash-dot lines), and true signals (black lines).

5.4.1 Estimation Results with Only Measurement Uncertainties

This section considers only the uncertainties due to measurement noise. This section conducts the Monte-Carlo simulation using two estimation algorithms (i)MHE, and (ii) a benchmark UKF. Moreover, the Monte-Carlo simulation results are presented and compared, which shows the difference in SOC estimation accuracy and convergence rate.

Each estimation scheme shares the same simulation parameters which are shown as follows. The parameters of the ECM-T model used in this chapter come from [78]. The battery's input current trajectory is produced by simulating the battery pack load associated with a 100-mile range electric vehicle (i.e., EV-100), then scaling the resulting simulated current down to match the capacity of the battery cell used in this study. The Federal Test Procedure 75 (FTP-75) cycle is adopted for the

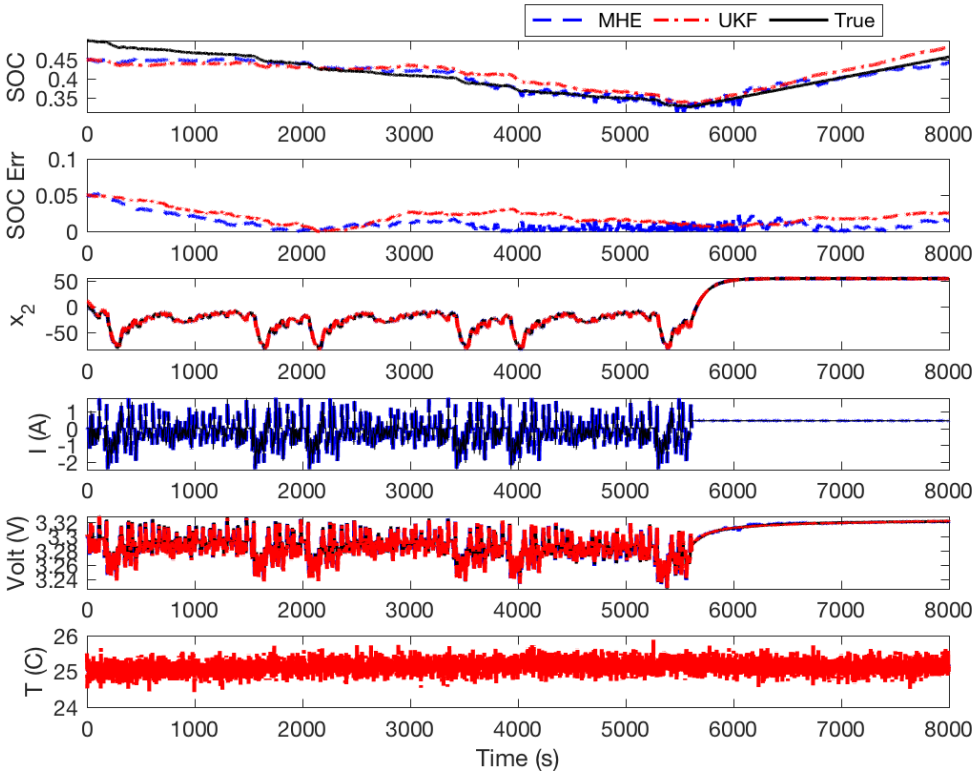

Figure 5.4: SOC estimation results comparison at mid-SOC region (starting from 50% SOC): MHE (blue dashed lines), UKF (red dash-dot lines), and true signals (black lines).

simulation study. The measurements are sampled at every second (i.e., $dt = 1s$). The length of the moving horizon is chosen to be 3, i.e., $N = 3$. The measurement noise is zero-mean Gaussian noise, i.e., $w_k \sim N(0, \sigma_w)$ and $v_k \sim N(0, \sigma_v)$. The standard deviation for the noise is: $\sigma_w = 0.02A$ and $\sigma_v = [0.02V, 0.02K]^T$. The problem (5.11) is solved in MATLAB with the *fmincon* function.

Table 5.1: The mean absolute error (MAE) and the root mean square error (RMSE) of estimators with different scenarios. Left table corresponds to the results shown in Fig. 5.3 and right table corresponds to the results shown in Fig. 5.4.

Error type	MHE	UKF
MAE	7.0393×10^{-4}	0.0132
RMSE	0.0859	1.4269

Error type	MHE	UKF
MAE	0.0058	0.0163
RMSE	0.8895	1.8442

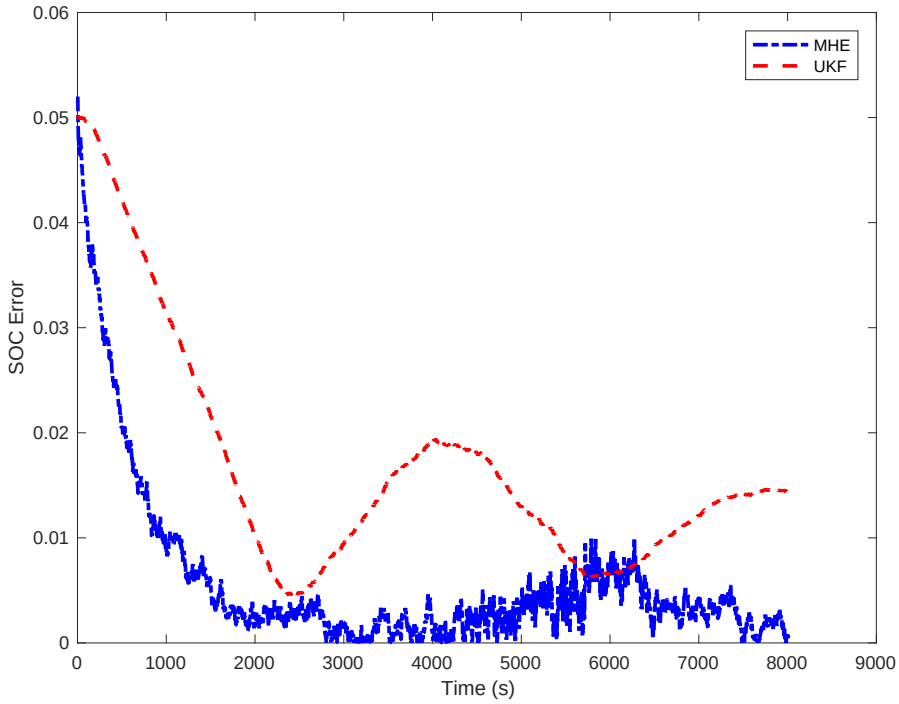

Figure 5.5: Monte-Carlo simulation results from (i) MHE and (ii) UKF. The initial SOC is 50% and this corresponds to the mid-range SOC where OCV curve is flat.

5.4.1.1 Comparative Study: MHE Vs. UKF

The SOC estimation accuracy of two estimators (MHE and UKF) are compared. The Kalman filters are widely used in battery SOC estimation. An introduction to UKF-based estimation can be found in [113]. The MHE and UKF share the same set of parameters to have a "fair" comparison. Note that although the computational efficiency of the TLS estimator is significantly improved with differential flatness, it still needs to solve optimization problem. Compared to the MHE, UKF does not need to solve optimization problem. Therefore, from the simulation time, the UKF is more efficient than the MHE. It takes about 26s computer time to give the estimated SOC for a 9000s simulation, compared to about 2000s computer time by MHE.

Figure 5.3 and Fig. 5.4 depict the state estimation results of the proposed moving horizon TLS estimation framework and the benchmark UKF. Figure 5.3 corresponds to the case starting at 95% SOC with the initial guess for each estimator to be $\hat{x}_0 = x_0 + [-0.05, 1, 0.1]^T$, where x_0 is the true initial state. Figure 5.4 corresponds to the case starting at 50% SOC with the initial guess for each estimator to be

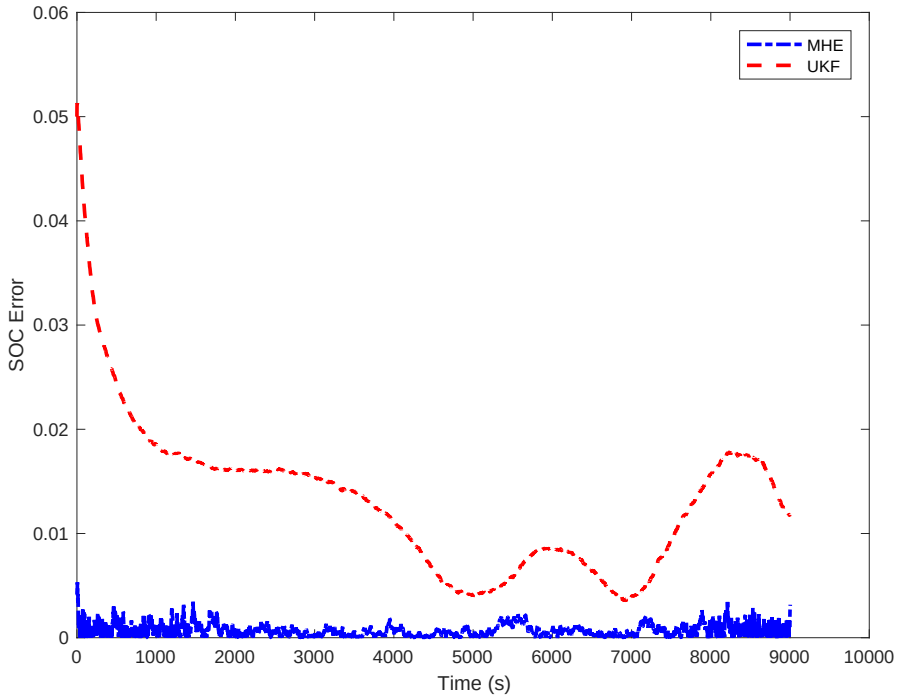

Figure 5.6: Monte-Carlo simulation results from (i) MHE and (ii) UKF. The initial SOC is 95% and this corresponds to the mid-range SOC where OCV curve has large slope.

$\hat{x}_0 = x_0 + [0.05, 1, 0.1]^T$, where x_0 is the true initial state. The MHE estimator provides relatively accurate SOC estimation and input current estimation. There is larger SOC error for this case due to the fact the SOC-OCV slope is flatter than the case at 95% SOC. The mean absolute error (MAE) and root mean square error (RMSE) for each case are listed in Table 5.1. For both cases (i.e., mid-SOC region and high SOC region), the MHE gives more accurate results in terms of the MAE and RMSE.

Additionally, this chapter conducts the Monte-Carlo simulation to further demonstrate the accuracy of both estimators with two initial SOCs: (i) 50% SOC (where the OCV-SOC curve is relatively flat) and (ii) 95% SOC (where the OCV-SOC curve has relatively large slope). Figure 5.5 and Fig. 5.6 show that the MHE scheme can provide the most accurate SOC estimation for both cases. This relates to the fact that (i) the MHE strategy includes the data from several sampling steps instead of one; and (ii) the weigh on the prior information in the MHE helps to estimate SOC with smaller variance (i.e., RMSE) and estimation bias (i.e., MAE).

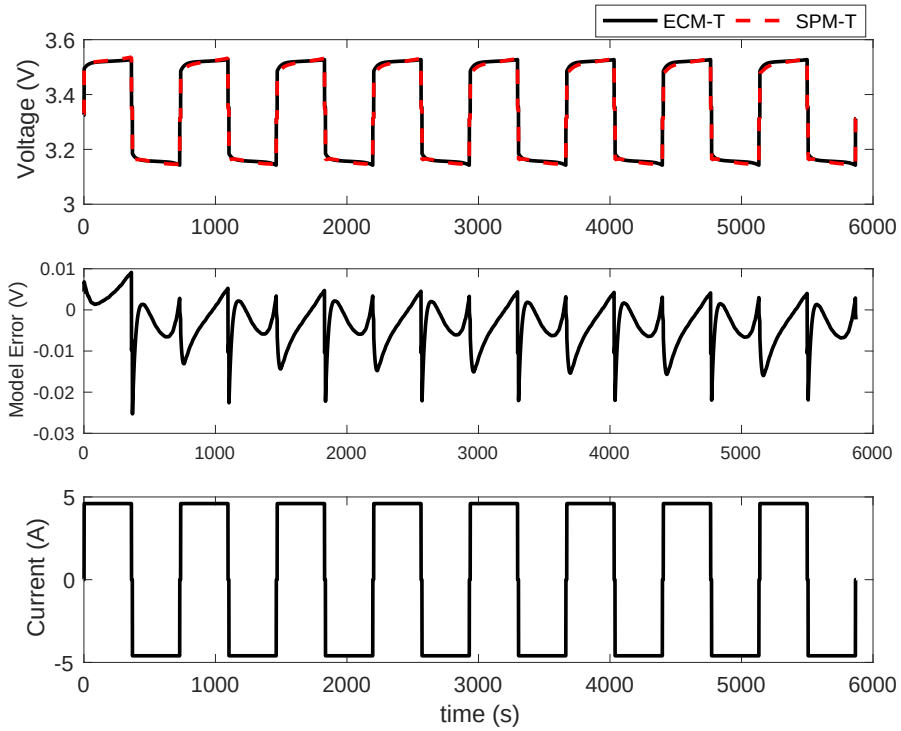

Figure 5.7: Model uncertainties: the ECM-T model used in the estimator is identified using the response generated with the SPM-T model which is considered as the "ture" model in section 5.4.2 .

Comparing the results shown in Fig. 5.5 and Fig. 5.6, the estimation results in the mid-SOC region are jeopardized by the slope of OCV curve. This relates to the fact that battery SOC is more observable in high SOC region than in the mid-range SOC region where SOC-OCV curve is flat, which is the same with the conclusions from some studies in the literature [32–34].

Table 5.2: The mean absolute error (MAE) and the root mean square error (RMSE) of estimators with model uncertainties and measurement uncertainties.

Error type	MHE	UKF
MAE	0.1205	0.2008
RMSE	5.4356	09.4653

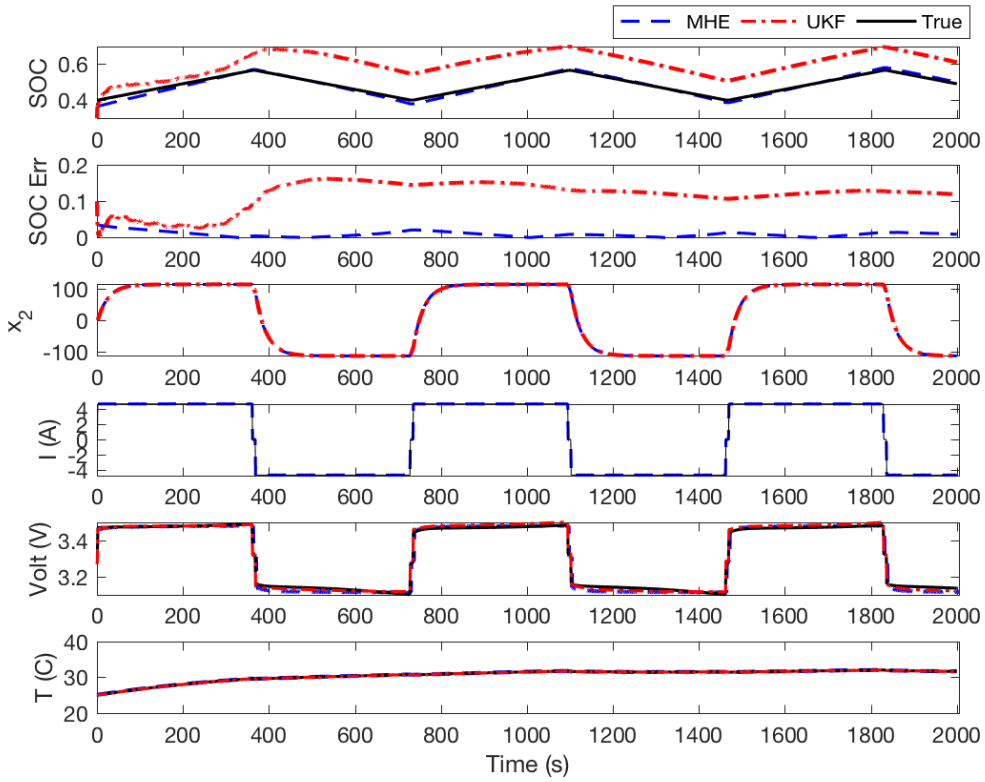

Figure 5.8: SOC estimation results with model uncertainties: MHE (blue dashed lines), UKF (red dash-dot lines), and true signals (black lines).

5.4.2 Estimation Results with Model and Measurement Uncertainties

This section investigates the effects of both measurement uncertainties and model uncertainties on estimation accuracy as illustrated in Fig. 5.2b. The SPM-T model is considered as the "true" battery model which generates the data by simulating the SPM-T model and the ECM-T model is used in the estimator. The parameters of the ECM-T are identified using the response from the SPM-T model. The identified ECM-T is used in the estimator to predict voltage. Figure 5.7 shows that using the ECM-T model in the estimator leads to relatively large voltage prediction error compared to the SPM-T model, which is considered as the true battery model.

Figure 5.8 depicts the simulation results of this study. The results show that the estimated SOC from the MHE is more accurate than the ones from the UKF.

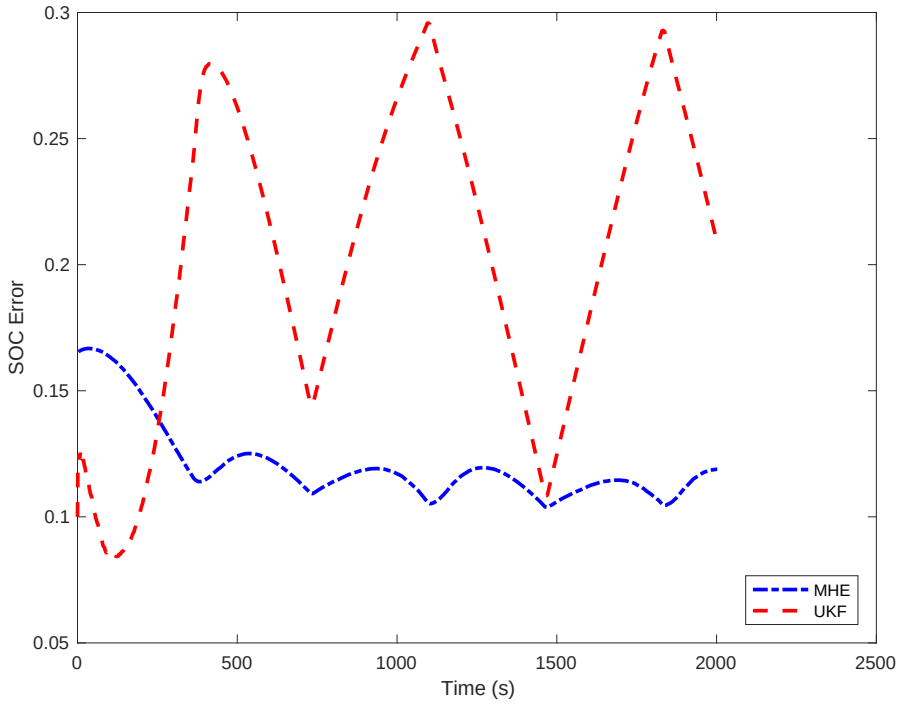

Figure 5.9: Monte-Carlo simulation results from (i) MHE and (ii) UKF.

Compared to the ones shown in Fig. 5.3 and Fig. 5.4, the estimation results shown in Fig. 5.8 has much larger estimation error. This is due to the fact that not only measurements are corrupted noise but also the model is not accurate any more. However, it shows that the MHE can still provide relative more accurate SOC estimates compared to the UKF. Moreover, this section also conducts a Monte Carlo simulation study using the same set of parameters for the MHE and UKF to study the accuracy of two estimators. The Monte Carlo results are shown in Fig. 5.9 and estimation error is shown in Table 5.2. The MHE is shown to give better estimates compared to the UKF.

5.5 Conclusions

This chapter proposes a computationally efficient framework for lithium-ion battery total least squares (TLS) state of charge (SOC) estimation. The proposed framework exploits the differential flatness property of battery dynamics, which makes it possible to represent battery dynamics using only flat output trajectories. An equivalent circuit model with thermal dynamics (ECM-T) is used to predict battery

dynamics. With the moving horizon strategy (MHE), the proposed TLS SOC estimation framework is demonstrated by comparing the results to a benchmark UKF. The results show that the MHE can achieve higher SOC estimation accuracy with (i) only measurement uncertainties and (ii) both measurement and model uncertainties.

Chapter 6
Experimental Validation of Total Least Squares SOC Estimation with A Moving Horizon Approach

6.1 Introduction

This chapter experimentally validates the proposed flatness-based total least squares (TLS) state of charge (SOC) estimation framework.[1] In addition, this chapter extends the proposed framework in Chapter 5 by using a physics-based electrochemical-thermal single particle model with thermal dynamics (SPM-T), instead of the ECM-T model.

Recently, several studies adopt MHE to estimate battery SOC with equivalent circuit models (ECM) [49–51]. There are two unique contributions of the work in this chapter. First, none of the MHE work exploits the additional computational gains with the exploitation of the differential flatness property. Additionally, the use of ECM, although simple, can bring a critical challenge for battery health management: unlike the physics-based battery models, ECM models are not designed to predict battery physical variables, such as electrode potentials, reaction rates or SEI layer thickness. Without estimating the physical variables, it is difficult to design health-conscious battery control algorithms.

[1] The work in Chapter 6 is in preparation for peer-reviewed publication.

To the best of authors' knowledge, this work is the first to study and experimentally validate battery TLS SOC estimation problem by (i) exploiting the differential flatness property of battery and (ii) using physics-based electrochemical-thermal battery model with a moving horizon estimation approach. Based on the literature and the simulation results using the ECM-T model in chapter 5, this chapter proposes several hypotheses to be validated via experimental data. The proposed hypotheses are listed as follows:

- State of charge estimation accuracy will increase as the size of the moving horizon used for estimation is increased: a hypothesis which, if validated experimentally, also suggests that the selection of the moving horizon's size involves a tradeoff between estimation accuracy and computational cost.
- The incorporation of prior information in the MHE strategy increases the accuracy of SOC estimation.
- The use of temperature measurements, in addition to current/voltage measurements (and therefore the use of a temperature-dependent model such as the SPM-T model), improves the accuracy of SOC estimation.

The remainder of the chapter is organized as follows. The TLS SOC estimation problem is first formulated in Section 6.2. Section 6.3 presents the details of the SPM-T model's system identification using experimental data. In Section 6.4, the SOC estimation results are compared to the experimental data and the hypotheses proposed in Section 1 are discussed. Finally, this chapter is concluded in Section 6.5

6.2 Problem Formulation

6.2.1 Total Least Squares Moving Horizon Estimation

This section formulates the TLS SOC estimation problem using the SPM-T model with a moving horizon estimation approach. The governing equations of the nonlinear SPM-T model can be found in chapter 3.

The MHE strategy is adopted for battery TLS SOC estimation in this chapter. Similar to the TLS SOC estimation problem using the ECM-T proposed in Chapter 5, the TLS SOC estimation problem can be formulated as follows

$$
\begin{aligned}
\min_{\{\hat{x}\}_{i=T-N}^{T},\{\hat{u}_1\}_{i=k-N}^{k}} \quad & J_k = \|(\hat{x}_{k-N} - \bar{x}_{k-N})\|_{\Pi^{-1}}^2 + \sum_{i=k-N}^{k} \|\hat{u}_i - u_i^m\|_{Q^{-1}}^2 \\
& \quad + \sum_{i=k-N}^{k} \|\hat{y}_i - y_i^m\|_{R^{-1}}^2 \\
\text{s.t:} \quad & \\
& \dot{\hat{x}}(t) = f(\hat{x}(t), \hat{u}(t)) \\
& \hat{y}_k = f(\hat{x}_k, \hat{u}_k)
\end{aligned} \tag{6.1}
$$

where the subscript k represents the corresponding values at k-th sampling instant. The symbol $\|\cdot\|$ represents the 2-norm. The goal of the optimization is to minimize the estimation error in input and output channels by estimating the state and input trajectories, $\{\hat{x}\}_{i=k-N}^{T}$ and $\{\hat{u}\}_{i=k-N}^{T}$. The error is defined as the difference between the estimated values, $\hat{u}_i$ and $\hat{y}_i$, and the measured values, u_i^m and y_i^m. One can choose to estimate the ambient temperature by adding another term in the cost function to minimize the difference between the measured and estimated ambient temperature. Moreover, to incorporate the previous information that is not included in the moving horizon, the arrival cost is added. The matrices Π, Q, R are tuning parameters with positive definite structures. These matrices represent the confidence for the initial guess, input measurements, and output measurements in the cost function J_k, respectively. The weight Π^{-1} for the arrival cost can be (i) a constant positive definite matrix as in [108, 109] or (ii) can be updated as the covariance matrix from the EKF [110]. The input noise is added to the input channel and the measured input is the true input u_k^t with noise w_k, i.e., $u_k^m = u_k^t + w_k$ and v_k is the output noise.

The MHE problem in Eq. (6.1) can be computationally expensive for TLS SOC estimation for two main reasons. First, due to the assumption of the TLS estimation problem that both input and output measurements are noisy, one needs to estimate all of the input, output, and state variables. This can lead to a high dimensional optimization problem. Second, battery SOC estimation problem in Eq. (6.1) is a nonlinear and nonconvex optimization problem. The nonlinearity is due to the coupled electrochemical-thermal dynamics of the SPM-T model shown in Chapter 2.2 and the nonconvexity comes from the the Butler-Volmer kinetics in Eq.

(2.13), the SOC-OCV curve, and the entropy curve (5.2). Therefore, the differential flatness property of the ECM-T model is exploited to increase the computational speed of battery TLS SOC estimation problem in Eq. (6.1).

6.2.2 Flatness-Based Estimation

The concept of differential flatness and how one can apply this concept to the SPM-T model are introduced in chapter 3. Based on the flatness-based analysis, the problem in Eq. (6.1) can be further transformed into the following problem

$$
\begin{aligned}
\min_{\{\hat{x}\}_{i=T-N}^{T},\{\hat{u}\}_{i=k-N}^{k}} \quad & J_k = \|(\hat{x}_{k-N} - \bar{x}_{k-N})\|^2_{\Pi^{-1}} + \sum_{i=k-N}^{k} \|\hat{u}_i - u_i^m\|^2_{Q^{-1}} \\
& \quad + \sum_{i=k-N}^{k} \|\hat{y}_i - y_i^m\|^2_{R^{-1}} \\
\text{s.t:} \quad & \\
& \hat{x}(\tau_i) = f_x(\hat{z}(\tau_i), \hat{\dot{z}}(\tau_i), \ldots, \hat{z}^{(\alpha)}(\tau_i)) \\
& \hat{u}(\tau_i) = f_u(\hat{z}(\tau_i), \hat{\dot{z}}(\tau_i), \ldots, \hat{z}^{(\beta)}(\tau_i)) \\
& \hat{z}(\tau_i) = f_z(\hat{x}(\tau_i), \hat{u}(\tau_i), \hat{\dot{u}}(\tau_i), \cdots, \hat{u}^{(\gamma)}(\tau_i)) \\
& \hat{y}_k = f(\hat{x}_k, \hat{u}_k) \\
& \text{where } i = 1, 2, \cdots, N
\end{aligned}
\tag{6.2}
$$

6.3 System Identification of SPM-T Model

This chapter briefly presents the details on system identification of the SPM-T model of commercial A123 26650 lithium iron phosphate (LFP) cells. Battery cells are placed in the thermal chamber which provides approximately constant ambient temperature. The Arbin battery cycler is used to measure input current and output voltage accurately. Additionally, battery surface temperature is measured with one thermocouple attached to the surface of the cell and the temperature data is collected with Arduino board and Matlab using a laptop computer.

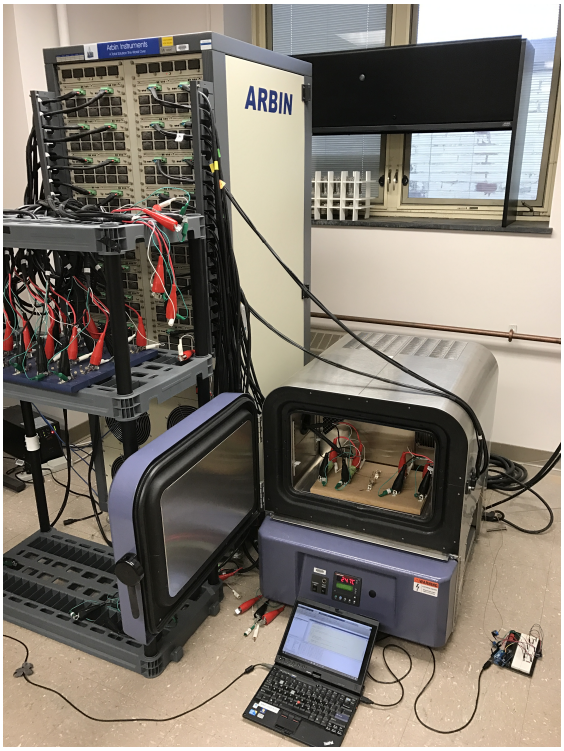

Figure 6.1: Experimental setup

6.3.1 SOC-OCV Curve

First, the SOC-OCV curve is measured and battery capacity is calculated by the following steps.

- First, the cell is discharged to empty, defined as 2V in this chapter.
- Second, the cell is charged with the CCCV strategy, where the constant current is 0.1C (i.e., 0.24A) and the cut off current is 0.01A, until the cell reaches 3.8V.
- Third, the cell is similarly discharged with the CCCV strategy until the cell reaches 2V.
- Fourth, battery charge and discharge capacity are calculated by integrating the current during the second and the third step, respectively. Battery SOC is calculated by dividing the charge in the cell by the charge/discharge capacity.

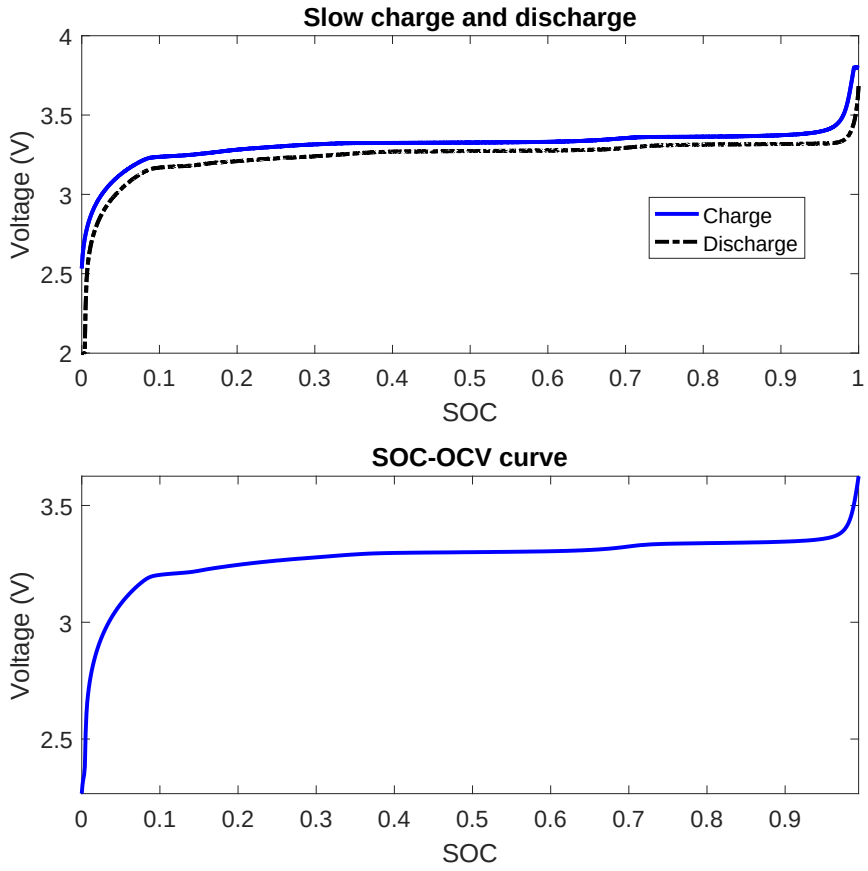

Figure 6.2: Measured OCV curve through slow charging and discharging

- Finally, the SOC-OCV curve is calculated by averaging the voltage responses during discharging and charging.

Figure 6.2 depicts the resulting experimental results of the above process and the resulting OCV curve.

6.3.2 Parameter Identification

This subsection presents the details on the parameter identification of the SPM-T model that is used in the online TLS SOC estimator. First, we introduce the parameters to be identified. Second, least squares estimation is adopted to identify the parameters using a set of different experiments.

Table 6.1 lists all the parameters that need to be estimated and other parameters

Table 6.1: The parameters to be estimated in the SPM-T model

Parameter	Type
Active material volume fraction ϵ_j	Static
Stoichiometry, $\theta_{n,0}$, $\theta_{p,0}$, $\theta_{n,100}$, $\theta_{p,100}$	Static
Solid state lithium diffusion coefficient, $D_{s,j}$	Electrochemical & Dynamic
reaction rate constant, k_j	Electrochemical & Dynamic
Effective internal resistance, R_{cell}	Electrochemical & Dynamic
Activation Energy, $Ea_{D,j}$	Thermal & Dynamic
Activation Energy, $Ea_{k,j}$	Thermal & Dynamic
Thermal time constant, $\frac{hA}{mCp}$	Thermal & Dynamic
Thermal capacity, mCp	Thermal & Dynamic

not listed are obtained from the literature.

In this chapter, as shown in Table 6.1, the parameters are grouped into 3 categories: (i) static parameters; (ii) electrochemical & dynamics parameters, and (iii) thermal & dynamics parameters. The parameters (including the identified ones) for the SPM-T model are shown in Table B.1. The details on the parameter identification are shown as below.

6.3.2.1 Static Parameters

Static parameters are the ones that can be estimated using only the SOC-OCV curve and do not need the data from battery dynamic tests. To identify the stoichiometry values of the tested cells, one needs to calculate the OCV curve using the reference potential curve from each electrode, U_j and match the measured OCV curve shown in Fig. 6.2. We formulate a least squares estimation problem to achieve this as follows:

$$\begin{aligned} \min_{\theta_{n,0},\theta_{p,0},\theta_{n,100},\theta_{p,100}} \; & J = \sum_{i=1}^{N} (OCV_{meas,i} - OCV_{est,i})^2 \\ \text{s.t.:} \; & SOC_{n,i} = SOC_{cell,i}(\theta_{n,100} - x_0) + \theta_{n,0} \\ & SOC_{p,i} = -SOC_{cell,i}(\theta_{p,100} - \theta_{p,0}) + \theta_{p,100} \\ & OCV_{est,i} = U_p(SOC_{p,i}) - U_n(SOC_{n,i}) \end{aligned} \tag{6.3}$$

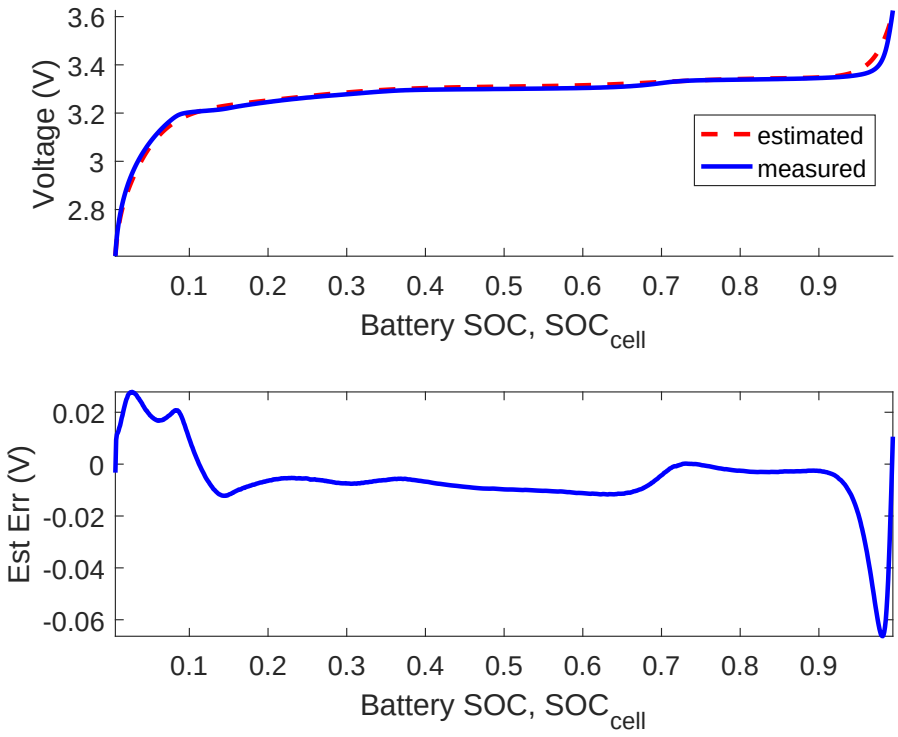

Figure 6.3: Identification of static parameters: Measured OCV curve through slow charging and discharging

Basically, one needs to discretize the range of cell SOC, $SOC_{cell} \in [0, 1]$ into N values. For each $SOC_{cell,i}$, one can calculate a corresponding OCV value, $OCV_{est,i}$. The goal of this optimization is to optimize the stoichiometry values such that the overall least squares error between the measured OCV, OCV_{meas}, and the optimized OCV, OCV_{est} is minimum. Figure 6.3 shows the estimated OCV OCV_{est}, measured OCV, OCV_{meas}, and the OCV estimation error. The problem is solved with using the fmincon function in Matlab with multiple initial guesses, which is known as multi-start strategy. This strategy is used for all the parameter identification optimization in this chapter, in order to increase the chance of reaching global optimum.

With the estimated stoichiometry values optimized in problem (6.3), one can calculate the active material volume fraction ϵ_n using the following relationship.

$$Q_{dis} = \epsilon_n(\theta_{n,100} - \theta_{n,0})S_n L_n F c_{s,n,max} \tag{6.4}$$

$$Q_{ch} = \epsilon_p(\theta_{p,100} - \theta_{p,0})S_p L_p F c_{s,p,max} \tag{6.5}$$

6.3.2.2 Dynamic Parameters

A dynamic cycling experiment is used for estimating the parameters pertaining to both the thermal and electrochemical battery parameters simultaneously. In this case, we solve the following least-squares parameter estimation problem:

$$\begin{aligned}
\min_{D_{s,j},k_j,R_{cell},Ea_{D,j},Ea_{k,j},\frac{hA}{mCp},mCp} \quad & J = \sum_{i=1}^{n} \left(Q(V_{meas,i} - V_{est,i})^2 + R(T_{meas,i} - T_{est,i})^2 \right) \\
\text{s.t:} \quad & \\
& V_{est} = y_1 \\
& T_{est} = y_2 \\
& \dot{x}(t) = f(x(t), u(t)) \\
& y = g(x(t), u(t)) \\
& SOC(0) = SOC_{ini}
\end{aligned} \tag{6.6}$$

where n is the number of data points in the experiment, V_m and T_m are measured voltage and temperature, and V_{est} and T_{est} are the simulated voltage and temperature from the SPM-T model. The terms Q and R are the weights for voltage and temperature error. The optimization is subject to the dynamics of the SPM-T model presented in chapter 3. We use least squares estimation to minimize the sum of the squared difference between the measured voltage and the output voltage from simulation at each data point. Before conducting the test, the cell is preconditioned to the initial SOC, SOC_{ini}, by (i) discharging the cell to empty (i.e., 2V) and (ii) then charging the cell to the target SOC_{ini} by coulomb counting using the Arbin battery cycler. Due to the high accuracy of the cycler, the initial SOC, $SOC(0)$ is assumed to be known a priori. A sequence of battery current pluses is used for parameter estimation. The optimization problem is scaled in MATLAB to avoid numerical issues due to very different ranges among estimated parameters.

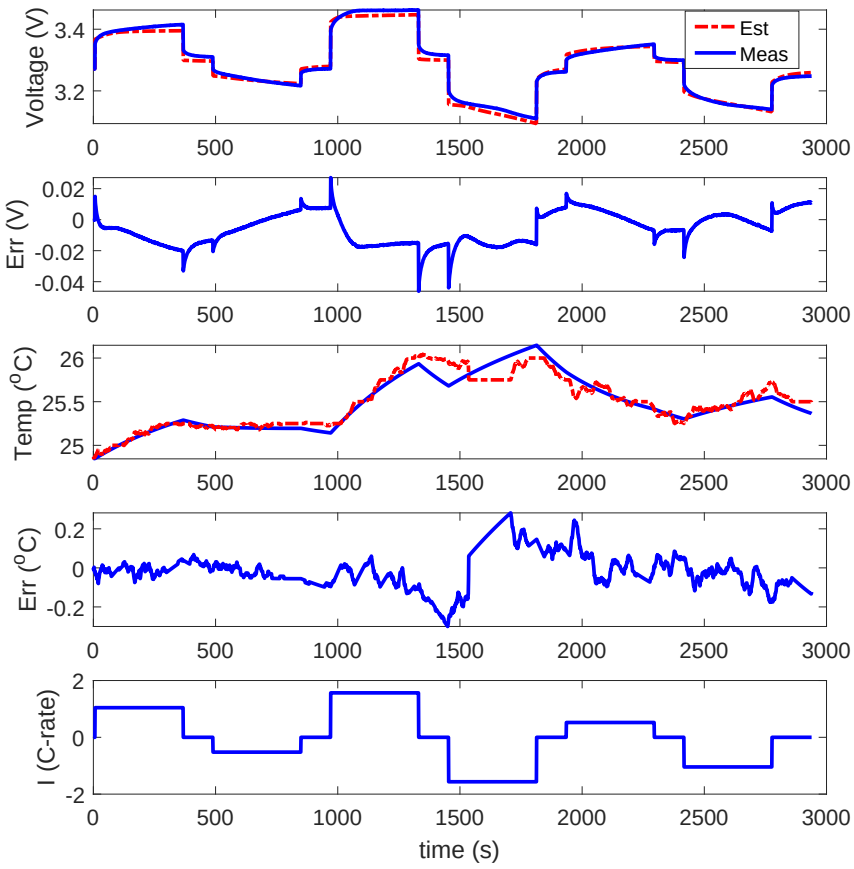

Figure 6.4: Response from measurement (Meas) and identified SPM-T model (Est)

The parameters that are not estimated in this chapter are obtained from [2, 3].

Figure 6.4 presents voltage and temperature response from measurements and model prediction error for both battery temperature and voltage. The model prediction error is defined as:

$$\text{Model Error} = y_{est} - y_{meas} \tag{6.7}$$

where y_{est} is the estimated or model predicted output and y_{meas} is the measured output in the tests. The means absolute error (AE) of the identified SPM-T model for the voltage and temperature is 9.5 mV and 0.07^oC, respectively. The root mean square error (RMSE) are 11.3 mV and 0.09^oC for the voltage and temperature, respectively. Figure 6.4 also depicts model errors in voltage (second subplot) and

temperature (fourth subplot) as a function of time. The identified parameters and other model parameters can be found in Table B.1.

6.4 Results and Discussion

Table 6.2: The mean absolute error (MAE) and the root mean square error (RMSE) of SOC estates with the MHE estimator.

Model	Prior info	Moving horizon	SOC range	MAE	RMSE
SPM	No, $\Pi^{-1} = \mathbf{0}$	$N = 1$	0.25-0.45	0.1413	0.1758
SPM	No, $\Pi^{-1} = \mathbf{0}$	$N = 3$	0.25-0.45	0.0586	0.0835
SPM	No, $\Pi^{-1} \neq \mathbf{0}$	$N = 1$	0.25-0.45	0.0519	0.0640
SPM	Yes, $\Pi^{-1} \neq \mathbf{0}$	$N = 3$	0.25-0.45	0.0192	0.0226
SPM-T	Yes, $\Pi^{-1} \neq \mathbf{0}$	$N = 3$	0.25-0.45	0.0175	0.0217

This section presents the SOC estimation results using the framework proposed in Sec. 6.2. The proposed hypotheses in Sec. 1 are examined using different setups of the MHE and different experiments. Table 6.2 summaries the mean AE and RMSE of different scenarios.

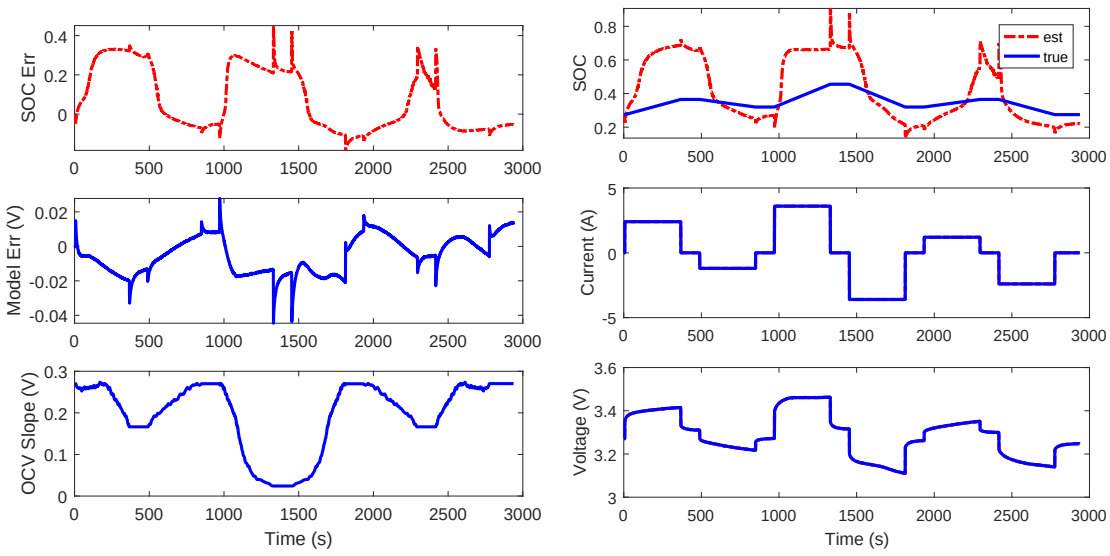

Figure 6.5: SOC estimation results using the SPM model, with $N = 1$, and without the prior information.

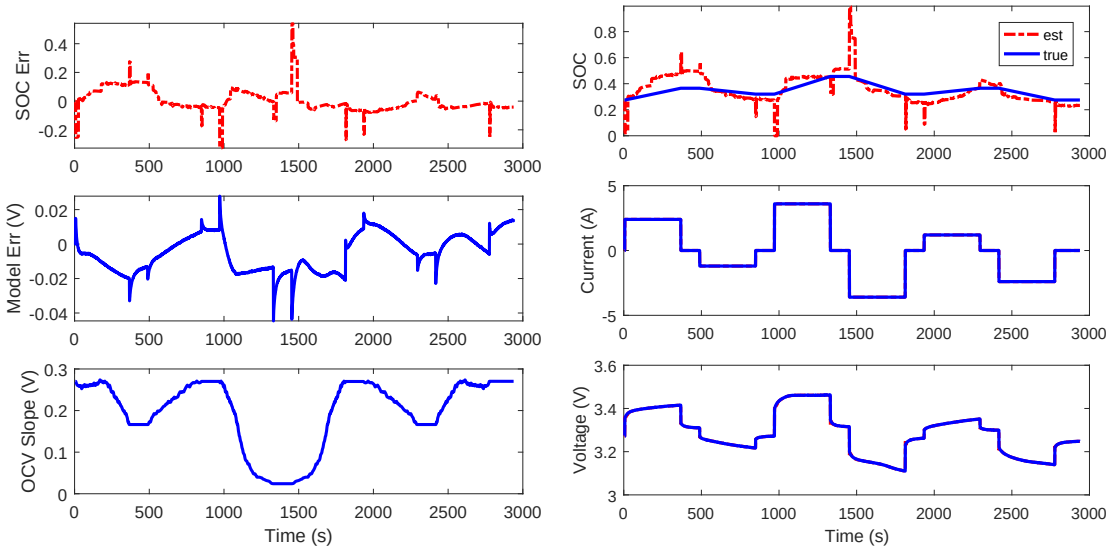

Figure 6.6: SOC estimation results using the SPM model, with $N = 3$, and without the prior information.

First, the effect of the size of the moving horizon (i.e., the number of measurements included) is studied. To make the comparison easier, we only change the moving horizon length from $N = 1$ to $N = 3$. The MHE uses the SPM model and does not include any prior information, i.e., $\Pi^{-1} = \mathbf{0}$. Although the SPM model is used, both scenarios share the same setup except N. One can see the difference from Fig. 6.5 and Fig. 6.6. Figure 6.5 depicts the estimation results and error with $N = 1$ and no prior information. One can see that in Fig. 6.5 the SOC estimation error is large and has very similar trend with the model voltage error. Since no prior information is used, every iteration is independent, and SOC estimates are essentially determined from instantaneous vltage/current measurements. Since the Arbin battery cycler is quite accurate, model prediction error dominates and shows up in SOC error. When three measurements are used ($N = 4$), as shown in in Fig. 6.6, the accuracy of the SOC estimation is significantly improved. When the length of the moving horizon is larger than one ($N > 1$), the MHE minimizes the estimation error in input and output measurements collected at each sampling time within the horizon. This averages the error due to model prediction and measurement at one time step. Therefore, by having longer horizon, one can estimate battery SOC more accurately.

Second, the effect of the inclusion of prior information is studied. The comparison

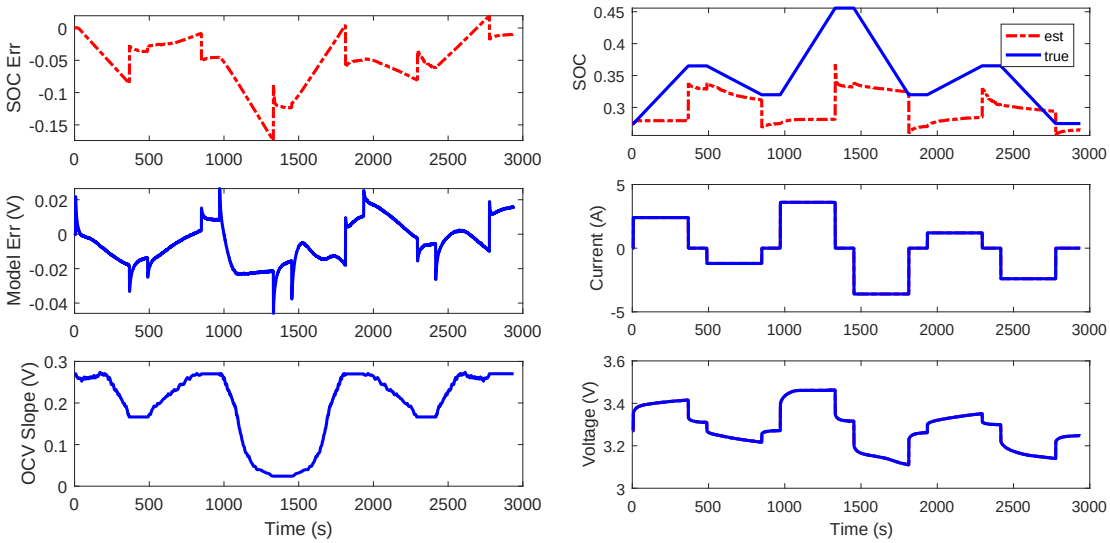

Figure 6.7: SOC estimation results using the SPM model, with $N = 1$, and with the prior information.

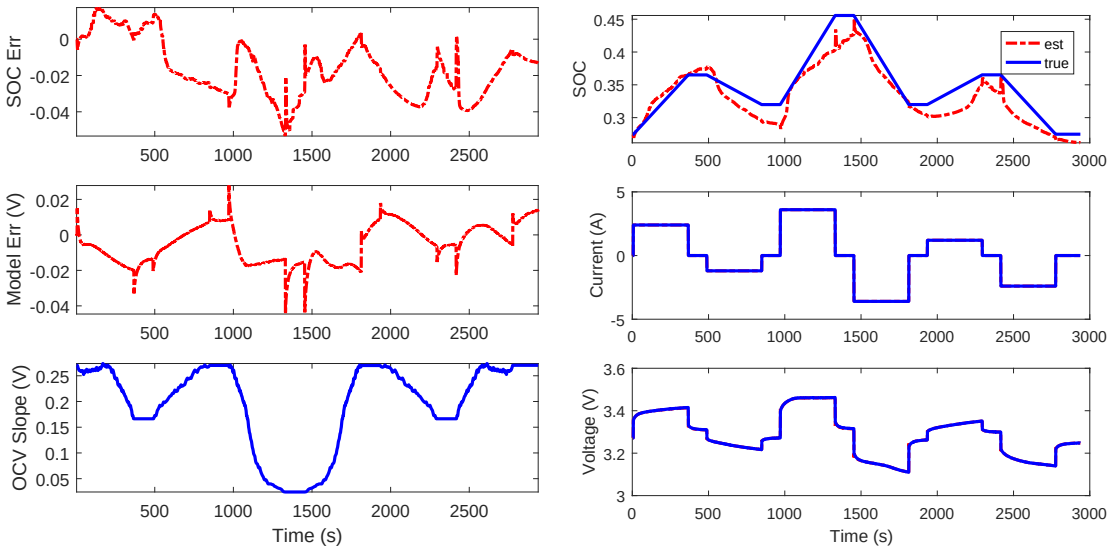

Figure 6.8: SOC estimation results using the SPM model, with $N = 3$, and with the prior information.

is made by including the prior information for $N = 1$ and $N = 3$, respectively. The SOC estimation error is significantly decreased by adding the prior information. For $N = 1$, by comparing the results shown in Fig. 6.5 and Fig. 6.7, one can see by adding the prior information, both the mean AE and RMSE of estimated SOC are decreased. Similar improvement can be seen in Fig. 6.6 and Fig. 6.8. The

improvement is due to the inclusion of prior information, which penalizes deviations of the initial estimate in the horizon at the current step from a prior estimate. The use of prior information is particularly valuable in mid-range SOCs, where the slope of the OCV-SOC curve is smaller and less conducive to accurate SOC estimation. In that scenario, propagation SOC estimates forward based on prior information provides an attractive accuracy benefit.

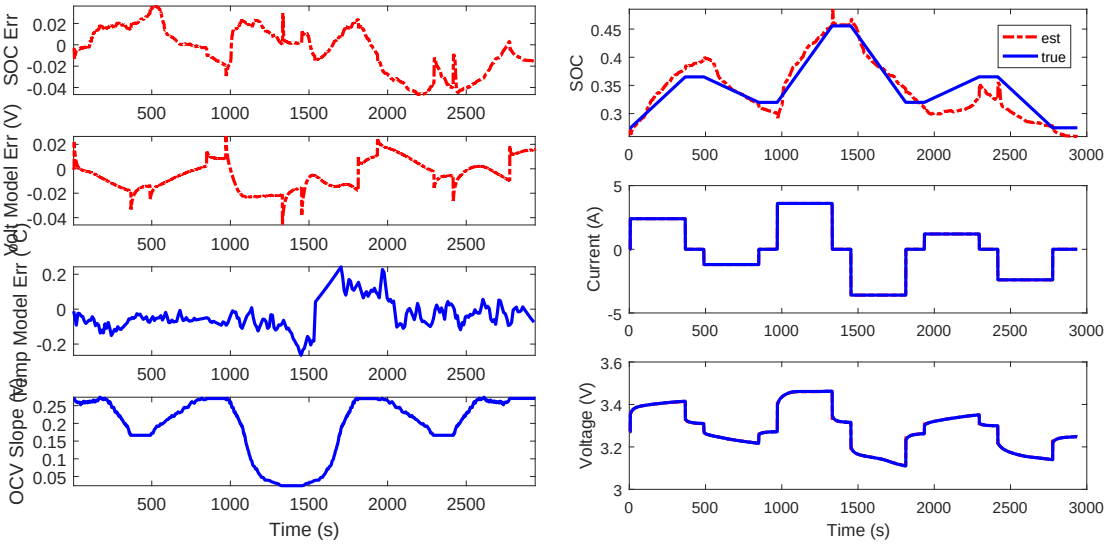

Figure 6.9: SOC estimation results using the SPM-T model, with $N = 3$, and with the prior information.

Third, the effect of adding the temperature model is investigated. Figure 6.9 presents the SOC estimation results using the SPM-T model. It may be difficult to observe apparent improvement from the plots, compared to the results shown in Fig. 6.8. It can be seen from Table 6.2 that the mean AE and the RSME are decreased slightly by adding the thermal sub-model. There are two possible factors contributing to this improvement. The first one is related to the fact that temperature and voltage measurements provide more information for the estimator than using only voltage measurement. At the region where only voltage measurement cannot achieve accurate SOC estimate, the added temperature measurement can provide extra information for the estimator. Specifically, the entropic heat generation term, which relates to electrode SOC, affects the thermal dynamics and hence battery temperature as shown in [114]. The second factor is that the SPM-T model gives smaller voltage model prediction error than the SPM

model. Based on the results, using the SPM-T model instead of the SPM model can improve the SOC estimation accuracy.

6.5 Conclusions

This chapter experimentally validates the previously proposed flatness-based total least squares (TLS) SOC estimation framework. The SPM-T model is identified with experimental data and used in the MHE. Four hypotheses are proposed and examined using the experiments. The conclusions of the hypotheses can be summarised as follows:

- Multiple measurements in the moving horizon can significantly improve the accuracy of SOC estimation.
- The incorporation of the prior information in the MHE strategy can significantly improve the accuracy of SOC estimation.
- The temperature measurement (i.e., using the SPM-T model instead of the SPM model) can slightly improve the accuracy of the SOC estimation.

Chapter 7
Conclusions

This dissertation presents an online framework for computationally efficient health-conscious model-based battery control and estimation by exploiting the differential flatness property. Each chapter of this dissertation is summarized in the follow list.

1. Chapter 1 presents the background and motivation of health-conscious model-based control and estimation and the literature review that emphasizes the importance of this dissertation. More specifically, this dissertation builds on the literature that highlights the fundamental challenge of (i) the computational complexity of online model-based battery control and estimation and (ii) accurate battery SOC estimation.

2. Chapter 2 presents a framework for the computationally-efficient, health-conscious optimization of battery charge trajectories. This framework brings together ideas from the battery model reformulation, differential flatness, and pseudo-spectral optimization literatures. The framework is 5 times faster than pseudo-spectral optimization alone, and generates battery charge trajectories that, unlike classical CCCV charging, are able to avoid side reaction overpotentials conducive to lithium plating: a critical degradation mechanism in lithium-ion batteries.

3. Chapter 3 extends the framework from Chapter 2 in three important ways. First, unlike Chapter 2, it does not assume significant time-scale separation between the diffusion dynamics of the positive and negative battery electrodes. This creates a redundancy between these electrodes' respective flat output variables. The law of conservation of charge is used for eliminating this

redundancy a priori, leading to an "extended" differential flatness-based optimization approach. Second, unlike Chapter 2, the battery model used for optimization is no longer assumed to be isothermal, and the optimization framework is extended to combined thermo-electrochemical models. Finally, Chapter 3 also utilizes the proposed framework for nonlinear model predictive control (NMPC), as opposed to offline optimization.

4. Chapter 4 presents a framework for the computationally efficient total least squares (TLS) combined state and parameter estimation in differentially flat systems. This framework forms a foundation for subsequent work in Chapters 5 and 6, but is initially demonstrated on a simple nonlinear mass-spring-damper problem.

5. Chapter 5 solves the battery state of charge (SOC) estimation problem with a total least squares (TLS) framework and a moving horizon approach. The battery TLS SOC estimation problem is then solved using the proposed flatness-based framework with a ECM-T model. It is shown in simulation that the moving horizon estimation (MHE) can achieve better accuracy than a benchmark unscented Kalman filter (UKF).

6. Chapter 6 validates the proposed TLS SOC online estimation framework presented in chapter 5 using experimental data. Instead of the ECM-T model, the chapter also extends the previous framework by using the SPM-T model. The SPM-T model parameters are first identified and then used in the moving horizon estimator for battery TLS SOC estimation. The experimental results show that it is possible to estimate battery SOC accurately using the flatness-based MHE.

Appendix A
Model Parameters: Equivalent Circuit Model with Thermal Dynamics (ECM-T)

This appendix provides the parameters for the ECM-T model used in chapter 5. The parameters are identified using commercial A123 26650 lithium iron phosphate (LFP) cells. The entropy coefficient curve is identified by measuring the voltage difference at different teesquares when the cell is at equilibrium. The details on the parameter identification can be found in [78].

Table A.1: The parameters of 2.3Ah 26650 $LiFePO_4$ cells.

Parameter	Value
Q (As)	8174.3
$R_1C_1(s)$	120.4
C_1 (F)	3960.9
$R_2(\omega)$	0.0192
$hA/mCp(s)$	0.0009
mCp (J/^{o}K)	50.8
θ_1	-2.43×10^{-4}
θ_2	3.325×10^{-4}
θ_3	2.3×10^{-3}
θ_4	-4.9×10^{-3}
θ_5	2.6×10^{-3}
$S(SOC) = \theta_1 + \theta_2 SOC + \theta_3 SOC^2 + \theta_4 SOC^3 + \theta_5 SOC^4$	

Appendix B
Model Parameters: Single Particle Model with Thermal Dynamics (SPM-T)

This appendix provides the parameters for the SPM-T model used in chapter 6. The parameters are identified using commercial A123 26650 lithium iron phosphate (LFP) cells. The parameters of the thermal dynamics shown in A.1 and B.1 are different. This is due to the fact that the parameters presented in Table B.1 correspond to the cells that are put in the thermal chamber whereas Table A.1 corresponds to the cells that are put in the test bed outside of the thermal chamber.

Table B.1: The parameters of 2.3Ah 26650 $LiFePO_4$ cells. e: identified parameters at 25^oC ambient temperature. Other parameters are obtained from [2,3]. Reference potential curve for each electrode is obtained from [2] and the entropy coefficient curve for each electrode is from [4].

Parameter	Negative electrode	Positive electrode
L_j (μm)	70	34
A_j (cm^2)	1694	1755
R_j (nm)	36.5	3500
$c_{s,j,\max}$ (mol/m^3)	22806	31370
$D_{s,j}$ (m^2/s)	1.26×10^{-15e}	$1.6.48 \times 10^{-15e}$
k_j ($A/m^2(mol/m^3)^{1.5}$)	8.692×10^{-7}	1.127×10^{-7}
$Ea_{D,j}$ (kJ/mol)	79.8^e	30.2^e
$Ea_{k,j}$ (kJ/mol)	55.6^e	174^e
α_j	0.5	0.5
ϵ_j	0.35^e	0.45^e
$\theta_{j,0}$	0^e	0.82^e
$\theta_{j,100}$	0.02^e	0.90^e
c_e (mol/L)	1	
R_{cell} (mΩ)	9^e	
F (C/mol)	96487	
R (J/(mol· K))	8.3143	
hA/mCp (1/s)	0.0026^e	
T_{ref} (^oC)	25	

Bibliography

[1] Liu, J., G. Li, and H. K. Fathy (2015) "Efficient Lithium-Ion Battery Model Predictive Control Using Differential Flatness-Based Pseudospectral Methods," in *ASME 2015 Dynamic Systems and Control Conference*, American Society of Mechanical Engineers, pp. V001T13A005–V001T13A005.

[2] Safari, M. and C. Delacourt (2011) "Modeling of a commercial graphite/LiFePO4 cell," *Journal of the Electrochemical Society*, **158**(5), pp. A562–A571.

[3] Forman, J. C., S. J. Moura, J. L. Stein, and H. K. Fathy (2011) "Genetic parameter identification of the Doyle-Fuller-Newman model from experimental cycling of a LiFePO 4 battery," in *American Control Conference (ACC), 2011*, IEEE, pp. 362–369.

[4] Viswanathan, V. V., D. Choi, D. Wang, W. Xu, S. Towne, R. E. Williford, J.-G. Zhang, J. Liu, and Z. Yang (2010) "Effect of entropy change of lithium intercalation in cathodes and anodes on Li-ion battery thermal management," *Journal of Power Sources*, **195**(11), pp. 3720–3729.

[5] Moura, S., N. Chaturvedi, and M. Krstic (2013) "Constraint management in Li-ion batteries: A modified reference governor approach," in *American Control Conference (ACC), 2013*, IEEE, pp. 5332–5337.

[6] Rahn, C. D. and C.-Y. Wang (2013) *Battery systems engineering*, John Wiley & Sons.

[7] Klein, R., N. A. Chaturvedi, J. Christensen, J. Ahmed, R. Findeisen, and A. Kojic (2013) "Electrochemical model based observer design for a lithium-ion battery," *Control Systems Technology, IEEE Transactions on*, **21**(2), pp. 289–301.

[8] Rothenberger, M. J. (2016) "Optimal input shaping for Fisher identifiability of control-oriented lithium-ion battery models," .

[9] Klein, R., N. Chaturvedi, J. Christensen, J. Ahmed, R. Findeisen, and A. Kojic (2011) "Optimal charging strategies in lithium-ion battery," in *American Control Conference (ACC), 2011*, pp. 382–387.

[10] Chaturvedi, N. A., R. Klein, J. Christensen, J. Ahmed, and A. Kojic (2010) "Modeling, estimation, and control challenges for lithium-ion batteries," in *American Control Conference (ACC), 2010*, IEEE, pp. 1997–2002.

[11] Rahimian, S. K., S. Rayman, and R. E. White (2011) "Optimal charge rates for a lithium ion cell," *Journal of Power Sources*, **196**(23), pp. 10297–10304.

[12] Smith, K. A., C. D. Rahn, and C.-Y. Wang (2010) "Model-based electrochemical estimation and constraint management for pulse operation of lithium ion batteries," *Control Systems Technology, IEEE Transactions on*, **18**(3), pp. 654–663.

[13] Suthar, B., P. W. Northrop, R. D. Braatz, and V. R. Subramanian (2014) "Optimal Charging Profiles with Minimal Intercalation-Induced Stresses for Lithium-Ion Batteries Using Reformulated Pseudo 2-Dimensional Models," *Journal of The Electrochemical Society*, **161**(11), pp. F3144–F3155.

[14] Tanim, T. R., C. D. Rahn, and C.-Y. Wang (2015) "A temperature dependent, single particle, lithium ion cell model including electrolyte diffusion," *Journal of Dynamic Systems, Measurement, and Control*, **137**(1), p. 011005.

[15] Doyle, M., T. F. Fuller, and J. Newman (1993) "Modeling of galvanostatic charge and discharge of the lithium/polymer/insertion cell," *Journal of the Electrochemical Society*, **140**(6), pp. 1526–1533.

[16] Ramadesigan, V., P. W. Northrop, S. De, S. Santhanagopalan, R. D. Braatz, and V. R. Subramanian (2012) "Modeling and simulation of lithium-ion batteries from a systems engineering perspective," *Journal of The Electrochemical Society*, **159**(3), pp. R31–R45.

[17] Smith, K. A., C. D. Rahn, and C.-Y. Wang (2008) "Model order reduction of 1D diffusion systems via residue grouping," *Journal of Dynamic Systems, Measurement, and Control*, **130**(1), p. 011012.

[18] Subramanian, V. R., V. D. Diwakar, and D. Tapriyal (2005) "Efficient macro-micro scale coupled modeling of batteries," *Journal of The Electrochemical Society*, **152**(10), pp. A2002–A2008.

[19] Cai, L. and R. E. White (2012) "Lithium ion cell modeling using orthogonal collocation on finite elements," *Journal of Power Sources*, **217**, pp. 248–255.

[20] Forman, J. C., S. Bashash, J. L. Stein, and H. K. Fathy (2011) "Reduction of an electrochemistry-based Li-ion battery model via quasi-linearization and Padé approximation," *Journal of the Electrochemical Society*, **158**(2), pp. A93–A101.

[21] Shi, Y., G. Prasad, Z. Shen, and C. D. Rahn (2011) "Discretization methods for battery systems modeling," in *American Control Conference (ACC), 2011*, IEEE, pp. 356–361.

[22] Kehs, M. A., M. D. Beeney, and H. K. Fathy (2014) "Computational efficiency of solving the DFN battery model using descriptor form with Legendre polynomials and Galerkin projections," in *American Control Conference (ACC), 2014*, IEEE, pp. 260–267.

[23] Mayhew, C., W. He, C. Kroener, R. Klein, N. Chaturvedi, and A. Kojic (2014) "Investigation of projection-based model-reduction techniques for solid-phase diffusion in Li-ion batteries," in *American Control Conference (ACC), 2014*, IEEE, pp. 123–128.

[24] Ross, I. M. and F. Fahroo (2006) "Issues in the real-time computation of optimal control," *Mathematical and computer modelling*, **43**(9), pp. 1172–1188.

[25] Moura, S. J., J. C. Forman, S. Bashash, J. L. Stein, and H. K. Fathy (2011) "Optimal control of film growth in lithium-ion battery packs via relay switches," *Industrial Electronics, IEEE Transactions on*, **58**(8), pp. 3555–3566.

[26] Bashash, S., S. J. Moura, J. C. Forman, and H. K. Fathy (2011) "Plug-in hybrid electric vehicle charge pattern optimization for energy cost and battery longevity," *Journal of Power Sources*, **196**(1), pp. 541–549.

[27] Mamun, A.-A., I. Narayanan, D. Wang, A. Sivasubramaniam, and H. K. Fathy (2015) "Multi-objective optimization to minimize battery degradation and electricity cost for demand response in datacenters," in *Dynamic Systems and Control Conference*, ASME.

[28] Rahimian, S. K., S. Rayman, and R. E. White (2011) "Optimal charge rates for a lithium ion cell," *Journal of Power Sources*, **196**(23), pp. 10297–10304.

[29] Methekar, R., V. Ramadesigan, R. D. Braatz, and V. R. Subramanian (2010) "Optimum charging profile for lithium-ion batteries to maximize energy storage and utilization," *ECS Transactions*, **25**(35), pp. 139–146.

[30] Hu, X., S. Li, H. Peng, and F. Sun (2013) "Charging time and loss optimization for LiNMC and LiFePO4 batteries based on equivalent circuit models," *Journal of Power Sources*, **239**, pp. 449–457.

[31] Inoa, E. and J. Wang (2011) "PHEV charging strategies for maximized energy saving," *Vehicular Technology, IEEE Transactions on*, **60**(7), pp. 2978–2986.

[32] Mendoza, S., J. Liu, P. Mishra, and H. Fathy K. (2016) "Statistical quantification of least-squares battery state of charge estimation errors," in *Dynamic Systems and Control Conference*, ASME.

[33] Mishra, P. P., M. Garg, S. Mendoza, J. Liu, C. D. Rahn, and H. K. Fathy (2017) "How Does Model Reduction Affect Lithium-Ion Battery State of Charge Estimation Errors? Theory and Experiments," *Journal of The Electrochemical Society*, **164**(2), pp. A237–A251.

[34] Lin, X., A. G. Stefanopoulou, Y. Li, and R. D. Anderson (2013) "State of charge estimation of cells in series connection by using only the total voltage measurement," in *2013 American Control Conference*, IEEE, pp. 704–709.

[35] Xing, Y., W. He, M. Pecht, and K. L. Tsui (2014) "State of charge estimation of lithium-ion batteries using the open-circuit voltage at various ambient temperatures," *Applied Energy*, **113**, pp. 106–115.

[36] Dey, S., B. Ayalew, and P. Pisu (2015) "Nonlinear robust observers for state-of-charge estimation of lithium-ion cells based on a reduced electrochemical model," *IEEE Transactions on Control Systems Technology*, **23**(5), pp. 1935–1942.

[37] Tanim, T. R., C. D. Rahn, and C.-Y. Wang (2015) "State of charge estimation of a lithium ion cell based on a temperature dependent and electrolyte enhanced single particle model," *Energy*, **80**, pp. 731–739.

[38] Camacho-Solorio, L., M. Krstic, R. Klein, A. Mirtabatabaei, and S. J. Moura (2016) "STATE ESTIMATION FOR AN ELECTROCHEMICAL MODEL OF MULTIPLE-MATERIAL LITHIUM-ION BATTERIES," in *ASME 2016 Dynamic Systems and Control Conference*, American Society of Mechanical Engineers.

[39] Tang, X., X. Mao, J. Lin, and B. Koch (2011) "Li-ion battery parameter estimation for state of charge," in *Proceedings of the 2011 American control conference*, IEEE, pp. 941–946.

[40] Zou, C., C. Manzie, D. Nešić, and A. G. Kallapur (2016) "Multi-time-scale observer design for state-of-charge and state-of-health of a lithium-ion battery," *Journal of Power Sources*, **335**, pp. 121–130.

[41] Santhanagopalan, S. and R. E. White (2010) "State of charge estimation using an unscented filter for high power lithium ion cells," *International Journal of Energy Research*, **34**(2), pp. 152–163.

[42] Chen, Z., Y. Fu, and C. C. Mi (2013) "State of charge estimation of lithium-ion batteries in electric drive vehicles using extended Kalman filtering," *IEEE Transactions on Vehicular Technology*, **62**(3), pp. 1020–1030.

[43] Chen, Z., B. Xia, and C. C. Mi (2015) "A novel state-of-charge estimation method for lithium-ion battery pack of electric vehicles," in *Transportation Electrification Conference and Expo (ITEC), 2015 IEEE*, IEEE, pp. 1–6.

[44] Moura, S. J., N. A. Chaturvedi, and M. Krstić (2014) "Adaptive partial differential equation observer for battery state-of-charge/state-of-health estimation via an electrochemical model," *Journal of Dynamic Systems, Measurement, and Control*, **136**(1), p. 011015.

[45] Dey, S., S. Mohon, P. Pisu, B. Ayalew, and S. Onori (2015) "Online State and Parameter Estimation of Battery-Double Layer Capacitor Hybrid Energy Storage System," in *2015 54th IEEE Conference on Decision and Control (CDC)*, IEEE, pp. 676–681.

[46] Xiong, R., F. Sun, X. Gong, and C. Gao (2014) "A data-driven based adaptive state of charge estimator of lithium-ion polymer battery used in electric vehicles," *Applied Energy*, **113**, pp. 1421–1433.

[47] Rausch, M., R. Klein, S. Streif, C. Pankiewitz, and R. Findeisen (2014) "Set-based state of charge estimation for lithium-ion batteries," in *2014 American Control Conference*, IEEE, pp. 1566–1571.

[48] Suthar, B., V. Ramadesigan, P. W. Northrop, B. Gopaluni, S. Santhanagopalan, R. D. Braatz, and V. R. Subramanian (2013) "Optimal control and state estimation of lithium-ion batteries using reformulated models," in *2013 American Control Conference*, IEEE, pp. 5350–5355.

[49] Yan, M., Z. Xiuwen, and Z. Jixing (2014) "Lithium-ion battery state of charge estimation based on moving horizon," in *Intelligent Control and Automation (WCICA), 2014 11th World Congress on*, IEEE, pp. 5002–5007.

[50] Pattel, B., H. Borhan, and S. Anwar (2014) "An evaluation of the moving horizon estimation algorithm for online estimation of battery state of

charge and state of health," in *ASME 2014 International Mechanical Engineering Congress and Exposition*, American Society of Mechanical Engineers, pp. V04BT04A049–V04BT04A049.

[51] Shen, J.-N., Y.-J. He, Z.-F. Ma, H.-B. Luo, and Z.-F. Zhang (2016) "Online state of charge estimation of lithium-ion batteries: A moving horizon estimation approach," *Chemical Engineering Science*, **154**, pp. 42–53.

[52] Fliess, M., J. Lévine, P. Martin, and P. Rouchon (1995) "Flatness and defect of non-linear systems: introductory theory and examples," *International journal of control*, **61**(6), pp. 1327–1361.

[53] Fliess, M. and R. Marquez (2000) "Continuous-time linear predictive control and flatness: A module-theoretic setting with examples," *International Journal of Control*, **73**(7), pp. 606–623.

[54] Meurer, T. (2011) "Flatness-based trajectory planning for diffusionâĂŞreaction systems in a parallelepipedonâĂŤA spectral approach," *Automatica*, **47**(5), pp. 935 – 949.

[55] Mahadevan, R. and F. J. Doyle III (2003) "Efficient optimization approaches to nonlinear model predictive control," *International Journal of Robust and Nonlinear Control*, **13**(3-4), pp. 309–329.

[56] Oldenburg, J. and W. Marquardt (2002) "Flatness and higher order differential model representations in dynamic optimization," *Computers & Chemical Engineering*, **26**(3), pp. 385 – 400.

[57] Laroche, B., P. Martin, and P. Rouchon (2000) "Motion planning for the heat equation," *International journal of robust and nonlinear control*, **10**(8), pp. 629–643.

[58] Liu, J., G. Li, and H. K. Fathy (2016) "A computationally efficient approach for optimizing lithium-ion battery charging," *Journal of Dynamic Systems, Measurement, and Control*, **138**(2), p. 021009.

[59] Liu, J., G. Li, and H. Fathy (2016) "An Extended Differential Flatness Approach for the Health-Conscious Nonlinear Model Predictive Control of Lithium-Ion Batteries," *IEEE Transactions on Control Systems Technology*, **PP**(99), pp. 1–8.

[60] Suthar, B., P. W. Northrop, R. D. Braatz, and V. R. Subramanian (2014) "Optimal Charging Profiles with Minimal Intercalation-Induced Stresses for Lithium-Ion Batteries Using Reformulated Pseudo 2-Dimensional Models," *Journal of The Electrochemical Society*, **161**(11), pp. F3144–F3155.

[61] Huntington, G. T. (2007) *Advancement and analysis of a Gauss pseudospectral transcription for optimal control problems*, Ph.D. thesis, University of Florida.

[62] Rao, A. V., D. A. Benson, C. Darby, M. A. Patterson, C. Francolin, I. Sanders, and G. T. Huntington (2010) "Algorithm 902: GPOPS, A MATLAB Software for Solving Multiple-phase Optimal Control Problems Using the Gauss Pseudospectral Method," *ACM Trans. Math. Softw.*, **37**(2), pp. 22:1–22:39.

[63] Benson, D. (2005) *A Gauss pseudospectral transcription for optimal control*, Ph.D. thesis, Massachusetts Institute of Technology.

[64] Gong, Q., W. Kang, N. Bedrossian, F. Fahroo, P. Sekhavat, and K. Bollino (2007) "Pseudospectral Optimal Control for Military and Industrial Applications," in *Decision and Control, 2007 46th IEEE Conference on*, pp. 4128–4142.

[65] Morari, M. and J. H. Lee (1999) "Model predictive control: past, present and future," *Computers & Chemical Engineering*, **23**(4), pp. 667–682.

[66] Fang, Y. and A. Armaou (2015) "Nonlinear Model Predictive Control using a bilinear Carleman linearization-based formulation for chemical processes," in *American Control Conference (ACC), 2015*, IEEE, pp. 5629–5634.

[67] Haseltine, E. L. and J. B. Rawlings (2005) "Critical evaluation of extended Kalman filtering and moving-horizon estimation," *Industrial & engineering chemistry research*, **44**(8), pp. 2451–2460.

[68] Moura, S., N. Chaturvedi, and M. Krstic (2013) "Constraint management in Li-ion batteries: A modified reference governor approach," in *American Control Conference (ACC), 2013*, IEEE, pp. 5332–5337.

[69] Smith, K. A., C. D. Rahn, and C.-Y. Wang (2010) "Model-based electrochemical estimation and constraint management for pulse operation of lithium ion batteries," *Control Systems Technology, IEEE Transactions on*, **18**(3), pp. 654–663.

[70] Ross, I. M. and F. Fahroo (2003) "Legendre pseudospectral approximations of optimal control problems," in *New Trends in Nonlinear Dynamics and Control and their Applications*, Springer, pp. 327–342.

[71] Guo, M., G. Sikha, and R. E. White (2011) "Single-particle model for a lithium-ion cell: thermal behavior," *Journal of The Electrochemical Society*, **158**(2), pp. A122–A132.

[72] Kehs, M. A., M. D. Beeney, and H. K. Fathy (2014) "On the solution of the DFN battery model using descriptor form with Legendre and Galerkin projections," To be presented at American Control Conference.

[73] Burns, J., D. Stevens, and J. Dahn (2015) "In-Situ Detection of Lithium Plating Using High Precision Coulometry," *Journal of The Electrochemical Society*, **162**(6), pp. A959–A964.

[74] Ross, I. M. and F. Fahroo (2004) "Pseudospectral methods for optimal motion planning of differentially flat systems," *Automatic Control, IEEE Transactions on*, **49**(8), pp. 1410–1413.

[75] Mutambara, A. G. (1999) *Design and analysis of control systems*, CRC press.

[76] Arora, P., M. Doyle, and R. E. White (1999) "Mathematical Modeling of the Lithium Deposition Overcharge Reaction in Lithium-Ion Batteries Using Carbon-Based Negative Electrodes," *Journal of The Electrochemical Society*, **146**(10), pp. 3543–3553.

[77] Liu, J., M. Rothenberger, S. Mendoza, P. Mishra, Y.-s. Jung, and H. K. Fathy (2016) "Can an identifiability-optimizing test protocol improve the robustness of subsequent health-conscious lithium-ion battery control? an illustrative case study," in *2016 American Control Conference (ACC)*, IEEE, pp. 6320–6325.

[78] Mendoza, S., J. Rothenberger, Michael Liu, and H. K. Fathy (2017) "Maximizing Parameter Identifiability of a Combined Thermal and Electrochemical Battery Model Via Periodic Current Input Optimization," in *IFAC World Congress, 2017*, accepted.

[79] Bernardi, D., E. Pawlikowski, and J. Newman (1985) "A general energy balance for battery systems," *Journal of the electrochemical society*, **132**(1), pp. 5–12.

[80] Dey, S., B. Ayalew, and P. Pisu (2014) "Combined estimation of State-of-Charge and State-of-Health of Li-ion battery cells using SMO on electrochemical model," in *2014 13th International Workshop on Variable Structure Systems (VSS)*, IEEE, pp. 1–6.

[81] Xiong, R., F. Sun, Z. Chen, and H. He (2014) "A data-driven multi-scale extended Kalman filtering based parameter and state estimation approach of lithium-ion olymer battery in electric vehicles," *Applied Energy*, **113**, pp. 463–476.

[82] Xia, B., X. Zhao, R. De Callafon, H. Garnier, T. Nguyen, and C. Mi (2016) "Accurate Lithium-ion battery parameter estimation with continuous-time system identification methods," *Applied Energy*, **179**, pp. 426–436.

[83] Yang, J., B. Xia, Y. Shang, W. Huang, and C. Mi (2016) "Improved Battery Parameter Estimation Method Considering Operating Scenarios for HEV/EV Applications," *Energies*, **10**(1), p. 5.

[84] Liu, J., S. Mendoza, G. Li, and H. Fathy (2016) "Efficient total least squares state and parameter estimation for differentially flat systems," in *American Control Conference (ACC), 2016*, American Automatic Control Council (AACC), pp. 5419–5424.

[85] Aoki, M. (1967) *Optimization of stochastic systems*, Academic Press New York.

[86] Plett, G. L. (2011) "Recursive approximate weighted total least squares estimation of battery cell total capacity," *Journal of Power Sources*, **196**(4), pp. 2319–2331.

[87] Van Huffel, S. and J. Vandewalle (1991) *The total least squares problem: computational aspects and analysis*, vol. 9, Siam.

[88] Markovsky, I. and S. Van Huffel (2007) "Overview of total least-squares methods," *Signal processing*, **87**(10), pp. 2283–2302.

[89] Markovsky, I., J. C. Willems, S. Van Huffel, B. De Moor, and R. Pintelon (2005) "Application of structured total least squares for system identification and model reduction," *Automatic Control, IEEE Transactions on*, **50**(10), pp. 1490–1500.

[90] Liu, Z. and L. Vandenberghe (2009) "Interior-point method for nuclear norm approximation with application to system identification," *SIAM Journal on Matrix Analysis and Applications*, **31**(3), pp. 1235–1256.

[91] Boggs, P. T., R. H. Byrd, and R. B. Schnabel (1987) "A stable and efficient algorithm for nonlinear orthogonal distance regression," *SIAM Journal on Scientific and Statistical Computing*, **8**(6), pp. 1052–1078.

[92] Li, G. (2015) "Predictive control of a wave energy converter with wave prediction using differential flatness," in *Decision and Control (CDC), 2015 IEEE 54th Annual Conference on*, IEEE, pp. 3230–3235.

[93] Simon, D. (2006) *Optimal state estimation: Kalman, H infinity, and nonlinear approaches*, John Wiley & Sons.

[94] Fliess, M., C. Join, and H. Sira-Ramirez (2008) "Non-linear estimation is easy," *International Journal of Modelling, Identification and Control*, **4**(1), pp. 12–27.

[95] Mahadevan, R. and F. J. Doyle III (2004) "A partial flatness approach to nonlinear moving horizon estimation," in *American Control Conference, 2004. Proceedings of the 2004*, vol. 1, IEEE, pp. 211–215.

[96] Mahadevan, R., S. K. Agrawal, et al. (2001) "Differential flatness based nonlinear predictive control of fed-batch bioreactors," *Control Engineering Practice*, **9**(8), pp. 889–899.

[97] Gong, Q., I. M. Ross, and W. Kang (2007) "A pseudospectral observer for nonlinear systems," *Discrete and Continous Dynamical System Serires B*, **8**(3), p. 589.

[98] Liu, J., S. Mendoza, and H. Fathy "Total Least Squares State of Charge Estimation of Lithium-Ion Batteries: An Efficient Moving Horizon Estimation Approach," in *IFAC World Congress, 2017*, accepted.

[99] Hu, X., S. E. Li, and Y. Yang (2016) "Advanced Machine Learning Approach for Lithium-Ion Battery State Estimation in Electric Vehicles," *IEEE Transactions on Transportation Electrification*, **2**(2), pp. 140–149.

[100] He, W., N. Williard, C. Chen, and M. Pecht (2014) "State of charge estimation for Li-ion batteries using neural network modeling and unscented Kalman filter-based error cancellation," *International Journal of Electrical Power & Energy Systems*, **62**, pp. 783–791.

[101] Plett, G. L. (2011) "Recursive approximate weighted total least squares estimation of battery cell total capacity," *Journal of Power Sources*, **196**(4), pp. 2319–2331.

[102] Hashemian, N. and A. Armaou (2016) "Simulation, model-reduction, and state estimation of a two-component coagulation process," *AIChE Journal*.

[103] Fang, Y. and A. Armaou (2016) "A Formulation of advanced-step bilinear Carleman approximation-based nonlinear model predictive control," in *Decision and Control (CDC), 2016 IEEE 55th Conference on*, IEEE, pp. 4027–4032.

[104] Xiao, Y. (2015) "Model-based virtual thermal sensors for lithium-ion battery in EV applications," *IEEE Transactions on Industrial Electronics*, **62**(5), pp. 3112–3122.

[105] Xiao, Y. and B. Fahimi (2014) "Electrothermal modeling and experimental validation of a LiFePO 4 battery cell," in *Transportation Electrification Conference and Expo (ITEC), 2014 IEEE*, IEEE, pp. 1–5.

[106] Forgez, C., D. V. Do, G. Friedrich, M. Morcrette, and C. Delacourt (2010) "Thermal modeling of a cylindrical LiFePO 4/graphite lithium-ion battery," *Journal of Power Sources*, **195**(9), pp. 2961–2968.

[107] Haseltine, E. L. and J. B. Rawlings (2005) "Critical evaluation of extended Kalman filtering and moving-horizon estimation," *Industrial & engineering chemistry research*, **44**(8), pp. 2451–2460.

[108] Alessandri, A., M. Baglietto, and G. Battistelli (2008) "Moving-horizon state estimation for nonlinear discrete-time systems: New stability results and approximation schemes," *Automatica*, **44**(7), pp. 1753–1765.

[109] Hashemian, N. and A. Armaou (2015) "Fast moving horizon estimation of nonlinear processes via Carleman linearization," in *2015 American Control Conference (ACC)*, IEEE, pp. 3379–3385.

[110] Rao, C. V., J. B. Rawlings, and D. Q. Mayne (2003) "Constrained state estimation for nonlinear discrete-time systems: Stability and moving horizon approximations," *IEEE transactions on automatic control*, **48**(2), pp. 246–258.

[111] Liu, J., Y. Chen, and H. Fathy "Nonlinear Model-Predictive Optimal Control of an Active Cell-to-Cell Lithium-Ion Battery Pack Balancing Circuit," in *IFAC World Congress, 2017*, accepted.

[112] Varigonda, S., T. T. Georgiou, and P. Daoutidis (2004) "Numerical solution of the optimal periodic control problem using differential flatness," *IEEE Transactions on Automatic Control*, **49**(2), pp. 271–275.

[113] Simon, D. (2006) *Optimal state estimation: Kalman, H infinity, and nonlinear approaches*, John Wiley & Sons.

[114] Dey, S. and B. Ayalew (2016) "Real-time Estimation of Lithium-ion Concentration in Both Electrodes of a Lithium-ion Battery Cell Utilizing Electrochemical-Thermal Coupling," *Journal of Dynamic Systems, Measurement, and Control*.

Vita

Ji Liu

Education:
Pennsylvania State University, Ph.D. Mechanical Engineering, May 2017.
Pennsylvania State University, M.S. Mechanical Engineering, Aug. 2015.
South China University of Technology, B.S. Mechanical Engineering, May 2012.

Experience:
Research Assistant, Pennsylvania State University, Jan. 2013 - Jan. 2017
Teaching Assistant, Pennsylvania State University, Jan. 2016 - May 2016
Personal Website:
https://www.linkedin.com/in/jiliupennstate
Selected Publications:

1. J. Liu, G. Li, and H. K. Fathy, "A computationally efficient approach for optimizing lithium-ion battery charging," Journal of Dynamic Systems, Measurement, and Control, vol. 138, no. 2, p. 021009, 2016.

2. J. Liu, G. Li, and H. K. Fathy, "An extended differential flatness approach for the health-conscious nonlinear model predictive control of lithium-ion batteries," IEEE Transactions on Control Systems Technology, 2016.

3. S. Mendoza, J. Liu, Mishra, Partha, H. Fathy, "On the Relative Contributions of Bias and Noise to Lithium-ion Battery State of Charge Estimation Errors," The Journal of Energy Storage, 2017.

4. M. J. Rothenberger, J. Safi, J. Liu, J. Anstrom, S. Brennan, and H. K. Fathy, "Improving li-ion battery pack diagnostics by optimizing the internal allocation of demand current for parameter identifiability," 2017.

5. P. P. Mishra, M. Garg, S. Mendoza, J. Liu, C. D. Rahn, and H. K. Fathy, "How does model reduction affect to ion battery state of charge estimation errors? theory and experiments," Journal of The Electrochemical Society, vol. 164, no. 2, pp. A237 - A251, 2017.

6. J. Liu, S. Mendoza, G. Li, and H. Fathy, "Efficient total least squares state and parameter estimation for differentially flat systems," in American Control Conference (ACC), 2016.

7. J. Liu, G. Li, and H. K. Fathy, "Efficient lithium-ion battery model predictive control using differential to based pseudospectral methods," in ASME 2015 Dynamic Systems and Control Conference. American Society of Mechanical Engineers, 2015.